EVALUATION OF NMR STRUCTURAL STUDIES ON A FAMILY OF MEMBRANE ACTIVE CHANNEL FORMING PEPTIDES

by

ALVARO IVAN HERRERA

B.E. Universidad Nacional de Colombia, 2002
M.S., Kansas State University, 2006

AN ABSTRACT OF A DISSERTATION

submitted in partial fulfillment of the requirements for the degree

DOCTOR OF PHILOSOPHY

Department of Biochemistry and Molecular Biophysics
College of Arts and Sciences

KANSAS STATE UNIVERSITY
Manhattan, Kansas

2015

Abstract

As part of the ongoing development of a channel forming peptide with the potential to be used clinically to treat cystic fibrosis, a number of structural studies using solution NMR spectroscopy have been carried out on a number of the test sequences. Given their structural similarities of the monomers it is important to evaluate whether or not there is a compelling need to determine the solution NMR structure of next-generation peptides. The determination of the NMR monomeric solution structure of peptides NK_4-M2GlyR-p22 and NK_4-M2GlyR-p20 T17R S20W in TFE solution and SDS micelles sample shows predominantly α-helical conformations for both sequences with an extended conformation for the N-terminal lysine residues. The I_{max}, $K_{1/2}$ and Hill coefficient, derived from data on ion conductance across monolayers of MDCK cells, were used to compare the ion conductance properties of the peptide sequences. Peptide NK_4-M2GlyR-p20 T17R S20W has both a higher I_{MAX} (43.8 ± 2.8 μA/cm^2) and a lower $K_{1/2}$ (58 ± 8 μM) compared to other M2GlyR derived peptides with calculated NMR structures. All available molecular structures calculated by NMR for M2GlyR derived peptides were compared and the correlation of the structural changes observed in the NMR structures with the ion conductance changes was evaluated. The NMR structures were found to have limited predicting potential over the ion conduction data. NMR determined structures have provided an experimentally based starting point for studies of the channels formed by the family of M2GlyR peptides. Computer simulations account for inter peptide interactions and packing effects that are not experienced by the monomeric form of the peptides in the NMR samples that have been used until now. The determination of the structure of the oligomeric peptide channels is deemed needed to improve the relevance of future use of NMR in this project. The use of larger

membrane mimicking agents, isotopically labeled (^{15}N, ^{13}C) samples, 3D NMR experiments and potentially solid state NMR would be required to accomplish that task.

EVALUATION OF NMR STRUCTURAL STUDIES ON A FAMILY OF MEMBRANE ACTIVE CHANNEL FORMING PEPTIDES

by

ALVARO IVAN HERRERA

B.E. Universidad Nacional de Colombia, 2002
M.S., Kansas State University, 2006

A DISSERTATION

submitted in partial fulfillment of the requirements for the degree

DOCTOR OF PHILOSOPHY

Department of Biochemistry and Molecular Biophysics
College of Arts and Sciences

KANSAS STATE UNIVERSITY
Manhattan, Kansas

2015

Approved by:

Co-Major Professor
John M. Tomich

Approved by:

Co-Major Professor
Om Prakash

Copyright

Abstract

As part of the ongoing development of a channel forming peptide with the potential to be used clinically to treat cystic fibrosis, a number of structural studies using solution NMR spectroscopy have been carried out on a number of the test sequences. Given their structural similarities of the monomers it is important to evaluate whether or not there is a compelling need to determine the solution NMR structure of next-generation peptides. The determination of the NMR monomeric solution structure of peptides NK_4-M2GlyR-p22 and NK_4-M2GlyR-p20 T17R S20W in TFE solution and SDS micelles sample shows predominantly α-helical conformations for both sequences with an extended conformation for the N-terminal lysine residues. The I_{max}, $K_{1/2}$ and Hill coefficient, derived from data on ion conductance across monolayers of MDCK cells, were used to compare the ion conductance properties of the peptide sequences. Peptide NK_4-M2GlyR-p20 T17R S20W has both a higher I_{MAX} (43.8 ± 2.8 μA/cm^2) and a lower $K_{1/2}$ (58 ± 8 μM) compared to other M2GlyR derived peptides with calculated NMR structures. All available molecular structures calculated by NMR for M2GlyR derived peptides were compared and the correlation of the structural changes observed in the NMR structures with the ion conductance changes was evaluated. The NMR structures were found to have limited predicting potential over the ion conduction data. NMR determined structures have provided an experimentally based starting point for studies of the channels formed by the family of M2GlyR peptides. Computer simulations account for inter peptide interactions and packing effects that are not experienced by the monomeric form of the peptides in the NMR samples that have been used until now. The determination of the structure of the oligomeric peptide channels is deemed needed to improve the relevance of future use of NMR in this project. The use of larger

membrane mimicking agents, isotopically labeled (^{15}N, ^{13}C) samples, 3D NMR experiments and potentially solid state NMR would be required to accomplish that task.

Table of Contents

List of Figures

List of Tables

List of Abbreviations

M2GlyR - second transmembrane sequence of the glycine receptor, α-subunit

AMP - antimicrobial peptide

CPP - cell penetrating peptide

CFP - channel/pore forming peptide

AP - amyloid peptide

SAAP - synthetic antimicrobial antibiofilm peptides

PSA - prostate-specific antigen

PSMA - prostate-specific membrane antigen

BAPS - branched amphiphilic peptide capsules

CFTR - cystic fibrosis transmembrane conductance regulator

NMR - nuclear magnetic resonance

DQF-COSY - double-quantum-filtered correlation spectroscopy

TOCSY - total correlation spectroscopy

NOESY - nuclear Overhauser effect spectroscopy

ROESY - rotating frame nuclear overhauser effect spectroscopy

TFE - 2,2,2-trifluoroethanol

SDS - sodium dodecyl sulfate

DMSO - dimethyl sulfoxide

1-EBIO - 1-ethyl-2-benzimidazolinone

I_{sc} - short circuit current

I_{max} - maximum short circuit current

MW - molecular weight

MD - molecular dynamics

FMOC - 9-fluorenyl methoxycarbonyl

HPLC - high performance liquid chromatography

TFA - trifluoroacetic acid

CD - circular dichroism

MALDI-TOF - matrix assisted-laser desorption time of flight mass spectroscopy

DI - deionized

RMSD - root mean square deviation

V_{TE} - transepithelial membrane potential

BSA - bovine serum albumin

POPC - 1-Palmitoyl-2-oleoyl-sn-glycero-3-phosphocholine

DPC - dodecylphosphocholine

DMPC - dimyristoylphosphatidylcholine

DHPC - 1,2-dihexanoyl-sn-glycero-3-phosphocholine

MAS - magic angle spinning

DARR - Dipolar Assisted Rotational Resonance

Acknowledgements

I want to thank my major professors: Dr. Om Prakash for his guidance, mentoring, trust, and kindness. Dr. John Tomich for his support, guidance and opportune advice regarding the research here presented, and for sharing with me his vision of science. To both of them my extensive gratitude for all the help during the writing of this dissertation. I would also like to thank the members of my committee Dr. Jianhan Chen and Dr. Paul Smith, and the outside chairperson Dr. Mark Weiss for their time and efforts in making this dissertation a better final product.

A special thanks to the people that have contributed to this project before me, and to those I had the opportunity to work with and learn from: Dr. Gabriel Cook, Dr. Ahlam Al-Rawi, Dr. Urška Bukovnik, Dr. Shawnalea Frazier, Dr. Sushanth Gudlur , Dr. Pinakin Sukthankar, Dr. Yasuaki Hiromasa, and Dr. Daisuke Takahashi. My gratitude to everyone in the department of Biochemistry and Molecular Biophysics as well for making my time here possible.

Finally I want to thank my family and friends, those far away and those close for their support and encouragement, and to God for facing me with challenges armed with the tools to solve them.

Dedication

Para Elisa,

In the stillness of a cold night while I rock my son to sleep, I can feel your embrace coming from a place in time beyond my memory. You are my foundation, and I can only wish you were here.

Para Sandra

Many days, many places, many stories and in all you've been there with me. Holding hands we have walk this path. You are my sunshine and I wish you're always by my side.

Y para Nicholas

Seeing you learn and discover the world every day gives meaning and purpose to my days. You are my fruit and I wish for you happiness and wisdom.

Chapter 1 - Membrane Active Peptides: A Review

Abstract

Membrane active peptides from natural or synthetic origins serve a variety of biological purposes. They have been extensively studied for their involvement in immunity, diseases, and for their potential as medical therapeutics and research tools. In this report a classification of membrane active peptides is presented, categorizing membrane active peptides according to their function such as antimicrobial peptides, cell-penetrating peptides, channel forming peptides and amyloid peptides. For each group a historical overview of the development, the current knowledge about their functional mechanism, and recent advances are presented. The large volume of current research on the field of membrane active peptides would make the task of covering it all an overwhelming one, but a representative sample of the latest research in each category is presented here. A set of common features among peptide groups emerges as the understanding of their action mechanisms increase. The possibility of a membrane centric general model for peptide-membrane interaction is also discussed.

Introduction

This review intends to give a general overview of peptides, natural and designed, having the ability to interact with cellular plasma membranes in a way that modifies the natural integrity and permeability of the lipid bilayer. Biological membranes are highly dynamic supramolecular

arrangements of lipids and proteins, which confine the cellular contents but also enforce a complex and highly regulated exchange with the surrounding environment (Bechinger, 2008).

Membrane active peptides fulfill many important functions in nature as they act as antimicrobials, transporters, channels, or hormones (Last and Miranker, 2013). The study of membrane active peptides has increased the understanding of polypeptide-membrane interactions and present unique opportunities for the intentional modulation of many cellular activities, with potential applications in medicine and in biological research in general.

As membrane active peptides with different activities were discovered new areas of study emerged and knowledge pertaining to each area developed mostly in an independent manner. It was not until recently that commonalities between peptides with different membrane activities have been widely recognized. Efforts to understand the interactions of these peptides with cellular membranes and develop a general peptide-membrane model have been published by others (Bechinger, 2008;Last and Miranker, 2013). In this report membrane active peptides are divided based on their reported function(s): antimicrobial peptides, cell-penetrating peptides, channel forming peptides and amyloid peptides.

General Properties

Membrane active peptides are short (less than 50 amino acids, in general), and soluble in both aqueous and membrane environments. Many natural membrane active peptides are the product of the cleavage of a precursor protein, and can also be post translationally modified. The

sequences of non-natural membrane active peptides could be the product of *de novo* design based on basic principles, or could be derived from naturally occurring proteins by truncations and or substitutions. Membrane active peptides have been described from species in all natural kingdoms as well as viruses (Frankel and Pabo, 1988;Phoenix et al., 2013). Non-natural membrane active peptides can be chemically synthesized or can be express in cells using common molecular biology techniques (Carmona-Ribeiro and Carrasco, 2014).

The current view of the structure of cellular membranes derives mainly from the fluid mosaic model proposed in 1972 (Singer and Nicolson, 1972). In this model the lipid bilayer forms a hydrophobic matrix with a distribution of embedded proteins of diverse functions in a mosaic-type fashion. Lateral diffusion within the plane of the bilayer is considered to occur in a manner comparable to viscous flow, and movements in the normal direction of the membrane are much more restricted (Bechinger, 2008). Solid-state NMR studies and molecular modeling have indicated considerable conformational flexibility of the lipid molecules within the bilayer (Feller et al., 1999;Huster et al., 1999). Membrane active peptides interact with the lipid components of membranes; the nature of these interactions is determined by the peptide sequence as well as by the composition of the membrane. The forces that control the membrane-peptide interaction are electrostatic as well as hydrophobic. The spatial distribution of charge and, hydrophobic and hydrophilic groups in the peptide as well as in the bilayer are determinant of the interactions.

Membrane active peptides are typically unstructured in aqueous solution, but undergo a disordered-to-ordered transition upon membrane association to either α-helical or β-strand secondary structural states that are generally amphipathic in nature (Herrera et al., 2010;Maler,

2013;Williamson et al., 2009). The amphipathic arrangement of the secondary structure allows the peptides to initially bind to membranes by orienting parallel to the plane of the bilayer with the polar side of the helix facing the lipid headgroups and the solvent, while the nonpolar side of the peptide is exposed to the membrane core (Huang, 2006;Jao et al., 2008).

Classification

Membrane active peptides can be classified in four broad categories according to their function: antimicrobial peptides, cell-penetrating peptides, channel/pore forming peptides and amyloid peptides. The classification used here is based in several factors including the function or activity for which each peptide is studied the most, common mechanisms of action within peptides groups, and the historical manner knowledge about each group of peptides developed. Some peptides could fit in more than one category depending on the context e.g. Tat peptide, a prototypical cell-penetrating peptide, is also known to have antimicrobial activity. As with any taxonomical effort the proposed boundaries between categories are a reflection of the limited knowledge available, and are subject to modification as greater understanding of the interactions between peptides and membranes becomes available.

Antimicrobial Peptides

According to the "Threat Report" of 2013, each year in the United States at least 2 million people become infected with bacteria that are resistant to antibiotics and at least 23,000 people die annually as a direct result of these infections (Center for Disease Control and Prevention,

2013). The prevalence of antibiotic resistant microorganisms has motivated an increasing interest in looking back at innate immunity and more specifically to the gene encoded protein elements of it. Antimicrobial peptides (AMPs), also known as host defense peptides, are part of the innate immune response. These peptides are found among all classes of life.

AMPs are generally defined as peptides consisting of less than 100 amino acid residues (usually between 12 and 50) with overall net charge of +2 to +9, due to the presence of positively charged amino acids such as lysine and arginine along with a substantial portion of hydrophobic residues (Pushpanathan et al., 2013). AMPs have been found to exist in a wide range of secondary structures such as α-helices, β-strands with one or more disulphide bridges, loops and extended structures (Hancock, 2001). AMPs present some degree of amphipathicity in the spatial distribution of its residue side chains.

Historical overview

The first reference to the antimicrobial activity of biological secretions appeared in 1922 when Alexander Fleming published his observations "On a Remarkable Bacteriolytic Element found in Tissues and Secretions" (Fleming, 1922). In this study, the ability of "Lysozyme" to kill a wide range of bacteria, and the ubiquitous presence of the protein in body secretions was reported. Because lysozyme lacked in killing most pathogen bacteria the search for an antibiotic drug took the path that resulted in the development of the variety of antibiotics available today. Initially the bacteriolytic properties found for body secretions, were credited to a single element, named "Lysozyme". In 1934 the nature of "Lysozyme" was studied in detail (Meyer et al., 1934) and it

was recognized as one or more protein enzymes. Through processes of purification and concentration the enzyme today know as lysozyme was isolated and characterized, but smaller non enzymatic antimicrobial agents present in low concentrations were ignored. The origins of research into AMPs came in the 1960s. In 1962, the first description of an animal AMP, named bombinin was reported in the orange speckled frog *Bombina variegate* (Bagnicka et al., 2011). The antimicrobial protein lactoferrin, isolated from milk (Groves et al., 1965) and small antimicrobial molecules observed to be induced in the hemolymph of wax moth larvae after challenge with *Pseudomonas aeruginosa* (Stephens and Marshall, 1962) were reported in during the 1960s as well (Phoenix et al., 2013).

In the following years after the initial reports many more AMPs have been reported from a wide variety of species. The "Antimicrobial Peptide Database" (Wang et al., 2009) contained 2531 entries from human, amphibians, fish, reptile, birds, arthropods, insects and more in its latest available statistic summary dated March 2015. Out of the 2531 entries in the database 340 have their atomic 3D structure determined. Antimicrobial peptides are evolutionarily ancient weapons; their widespread distribution throughout the animal and plant kingdoms suggests that they have served an important role in the successful evolution of complex multicellular organisms (Zasloff, 2002). The diversity of antimicrobial peptides is so great that a consensus on classification and categorization is difficult. AMPs are generally categorized broadly in three groups on basis of their secondary structure.

-Small Linear peptides, such as the silk moth's cecropin and the African clawed frog's magainin that adopt an amphipathic α-helical secondary structure in the membrane (Zasloff, 1987).

- Peptides with an even number of Cys, always intralinked, with a relatively rigid antiparallel β-sheet structures like bactenecin and defensins (Selsted et al., 1985).
- Linear Peptides with a high proportion of one or two amino acids, most often Pro, Arg. Like the Pro-Arg rich PR39 of the pig neutrophil (Agerberth et al., 1991) and cationic peptides such as cathelicidins.

Naturally occurring AMPs are derived from larger precursor proteins, which contain a signal sequence. Post-translational modifications include proteolytic processing, and in some cases glycosylation, carboxy-terminal amidation, amino acid isomerization and halogenation (Zasloff, 2002). The number of amino acid residues in most of the mature antimicrobial peptides is between 13 and 39. In addition to the naturally occurring AMPs, peptides with the same biological activity have been designed de novo (Blazyk et al., 2001), engineered from natural sequences (Avrahami and Shai, 2002;Hilpert et al., 2006) or selected from combinatorial libraries (Rathinakumar et al., 2009;Rausch et al., 2005).

Mode of action

The term antimicrobial peptide includes peptides with a range of additional biological activities such as antiviral, antifungal, and antitumor. Also the locations of expression of antimicrobial peptides are diverse; AMPs have been found to be produced by the epithelia of amphibian, mammals, and insects. They are secreted into internal body fluids in arthropods and stored in the cytoplasmic granules of professional phagocytes of mammals and birds (Zanetti et al., 1995).

AMPs are cationic, amphipathic peptides with broad spectrum microbicidal activity which is associated with membrane permeabilization. Unlike nonspecific membrane lytic peptide toxins, such as melittin from the venom of the Honey Bee (*Apis mellifera*), AMPs have little cytolytic or cytotoxic activity against host cells (Herrera et al., 2009;Wimley, 2010). Most AMPs are believed to kill microorganisms via a non receptor-mediated mechanism. These peptides are active in vitro at micromolar concentration, which is their biologic concentration at the sites of infections. Most AMPs can be subjected to pronounced sequence alterations without affecting significantly their function.

AMPs target a fundamental difference between the membranes of microbes and multicellular animals for their preferential binding affinity. Microbial membranes are organized such that the outermost leaflet of the bilayer, the surface exposed to the outer environment, is populated by lipids with negatively charged phospholipid headgroups (phosphatidylglycerol, cardiolipin), in contrast the outer leaflet of the membranes in plants and animals is composed mainly of lipids with no net charge (phosphatidylethanolamine, cholesterol, sphingomyelin). Most of the lipids with negatively charged headgroups are segregated into the inner leaflet (Zasloff, 2002). This characteristic gives AMPs a greater affinity for microbial membranes than for eukaryotic membranes. The binding forces between the AMPs and the membrane are: electrostatic interactions (charged residues to negative charges in head groups of the lipids), and hydrophobic interactions (non-polar residues to the membrane core). There is direct evidence that most AMPs permeabilize the cytoplasmic membrane of the target and that often this permeabilization increases in severity with time. AMPs have the ability to dissipate the electrochemical gradient of the microbial plasma membranes within seconds after contact (Matsuzaki et al., 1997). In

order to achieve their intended activity in the observed time frame, AMPs must be able to rapidly pass through the proteoglycan layer of Gram positive bacteria and the outer membrane lipopolysaccharide layer of Gram negative bacteria. The timescale for the AMP induced permeation of larger markers, including dye markers, metabolites and cytosolic proteins, through the cytoplasmic membrane is of minutes to tens of minutes (Rathinakumar et al., 2009;Rausch et al., 2007). A numbers of models have been proposed to explain the mechanism by which AMPs permeate the phospholipids membrane. The amount of evidence supporting different models for different AMPs, suggests diversity on the mode of action within the compendium of AMPs (Wimley, 2010). The classical models can be divided into the "pore models" and the "non-pore models".

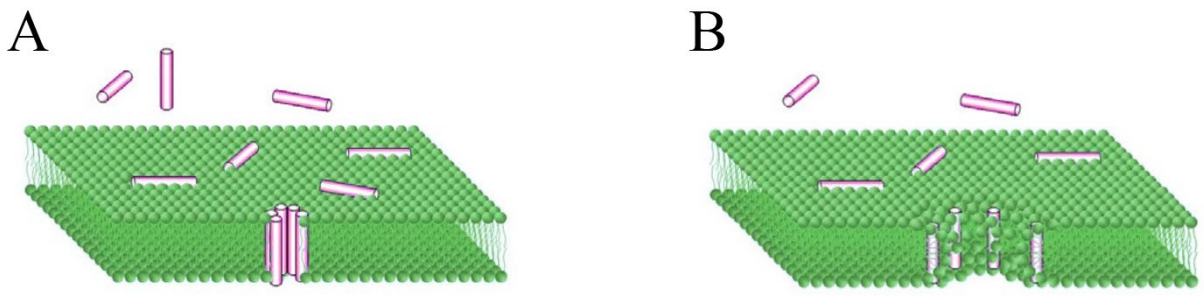

Figure 1-1. Pore Models of action of AMPs. A. Barrel Stave Model B. Torodial Model. Adapted with permission from Describing the Mechanism of Antimicrobial Peptide Action with the Interfacial Activity Model. Copyright 2010 American Chemical Society

The pore models implicate the formation of a transient transmembrane pore or channel. In the barrel stave model, the interior of the formed pore is lined by the hydrophilic surfaces of the AMP, while peptides interact with each other laterally, in a manner similar to the channels formed by membrane proteins (Figure 1-1A). The other classic pore forming model is the

Toroidal model. According to this model the peptide interaction with the bilayer affect the local curvature inducing a continuous bend through the pore, there are no specific peptide-peptide interactions and the interior of the pores is lined by both the peptides and the lipid head groups (Figure 1-1B).

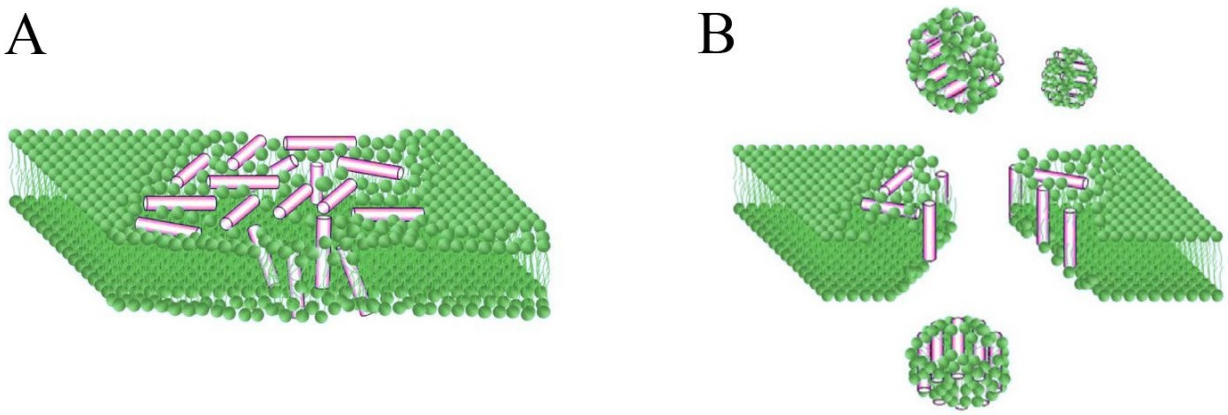

Figure 1-2. Non-pore models of action for AMPs. A. Carpet Model B. Detergent Model. Adapted with permission from Describing the Mechanism of Antimicrobial Peptide Action with the Interfacial Activity Model. Copyright 2010 American Chemical Society

A model by Gazit et al. proposes an AMP mode of action where the formation of a pore is not necessary. It is suggested that peptides are always oriented parallel to the membrane surface and at high concentration the peptides form a "carpet" that distorts the bilayer enough to allow permeation (Figure 1-2A) (Gazit et al., 1996). The other commonly cited non-pore forming model is the "detergent model", that describes the catastrophic collapse of the membrane integrity and a probe-size independent permeation observed at high peptide concentration for some AMPs (Figure 1-2B) (Hristova et al., 1997).

The descriptive models of AMP action have a limited predicting potential and applicability in optimization or design of engineered peptides. Recently a new set of descriptions aimed to provide a physicochemical understanding that would be potentially more comprehensive and useful has been proposed. A model based on molecular shape that describes the physical chemistry of AMPs and membranes in a phase diagram was presented by Bechinger and Lohner (Bechinger, 2009;Bechinger and Lohner, 2006). Experimental evidence supporting that membrane leakage could occur at phase boundary defects has been presented by Epand et al., they proposed that lateral lipid phase separation, or lipid clustering, induced by cationic antimicrobial peptides explains the AMPs biophysical properties as well as their selectivity and biological activity. (Epand et al., 2010;Epand and Epand, 2009).

The computational simulations of uncharged small molecule release from single vesicles through single pores predict complete release of the vesicular content within a few tenths of a second. However, available experimental data on vesicle-based leakage studies show that vesicles with 1000 bound AMPs typically release only a portion of their content over several minutes. Based on these discrepancies, Wimley in 2009 postulated that most AMPs do note ever form true pores in unilamellar vesicles, instead content leaking occurs by transient disruption of the membrane integrity. To describe the non-equilibrium events that allow content release Wimley proposed the "interfacial activity model" (Rathinakumar et al., 2009;Wimley, 2010). Interfacial activity was defined as "the ability of a molecule to bind to a membrane, partition into the membrane-water interface, and to alter the packing and organization of the lipids". Interfacial activity is a quantifiable property assigned to a peptide based on amino acid sequence, structure and the physical chemical balance between hydrophobic and polar groups. According to this model an

imperfect amphipathic peptide would have a greater interfacial activity comparted to a perfect amphipathic one because the membrane packing and arrangement would have to be further disturbed to accommodate the imperfections. The structural and biological findings of our studies on AMPs identified from the chicken genome support the concept of interfacial activity (Herrera et al., 2009;Xiao et al., 2006).

Recent developments

Although in the last decade a number of AMPs had been considered promising candidates for antibacterial drug development, currently the only AMPs approved for medical use are gramicidin, nisin, daptomycin, and polymyxins (Carmona-Ribeiro and Carrasco, 2014), all of them restricted to topical agents. AMP based applications of magainins, cecropins and defensins have failed to translate into approved anti-infective agents. However interest in the development of AMP based antibiotic agents has seen resurgence with recent policy changes and incentives. Recognizing that approval of new antibiotics was declining, FDA officials launched the Antibacterial Drug Development Task Force to address a mandate that was part of the 2012 FDA Safety and Innovation Act (FDASIA), also called PDUFA 5, which incorporated parts of the Generating Antibiotic Incentives Now (GAIN) Act (Fox, 2012).

The current approach for the development of successful clinical agents based on AMPs is centered on new formulations that could potentially overcome the challenge of delivering the peptides to the site of infection with sufficient bioavailability, while protecting their activity. The potential use of electrospun nanofibers as a drug delivery system has been explored. The release

properties and the loading density of the synthetic AMP fluorescein incorporated into electrospun nanofibres of poly(ε-caprolactone) were studied by Eriksen et al. (Eriksen et al., 2013), a release of 85% of the AMP after 60 minutes was reported. Recently Zaat reported on behalf of the European Union's Biofilm Alliance (BALI), the development of novel synthetic antimicrobial antibiofilm peptides (SAAPs) based on the primary structures of the antimicrobial proteins LL-37 and thrombocidin-1. SAAPs are a solution against infection of inserted and implanted medical devices predominantly caused by staphylococci. The novel peptides kill a wide spectrum of Gram-positive and -negative (antibiotic resistant) bacteria at concentrations ranging from 0.8 - 8 μM in phosphate-buffered saline. The SAAPs have been shown to prevent biofilm formation of *Staphylococcus aureus* at concentrations of 3.2 – 12.8 μM. These peptides also have potent anti-inflammatory activity: they inhibit production of IL-12 and IL-8 by cells in whole blood upon stimulation with lipopolysaccharide and UV-killed *S. aureus* (Zaat, 2014). The conjugation of AMPs to magnetic nanoparticles has also been suggested (Lopez-Abarrategui et al., 2013).

Advances have also been made in the use of the antitumor activity found in some AMPs, LeBeau et al. reported on a protease-activated pore-forming peptide for the treatment and imaging of prostate cancer (LeBeau and Denmeade, 2014). Taking advantage of the peritumoral proteolytic activity of prostate cancer, a propeptide construct made of a cationic diastereomeric pore-forming peptide linked to an inactivating acidic peptide domain, gets activated by the serine protease prostate specific antigen (PSA) or the transmembrane metalloprotease prostate-specific membrane antigen (PSMA)). PSA and PSMA activated propeptides were found to be cytotoxic

to prostate cancer cells *in vitro*. *In vivo*, PSMA activated propeptide also proved to be an effective optical imaging probe when labeled with a near-infrared fluorophore.

New fields of action and modes of application for AMPs are been explored - e.g. recently Veldhuizen reported the *in ovo* administration of chicken cathelicidin peptide analog DCATH-2 and its efficacy to reduce experimentally induced salmonellosis in young broiler chickens (Ordonez et al., 2014), In another study Li et al. reported the development of a peptide-based biosensor for the detection of *Escherichia coli* O157:H7 using a ruthenium complex labeled Magainin I peptide as capture/signal probe (Li et al., 2015). Puig et al. published the successful use *in vitro* of 12 synthetic AMPs against the fungal disease produced by *Stemphylium vesicarium* that causes brown spots in pears (Puig et al., 2014)

A new universal classification system (UC) intended to facilitate the study and development of AMPs has been proposed (Wang, 2015). The UC groups AMPs into four classes based on the covalent bonding pattern of polypeptide chains: 1) UCLL- linear one-chain peptides (e.g. LL-37 and magainins) or two linear peptides not connected via a covalent bond (e.g. enterocin L50); 2) UCSS -sidechain-linked peptides (e.g. disulfide-containing defensins or ether bond-containing lantibiotics); 3) UCSB -polypeptide chains with a sidechain to backbone connection (e.g. bacterial lassos and fusaricidins); 4) UCBB -circular polypeptides with a peptide bond between the N- and C-termini (e.g. bacterial AS-48, plant cyclotides, animal theta-defensins). The new classification system aims to unify innate immunity peptides from a variety of biological sources; implemented into the AMP database the new classification improves its search engine and the usability of the database on the design of novel antimicrobials.

Though AMPs have been touted as a potential solution to the antibiotic drug resistance crisis, concerns have been raised about the risk of developing AMPs based therapeutics. In a 2012 report, *S. aureus* was shown to rapidly evolve resistance to pexiganan (currently at Phase 3 clinical studies as Locilex) under laboratory conditions (Habets and Brockhurst, 2012). In some of the populations studied in this report, the adaptation to pexiganan provided *S. aureus* with cross-resistance to human-neutrophil-defensin-1, a key component of the innate immune response to infection; presenting the potential risk of compromising the innate human immune system.

Cell-Penetrating Peptides

Cell-Penetrating Peptides (CPPs) are generally comprised of 40 amino acids residues of less, and have the ability to translocate cell membranes and enter cells promoting the delivery of a variety of cargos. The property of CCPs to deliver therapeutic molecules (nucleic acids, drugs, imaging agents and even proteins) to cells and tissues in a nontoxic manner makes them potential components of future drugs and disease diagnostic agents (Copolovici et al., 2014).

Historical overview

The HIV Tat factor discovered in 1988 and the Drosophila Antennapedia transcription factor a few years later, were the first sequences reported to translocate molecules across cell membranes into cells (Derossi et al., 1994;Frankel and Pabo, 1988). Shorter sequences derived from these

natural peptides (16 residues from third helix homeodomain of Antennapedia named penetratin and 11 residues from Tat) preserve the cell penetrating activity. Tat and penetratin were the basis for the study and development of CPPs, as a new type of molecular vectors with the ability to promote the delivery of a variety of cargos (Copolovici et al., 2014). In 1997, the first non-covalent CPP for delivery of nucleic acids, Pep-1, was designed by the group of Heitz and Divita (Morris et al., 1997). The development of Pep-1 for non-covalent cellular delivery of proteins and peptides was reported a few years later (Morris et al., 2001). This sequence is commercially available under the trade name *Chariot* (Active Motif, Carlsbad, California). Polyarginine sequences (R8) were also demonstrated to be sufficient to drive molecules into cells by Wender and Fukati (Futaki et al., 2001;Wender et al., 2000). Since then, many novels synthetic or chimeric CPPs have been discovered and tested. Table 1-1 presents the amino acid sequence of some common CPPs (Farkhani et al., 2014).

Table 1-1. Amino Acid sequence of some common CPPs

Type	*Name*	*Amino acid sequence*
Amphipathic	Transportan	GWTLNSAGYLLGKINLKALAALAKKIL
	Pep-1	KETWWETWWTEWSQPKKKRKV
	MPG	GLAFLGFLGAAGSTMGAWSQPKKKRKV
	pVEC	LLIILRRRIRKQAHAHSK
	MAP	KLALKLALKALKAALKLA
	CADY	GLWRALWRLLRSLWRLLWRA
Cationic	Polyarginine	R8, R9, R10, R12
	Tat 49–57	RKKRRQRRR
	Penetratin	RQIKIWFQNRRMKWKK
	P22N	NAKTRRHERRRKLAIER
	DPV3	RKKRRRESRKKRRRES

Hydrophobic	DPV6	GRPRESGKKRKRKRLKP
	K-FGF	AAVLLPVLLAAP
	C105Y	CSIPPEVKFNKPFVYLI

Mode of action

The characteristics of CPPs include: low cytotoxicity, dose-dependent efficiency, the ability to be taken up by a variety of cell types and no restriction on the size or type of cargo (Heitz et al., 2009). CPPs have been reported in the delivery of multiple types of cargo like: nucleic acids, liposomes, low molecular weight drugs, nanoparticles and polymers. One group even delivered a small protein using a Tat-fusion (Watanabe et al., 2003). CPPs are grouped into two main classes according to the nature of the association between the peptide and the cargo. The first group requires chemical linkage between peptide and cargo, and the second involves the formation of stable, non-covalent complexes. From a structural point of view CPPs can be classified into amphipathic, cationic (containing clusters of polyarginine or polylysine), or amphipathic (Heitz et al., 2009).

For CPPs that are covalently linked to the cargo, the formation of the covalent conjugate between the cargo and the carrier peptide is achieved by chemical cross-linking or by cloning followed by expression of a CPP fusion protein (Moulton, 2012;Zatsepin et al., 2005). Different chemical compositions have been reported for stable or cleavable conjugation mostly involving disulfide or thio-esters linkages (Heitz et al., 2009). Covalent strategies have been mainly reported for the delivery of DNA mimic molecules or steric block oligonucleotides (Abes et al., 2008;Lebleu et al., 2008). Conjugation methods offer reproducibility of the procedure, rationalization, and

control over the stoichiometry of the CPP-cargo; however the conjugation technology risks altering the biological activity of the cargo. The non-covalent strategy is mainly based on short amphipathic peptide carriers, where the amphipathic character may be a result of the primary structure or of the secondary structure. Non-covalent CPPs form stable complexes with their respective cargo (oligonucleotide or protein/peptide) through non-covalent electrostatic and hydrophobic interactions (Gros et al., 2006;Munoz-Morris et al., 2007).

Elucidation of the mechanism of internalization of CPPs proved puzzling for a long time, as it had early been reported as independent of endocytosis, of energy and of specific receptor. These studies, however, were showed to be affected by experimental artifacts (Copolovici et al., 2014). For example, contradictory results are obtained through the use of different peptide concentrations, cell types, incubation time, and various physiochemical parameters of the CPPs, including hydrophobicity and net charge (Jones and Sayers, 2012;Madani et al., 2011). It has been proposed that some CPPs, like Tat, Antennapedia, Poly-Arg, and Pep-1, can pass through the plasma membrane via at least one energy-independent pathway (Vives et al., 2008). It is likely that CPPs without cargo can be taken up by cells via multiple pathways, including direct penetration of the plasma. In 2014, Herce et al. described a complete cellular uptake mechanism for arginine-rich peptides based on the interplay between fatty acids and the plasma membrane pH gradient. They proposed that at high pH fatty acids bind extracellular arginine-rich peptides, mediate their membrane transport, and release them into the lower-pH environment of the cytosol. In vitro experiments showed the major steps of this mechanism. Computational simulations showed that deprotonated fatty acids reduce the free energy of insertion of the arginine-rich peptides into model phospholipid bilayers and that this insertion leads to the

formation of a channel across the lipid bilayer (Herce et al., 2014). Figure 1-3 shows the steps of the proposed mechanisms as: (a) the peptide located in the extracellular medium is attracted by electrostatics; (b) the peptide binds to deprotonated fatty acids; (c) the peptide–fatty acid complex nucleates a water channel; (d) the peptide–fatty acid complex diffuses across the channel while simultaneously protons from the cytosolic side compete for the binding of the guanidinium groups to fatty acids; (e) the high density of protons in the cytosol protonates the fatty acids, and the peptide gets released into the cytosol; (f) the channel closes, and neutral fatty acids freely diffuse across the plasma membrane.

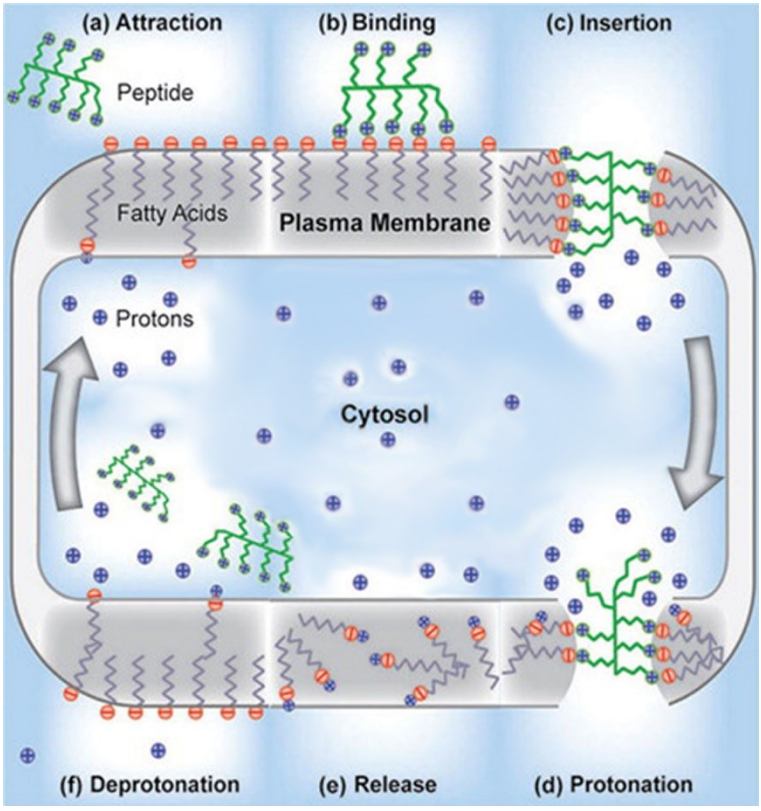

Figure 1-3. Cellular Uptake Mechanism for Arginine-Rich Cell-Penetrating Peptides. Adapted with permission from Fundamental Molecular Mechanism for the Cellular Uptake of Guanidinium-Rich Molecules. Copyright 2014 American Chemical Society

There is still no consensus on the mechanisms of cellular uptake and internalization of CPP--cargo complexes. Many researches claim that most CPP-cargo complexes do not translocate by direct penetration of the plasma membrane, instead they are taken up by various types of endocytosis. Endocytosis occurs through the action of various pathways and can be classified into: caveolae and/or lipid-raft-mediated endocytosis, macropinocytosis, cholesterol-dependent clathrin-mediated endocytosis, or caveolae- and clathrin-independent endocytosis. It is proposed that the mechanism of entry into the cell is influenced by a variety of factors, including the nature of the conjugated cargo (type, size, charge), differences in the physicochemical properties of CPPs (such as molecule length, charge delocalization, and hydrophobicity), the cell line being utilized, and the concentration of the CPP (Copolovici et al., 2014).

By endocytosis, CPPs may or may not be released into the cytosol or can even end up in intracellular vesicular compartments (Patel et al., 2007). The presence of membrane-associated proteoglycans has been reported as an important factor for both uptake and micropinocytosis (Futaki et al., 2007). Macropinocytosis is activated only when a specific stimuli is applied (e.g. growth factors or viruses). Membrane associated proteoglycans serve as one of the primary receptors that induce macropinocytosis. Macropinocytosis may be one of the preferred pathways in some cell types for the uptake of arginine-rich CPPs and larger CPP conjugates. A general scheme for CPP uptake mechanisms is still a matter of investigation and debate; nonetheless, there is consensus that the initial contact between the CPPs and proteoglycans on the cellular surface takes place through electrostatic interactions. After initial interaction the cellular uptake pathways are driven by several parameters: -the primary and secondary structure of the CPP; - The CPP's ability to interact with cell surface and membrane lipid components; - the nature,

type, and active concentration of the cargo; -the cell type and membrane composition (Copolovici et al., 2014).

Recent developments

Advances in drug delivery have been reported using CPPs to address the challenges in targeted delivery of pharmaceutical compounds having low efficacy *in vivo* for the treatment of cancer (Araki et al., 2010;Ueda et al., 2012;Wender et al., 2012). One particularly novel approach is the system made using CPPs as part of a combinatorial approach. Ringhieri et al. reported the synthesis of a dual-ligand liposomal doxorubicin delivery system, which couples targeting to enhanced cellular uptake by anchoring cell penetrating peptide R8 and targeting peptide CCK8 to the surface of liposomes. A characterization by spectroscopic methods confirmed the obtainment of liposomes in which both peptides are durably linked to the external liposome surface while doxorubicin is efficiently loaded in the inner water liposome compartment, effectiveness of the system *in vivo* is yet to be demonstrated (Ringhieri et al., 2015).

A major limitation in using CPPs as a delivery system is limited release of the cargo to the cytoplasm once the peptide-cargo complex has enter the cell via the endocytosis mediated mechanism. In the search of more efficient cargo delivery peptides, a method for high-throughput screening of spontaneous membrane-translocating peptides has been proposed (Marks et al., 2011). He et al. reported the effectiveness of three peptides (TP1, TP2 and TP3) identified by the high-throughput screening method, to deliver the zwitterionic, membrane-impermeant dye tetramethylrhodamine to cells under conditions not permissive for endocytosis

(He et al., 2013). Peptide TP2 was reported to translocate lipid bilayers at a concentration independent rate and without significant bilayer perturbations (Cruz et al., 2013).

Jianquan et al. reported the development of a CPP based approach for the delivery of quantum dots into mammalian cells with high reproducibility and efficiency, and with minimal cytotoxicity (Jianquan et al., 2014). Advantages of quantum dots over traditional dyes consist of high quantum yield, narrow emission peak, excellent resistance to photobleaching, and broad size-dependent photoluminescence (Chen and Gerion, 2004). These unique fluorescence properties make quantum dots desirable biological imaging probes, however, reliable and efficient cellular delivery of quantum dots has proven technically challenging. To address this problem the authors conjugated Tat and HA2 peptides to quantum dots (CPP-QDs) and analyzed their internalization and endosomal trapping and release in mammalian PC12 cells using high-resolution live cell imaging. It was found that the CPP-QDs were mainly internalized through the endocytosis pathway. However, a small number of CPP-QDs were internalized through direct membrane permeation. It was also reported that CPP-QDs could be released to the cytoplasm when conjugated to membrane disrupting HA2 peptide (Jianquan et al., 2014).

Recently, several studies have explored the possibility of using CPPs as a nonviral gene delivery system (Bolhassani, 2011). Liu et al. reported the use of arginine-rich CPPs for gene delivery into human cells in a noncovalent fashion (Liu et al., 2012), while Chen et al. reported a similar approach for gene delivery into insect cells (Chen et al., 2012). They indicated that SR9, PR9 and especially HR9 CPPs are able to transfer plasmid DNA into the target cells with the following transfection efficiencies: HR9 (18.76 ± 1.09%) > PR9 (2.73 ± 0.25%) > SR9 (2.03 ±

0.21%). Liu et al also reported that although treatment with $CaCl_2$ did not facilitate the CPP-mediated transfection efficiency, it improved the gene expression intensity.

Another field where CPPs present promising prospects is the development of antiviral applications; the most widely used antiviral cargos conjugated to CPPs are phosphorodiamidate morpholino oligomers (PMOs) (Delcroix and Riley, 2010). Peptide-conjugated PMOs are water-soluble, nuclease-resistant, and act as steric-blocking antisense agents due to the formation of stable duplexes with complementary RNA. CPP-PMOs conjugates act on non-retroviral RNA virus infections in a dose dependent and highly specific on the nature of the CPP and PMOs manner. These conjugates act by reducing viral replication and significantly increase survival in mice experimentally infected with polio virus, coxsackie virus B2 and B3, dengue virus, West Nile virus, Japanese and St. Louis encephalitis virus, Venezuelan equine encephalitis virus, equine encephalitis virus, respiratory syncytial virus, Ebola virus, SARS coronavirus, mouse hepatitis virus, porcine reproductive and respiratory syndrome virus, human rhinovirus 14, foot and mouth disease virus, measles virus, and the influenza A virus (Delcroix and Riley, 2010). A new cationic lipid peptide, Deca-$(R)_8$, was demonstrated to inhibit duck hepatitis B virus replication, the peptide led to a decrease in virus secretion in HepG2.2.15 cells without targeting the viral polymerase (Abdul et al., 2012).

Channel/pore Forming Peptides

Channel/pore Forming Peptides (CFPs) are designed peptides (*de novo* or derived from the sequence of a channel protein) with less than 40 amino acid residues. CFPs have the ability to

insert into lipid bilayers adopting an amphipathic helical conformation. CFPs associate and assemble to form ion conducting channels. CFPs synthesized with D-enantiomers conserve the channel forming capability of their L-enantiomer versions, suggesting CFP's interact with the membrane without the need for receptors (Wade et al., 1990). CFPs differ from AMPs as their intended purpose is not the destruction of the target cell, but the creation a transient membrane ion channels. This differentiation is somehow arbitrary, as cytotoxicity could be achieved with most CFPs at high enough concentration.

A special class of CFP uses a peptide scaffold to create co-facial organization of crown ethers (Fyles, 2007). The ion conductance of these synthetic ion channels is achieved through the interior of the crown ethers, while the peptide elements serve a structural function. Peptides that are part of the immune complement system are not included in this category because their pore forming activity requires them to be associated with a protein complex.

Historical overview

The first peptides belonging to this category to be studied were *de novo* simple sequences, based on the amphipathic side chain distribution of transmembrane α helices. These peptides were created in order to evaluate the basic principles of CFPs. Ion channel forming peptide P from 1985 with 12 leucines out of its18 residue (Spach et al., 1985) and from 1988 peptides $[LSSLLSL]_3$, and $[LSLLLSL]_3$ (Lear et al., 1988) are two of the earliest efforts to understand the role of the individual sidechains in the interaction of peptides with the lipid bilayer.

Since the late 1980s a number of peptides with sequences derived from the pore lining segments of naturally occurring ion channels have been shown to have the ability to spontaneously insert into lipid bilayers and to self-assemble into ion channels that retain some of the characteristics of the parent ion channel. A 23 amino acid residues peptide from the M2 transmembrane segment of the acetylcholine receptor (AcChoR) δ subunit was reported to form cationic channels in phosphatidylcholine bilayers (Oiki et al., 1988). A synthetic peptide modelled after the transmembrane domain M2 of the Glycine receptor (M2GlyR) channel was reported to form ion channels in lipid bilayers (Langosch et al., 1991). In 1997, Tomich's lab first suggested delivery of Cl^- channel-forming peptides derived from the M2GlyR, to the apical membranes of airway epithelial cells of patients suffering from cystic fibrosis (CF) (Wallace et al., 1997). The formulation of efficient peptides with pharmaceutical applications has been an ongoing project at this lab and advances on this task are discussed in the following sections (Tomich et al., 2012).

Mode of action

Channel forming peptides in solution spontaneously insert into lipid bilayers on a matter dependent of aqueous solubility, and lipid composition of the bilayer (Tomich et al., 1998). The peptides undergo a conformational change, from unstructured in the aqueous environment to an amphipathic helical structure when inserted into lipid bilayers (Bukovnik et al., 2012;Cook et al., 2004;Herrera et al., 2010). In order to form functional ion channels monomers need to assemble into an oligomeric functional state. The question of successive order on which the events of folding, insertion and assembly formation occur, or whether these events occur independently or coupled is still unresolved. Figure 1-4 shows the possible routes to get to the functional ion

channel. The path to the right has the peptide insertion and folding as a single step followed by assembly. The path to the left has peptide folding occurring at the bilayer surface followed by assembly before insertion (Tomich et al., 2012). In addition folded states could be sampled by the peptide prior to membrane interaction; the folded states would be stabilized by binding to the bilayer surface.

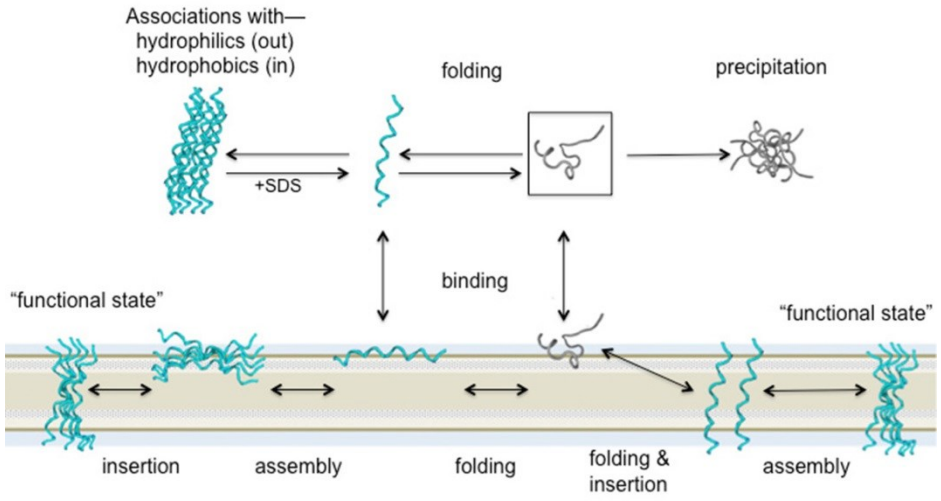

Figure 1-4. Possible paths for the assembly of CFP monomers into ion conducting channels. Figure from Tomich et at., 2012 (Intech Open access)

The formation of assembled channels is concentration dependent (Wallace et al., 2000). The number of monomers that comprise an individual channel is dependent on the peptide sequence, and in the case of sequences derived from naturally occurring ion channels, is related to the number of helices lining the interior of the parent channel (Krittanai and Panyim, 2004;Reddy et al., 1993;Wallace et al., 1997). Ion selectivity, voltage dependence and ion conductance are also dependent of the peptide sequence, and although these properties are related to those of the parent channel, they are not always conserved (Bukovnik et al., 2012;Cook et al., 2004;Wallace et al., 2000).

Ions and other molecules that fit through the channel diffuse driven by its particular concentration gradient. The ion conductance and ion selectivity of a single assembled channel depends primarily of the amino acid residue side chains oriented to the lumen of the channel (Bukovnik et al., 2012). The ion conductance measured on cells also depends on the rates of folding, insertion, and assembly. These rates are dependent to some degree on every amino acid residue in the peptide (Broughman et al., 2002;Cook et al., 2004;Herrera et al., 2010;Shank et al., 2006). The ion conductance induced by CPPs is transitory, possibly due to membrane recycling and proteolytic activity.

Recent developments

By covalently attaching functional groups to CFPs, new analytical applications have been developed. Mayer et al. reported a method to quantify protein-ligand interactions by measuring the flux of ions through pores of a synthetically-modified, CFP in planar lipid bilayers. The method is based on the reduction of conductivity through the channels of a derivative of alamethicin, which carries a covalently attached benzenesulfonamide group on its C-terminus. In the assay reported, reduction of the ion current is triggered by binding of carbonic anhydrase II to the sulfonamide moiety on the CFP (Mayer et al., 2008). Another application of covalently attaching functional groups to CFPs was reported by the Voyer's laboratory in 2012. By attaching a fluorescent marker (fluorescein isothiocyanate) to LS2 and LS3 CFPs, the authors were able to study by attenuated total reflectance the incorporation equilibrium of the peptide between two forms: adsorbed at the surface or incorporated within the bilayer. These results

showed that the incorporation equilibrium is highly dependent on the lipid composition, with a lower incorporation level when lipids have longer alkyl chains. Confocal microscopy studies also showed that fluorescent CFP analogs internalized into HeLa cells and localized into both the membranes of inner organelles and the cell membrane (Arseneault et al., 2012).

With the purpose of developing artificial sensing systems Futaki et al. attached leucine-zipper extra-membrane peptide segments to CFP alamethicin. The idea being that the extra-membrane segment would acts in a similar way to the large extra-membrane domains present in natural-ion channel proteins. Ligand binding could alter the structure of the extra-membrane domains and influence the association states or association numbers of alamethicin in the membranes. Using conformationally switchable leucine-zipper extra-membrane segments that respond to Fe^{3+}, Futaki et al. fabricated an artificial Fe^{3+}-sensitive ion channel, and showed that a decrease in the helical content of the extra-membrane segment led to an increase in the channel current (Futaki et al., 2013).

Recently novel medical uses of CFPs have also been reported and efforts have been made to study the effect of CFP NC-1059 on riboflavin diffusion across an intact corneal epithelium. Efficient riboflavin diffusion is needed for the corneal cross-linking treatment of the vision disorder Keratoconus. The study demonstrated that peptide NC-1059 enhances the diffusion of riboflavin into the corneal stroma, without causing any measurable cytotoxicity to corneal epithelial cells (Zhang et al., 2012).

Ion channels formed by CFPs are composed of simple elements and contain fewer atoms compared with natural ion channels; this makes them a suitable subject for computational studies. Li-Hu et al. performed a computational fine-grained docking with molecular dynamics simulations, to explore the geometry and orientation of homo-pentameric bundles of CFP Vpu_{1-32}. The Vpu_{1-32} sequence comes from channel-forming membrane protein Vpu of the HIV virus. Computational methods have also been used by Dr. Chen's lab to evaluate the charge selectivity of M2GlyR derived ion channels (Chen and Tomich, 2014). In 2013 Bukovnik et al. reported increased conductivity of NK_4-M2GlyR p22 T19R, S22W channels by the substitution of pore lining threonine residues 13, 17 and 20 by non-encoding amino acid 2,3-diaminopropionic acid (Dap) (Bukovnik et al., 2013). The increase in conductivity was accompanied by decreased ion selectivity, to analyze the conductance and charge selectivity of M2GlyR-derived synthetic channels Chen et al. performed free energy simulations on the peptide assembly. The simulations showed the pentameric p22 pores to be non-selective, with moderate barriers for permeation of both K^+ and Cl^- dominated by the desolvation cost (Chen and Tomich, 2014).

CFPs have also found applications into unexpected fields, in 2012 Gudlur et al. first reported the development of peptide nanovesicles formed by the self-assembly of branched amphiphilic peptides (BAPCs) (Gudlur et al., 2012). The hydrophobic core sequences of the nanovesicle forming peptides are derived from an internal fragment of CaIVS3, the human dihydropyridine sensitive L-type calcium channel segment. BAPCs have potential as a novel cellular delivery system, as they are taken up by cells. BAPCs undergo thermosensitive conformational transitions

as a function of both time and temperature; the properties of BAPCs vary based on the temperature of assembly (Sukthankar et al., 2015).

Amyloid Peptides

Amyloid peptides (AP) are a class of proteins characterized by their ability to form stable β-sheet-rich structures known as amyloid fibrils (Sunde and Blake, 1998). APs are involved in a number of degenerative diseases, and despite of origin and amino acid sequence differences they behave structurally on a similar way. Non-fibrillar oligomers of APs are known to alter membrane structure, and are suspected to be the main disease causative agent of amyloidoses (Bartels et al., 2011;Hebda et al., 2009;Nerelius et al., 2009).

Historical overview

The term 'amyloid' was coined initially by Schleiden and then by Virchow in the mid-19th century to describe the iodine stained deposits seen in liver at autopsy (Virchow, 1854). Consequently the deposits were thought to be carbohydrate in nature (Latin word for starch: *amylum*) until their high nitrogen content was later established, and their proteinaceous nature determined (Friedrich and Kekulé, 1859). Amyloid deposits bind to Congo Red dye producing an apple green birefringence when examined between cross polarizers in a light microscope (Divry and Florkin, 1927). This characteristic suggested that amyloid had a fibrillary structure, which was confirmed by electron micrographs (Cohen and Calkins, 1959). The β-sheet nature of the fibrils was determined by X-ray diffraction studies (Eanes and Glenner, 1968).

In 1906, Alois Alzheimer gave a lecture, in which he described for the first time a form of dementia that subsequently, at the suggestion of Emil Kraepelin, became known as Alzheimer's disease. In his lecture Alzheimer described a patient called Auguste D, a 51-year-old woman who had shown progressive cognitive impairment, focal symptoms, hallucinations, delusions, and psychosocial incompetence. Autopsy of the brain tissue revealed the presence of plaques, neurofibrillary tangles, and arteriosclerotic changes. Alzheimer mentioned the miliary foci (later called senile plaques), which represented the sites of deposition of an amyloid protein (Maurer et al., 1997). In a similar way many other diseases were described to be associated with amyloid deposits, collectively these disorders became known as amyloidoses. Amino acid composition and sequence analysis of the proteins comprising a range of *ex vivo* amyloid fibrils revealed that each amyloid disorder was associated with a particular protein or peptide (Glenner et al., 1971). Amyloidoses have traditionally been defined as diseases in which normally soluble proteins accumulate in the extracellular space of various tissues as insoluble deposits of fibrils (Selkoe, 2003). Another general feature of these protein-folding disorders is the prolonged period before clinical manifestations appear. To date more than 20 diseases have been associated with amyloid formation. Many amyloid forming peptides are produced by the proteolytic processing of a precursor protein. Table 1-2 presents a list of the most common amyloidoses with their corresponding precursor protein and amyloid forming peptide (Rambaran and Serpell, 2008).

Table 1-2. Amyloidoses with their precursor protein and amyloid peptide

Disease	*Precursor protein*	*Amyloid Peptide*
Alzheimer's disease	Amyloid precursor protein	Aβ peptides
Atrial amyloidosis	Atrial natriuretic factor (ANF)	Amyloid ANF
Spongiform encephalopathies	Prion protein (PrPc)	PrPsc
Primary systemic amyloidosis	Immunoglobulin light and heavy chains	AL and AH
Senile systemic amyloidosis	Wild-type transthyretin	ATTR
Haemodialysis-related amyloidosis	β2-microglobulin	Aβ2M
Hereditary nonneuropathic systemic amyloidosis	Lysozyme	ALys
Type II diabetes	Pro-IAPP	IAPP or "amylin"
Injection-localized amyloidosis	Insulin	AIns
Secondary systemic amyloidosis	(Apo) serum amyloid A	Serum amyloid A
Hereditary cerebral amyloid angiopathy	Cystatin C	ACys
Finnish hereditary systemic amyloidosis	Gelsolin	AGel
Familial amyloid polyneuropathy	Transthyretin variants	ATTR
Parkinson's disease		α-synuclein
Ageing pituitary, prolactinomas	Prolactin	APro
Familial amyloidosis	Fibrinogen αA-chain	AFib
British familial dementia	Amyloid Bri Precursor Protein	ABri

Adapted from (Rambaran and Serpell, 2008)

Prusiner in 1982 proposed the 'prion' hypothesis that described an infectious protein particle capable of causing a fatal neurodegenerative disease in sheep (scrapie) (Prusiner, 1982) .The causative peptide of scrapie was amyloidogenic but unlike other amyloid forming proteins it was infective and was termed: prion. In 1984 the Aβ peptide that composes the bulk of amyloid

plaques in Alzheimer's disease was identified and biochemically characterized (Glenner and Wong, 1984). Not all amyloid forming peptides are disease related. Amyloids play a role in functional biological process including: biofilm formation (Barnhart and Chapman, 2006), hormone storage (Maji et al., 2009), and gas vesicles formation (Bayro et al., 2012).

Historically the main focus of amyloid research has been the fibrillary state, as it has been considered a hallmark of disease progression, and a probable causative agent. Recently, however, it has been shown that nonfibrillar preamyloid toxins induce membrane disruptions in cells and in synthetic liposomes. These nonfibrillar forms of APs are known now to be the toxic species, while the fibers are considered relatively benign (Hebda and Miranker, 2009). Here the focus is the interactions between APs and cellular plasma membranes, in particular peptides that are disease related, like Aβ, α-Syn and IAPP.

Mode of action

Development of a single antibody selective for the amyloid oligomers of a variety of APs has suggested that there is a structural commonality among oligomers of different APs (Kayed et al., 2003). However, amyloid precursor proteins have been observed to form a number of unique structures on membranes. A large number of oligomer structures has been observed for Aβ peptides, ranging from dimers to large oligomers (Schauerte et al., 2010). Structures that are unique to preamyloid states on membranes have been identified in a number of studies, interestingly the prefibrilar membrane-bound states, that precede rapid formation of β-sheet filaments, were found to be α-helical for many AP including Aβ (Kayed et al., 2003), IAPP

(Apostolidou et al., 2008) and α-Syn (Jao et al., 2008). Membrane binding has been determined to be driven predominantly by electrostatic forces for these slightly cationic helixes (Knight and Miranker, 2004;Shvadchak et al., 2011). It has been proposed that in the case of Aβ peptides the specific interaction with gangliosides (Yanagisawa et al., 1995), a major lipid component in neural cell membranes, cholesterol (Simons et al., 1998;Yip et al., 2001) or with phosphatidylinositol (McLaurin et al., 1998) is involved in cytotoxicity.

The helical structures of APs have been strongly correlated with cytotoxicity, small molecules designed to interact with the helical portions of Aβ reduce toxicity (Nerelius et al., 2009). A tetramer of helically folded α-Syn is capable of binding to membranes or existing in solution (Bartels et al., 2011). A mutant of IAPP that affect helix formation presents no toxicity to insulin secreting cell lines (Hebda et al., 2009).

The actual mechanism of membrane disruption and cytotoxicity by APs has yet to be elucidated. One possibility is that the AP oligomers form a well-defined pore; another is that bilayer permeation could be caused by interactions that induce distortions to the membrane like removal of one leaf of the bilayer by the detergent effect of the amphipathic helices. A third possibility is the induction of curvature changes to the bilayer upon peptide binding (Last and Miranker, 2013). Preference for membrane regions of negative or increased positive curvature have been reported for Aβ (Matsuzaki and Horikiri, 1999) , IAPP (Smith et al., 2009) and α-Syn (Middleton and Rhoades, 2010).

Recent developments

Since APs are studied mainly because of their role in diseases, recent developments on the area of APs are mostly related to the development of treatment options for the corresponding diseases. One treatment option being explored is the modulation of the oligomeric state of APs, in order to decrease toxicity. Smaoui et al. worked on a computational binding affinity method that optimizes mutations of the IAPP sequence in order to produce an analog with increased affinity for the natural IAPP. Their rational is that the analog will bind IAPP oligomers and promote extension of their length, favoring the formation of fibrils (Smaoui et al., 2015). On the opposite end of oligomeric modulation efforts, Xiong et at. have developed a peptide functionalized nanoparticle that shows inhibitory capability against Aβ42 aggregation, and fibril formation (Xiong et al., 2015). Although the aforementioned reports concern different APs (IAPP and Aβ), clearly their approaches are mutually contradictory. This highlights the need for better understanding of the role that the different sizes of AP oligomers play in cytotoxic, and of the details of the peptide-membrane interactions involved.

Conflicting results reported on the folding state of the monomeric and oligomeric APs have made it harder to have a complete and definitive understanding of the conformational transitions APs undergo, and their role on cytotoxicity (Bartels et al., 2011;Fauvet et al., 2012). Bartels et al. have recently addressed this issue, bringing attention to the importance of post-translational modifications to APs in their natural environment. The authors showed that N-terminal acetylation, the predominant post-translational modification of mammalian α-Syn, increases the helical folding propensity and resistance to aggregation of α-Syn (Bartels et al., 2014). This

result suggests that the absence of post-translational modification of α-Syn peptides used in some *in vitro* studies is a probable cause of conflicting results.

A different approach to treat Alzheimer's disease with a potential of extension to other amyloidoses, has been recently reported with promising prospects. A large collaborative group headed by Dr. Sudhir Paul, from the Department of Pathology and Laboratory Medicine, at the University of Texas Medical School reported on the specificity and Aβ clearing effect of a catabody (catalytic antibody) construct engineered from innate immunity principles. Intravenous catabody treatment reduced brain Aβ deposits in an Alzheimer's disease model mouse without inducing microgliosis or microhemorrhages (Planque et al., 2015).

Concluding remarks

This review of membrane active peptides highlights the diversity of origins as well as activities found for these macromolecules. Membrane active peptides appear to be as ubiquitous in nature as membranes themselves. Many peptides share the activity of more than one membrane active category, e.g. Human AMP LL-37 can transfer DNA into cells (Sandgren et al., 2004) , Aβ amyloid also shows antimicrobial activity against a wide spectrum of bacteria and fungi (Soscia et al., 2010), Protegrin-1 a porcine AMP has been found to form amyloid fibrils upon deposition on hydrophilic surfaces (Jang et al., 2011), IAPP the AP related with Type II diabetes has been found to be able to cross plasma membranes to access mitochondrial membranes (Magzoub and Miranker, 2012).

The classification presented here, shows how biophysical knowledge about each group has developed on an independent manner, but as better understanding of the mechanisms of interaction for each group emerges similarities and commonalties become more evident. Helixes as the predominant structural feature for membrane interaction, amphipathic distribution of residues, and high content of one or two amino acids residues are common in all peptide classes, and are likely to have common mechanistic significance. This has motivated a number of groups to propose a general model for peptide-membrane interaction, based on a small set of governing principals. The proposed models focus on the membrane as an active participant in the formation of pores (Fuertes et al., 2011;Lee et al., 2004;Wimley, 2010).

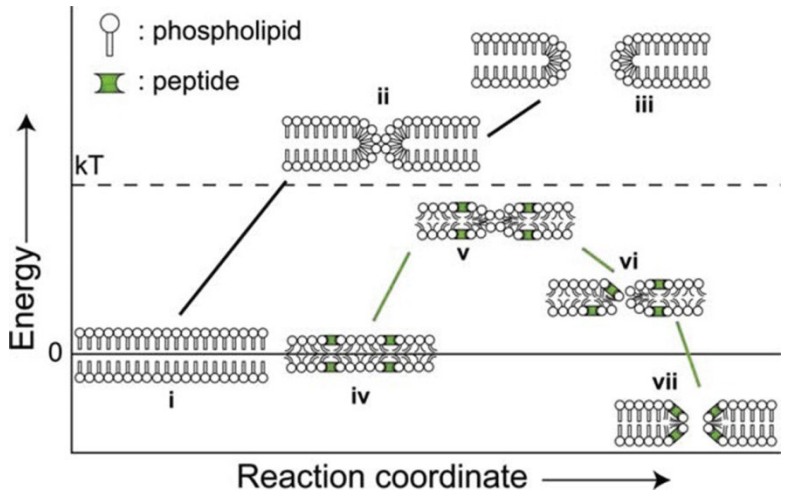

Figure 1-5. The Effect of peptide binding on the lipid bilayer integrity. Figure from Last and Miranker, 2013

Figure 1-5 illustrates the energetics of the proposed membrane centric models: (i) an intact phospholipid bilayer is the reference state for energy change. (ii) Spontaneous fluctuations result in the sampling of energetically unfavorable membrane defects. (iii) Widening of the defect to permit leakage results in a further energetic penalty. (iv) Peptide binding to the surface induces

membrane tension. (v) Peptide binding increases the frequency of defect formation. (vi) Surface tension is released by pore formation. (vii) Stabilization by peptide binding results in equilibrium pore formation (Last and Miranker, 2013).

This review establishes a framework for the experimental undertakings presented on a family of CFPs in the following chapters of this dissertation. It intends to aid in the interpretation, and underline the relevance of the structural and biophysical finding, within the context of not only CPPs but all classes of membrane active peptides.

References

Abdul, F., Ndeboko, B., Buronfosse, T., Zoulim, F., Kann, M., Nielsen, P. E. and Cova, L. (2012). Potent inhibition of late stages of hepadnavirus replication by a modified cell penetrating peptide. *PloS one* **7**, e48721.

Abes, R., Arzumanov, A., Moulton, H., Abes, S., Ivanova, G., Gait, M. J., Iversen, P. and Lebleu, B. (2008). Arginine-rich cell penetrating peptides: design, structure-activity, and applications to alter pre-mRNA splicing by steric-block oligonucleotides. *Journal of peptide science : an official publication of the European Peptide Society* **14**, 455-460.

Agerberth, B., Lee, J. Y., Bergman, T., Carlquist, M., Boman, H. G., Mutt, V. and Jornvall, H. (1991). Amino acid sequence of PR-39. Isolation from pig intestine of a new member of the family of proline-arginine-rich antibacterial peptides. *Eur J Biochem* **202**, 849-854.

Apostolidou, M., Jayasinghe, S. A. and Langen, R. (2008). Structure of alpha-helical membrane-bound human islet amyloid polypeptide and its implications for membrane-mediated misfolding. *Journal of Biological Chemistry* **283**, 17205-17210.

Araki, D., Takayama, K., Inoue, M., Watanabe, T., Kumon, H., Futaki, S., Matsui, H. and Tomizawa, K. (2010). Cell-penetrating D-isomer peptides of p53 C-terminus: long-term inhibitory effect on the growth of bladder cancer. *Urology* **75**, 813-819.

Arseneault, M., Dumont, M., Otis, F. and Voyer, N. (2012). Characterization of channel-forming peptide nanostructures. *Biophysical Chemistry* **162**, 6-13.

Avrahami, D. and Shai, Y. (2002). Conjugation of a magainin analogue with lipophilic acids controls hydrophobicity, solution assembly, and cell selectivity. *Biochemistry* **41**, 2254-2263.

Bagnicka, E., Jozwik, A., Strzalkowska, N., Krzyzewski, J. and Zwierzchowski, L. (2011). Antimicrobial peptides - outline of the history of studies and mode of action. *Medycyna Weterynaryjna* **67**, 444-448.

Barnhart, M. M. and Chapman, M. R. (2006). Curli biogenesis and function. *Annual Review of Microbiology* **60**, 131-147.

Bartels, T., Choi, J. G. and Selkoe, D. J. (2011). alpha-Synuclein occurs physiologically as a helically folded tetramer that resists aggregation. *Nature* **477**, 107-U123.

Bartels, T., Kim, N. C., Luth, E. S. and Selkoe, D. J. (2014). N-Alpha-Acetylation of alpha-Synuclein Increases Its Helical Folding Propensity, GM1 Binding Specificity and Resistance to Aggregation. *Plos One* **9**, e103727

Bayro, M. J., Daviso, E., Belenky, M., Griffin, R. G. and Herzfeld, J. (2012). An Amyloid Organelle, Solid-state NMR Evidence for Cross-beta Assembly of Gas Vesicles. *Journal of Biological Chemistry* **287**, 3479-3484.

Bechinger, B. (2008). A dynamic view of peptides and proteins in membranes. *Cellular and molecular life sciences : CMLS* **65**, 3028-3039.

Bechinger, B. (2009). Rationalizing the membrane interactions of cationic amphipathic antimicrobial peptides by their molecular shape. *Current Opinion in Colloid & Interface Science* **14**, 349-355.

Bechinger, B. and Lohner, K. (2006). Detergent-like actions of linear amphipathic cationic antimicrobial peptides. *Biochimica Et Biophysica Acta-Biomembranes* **1758**, 1529-1539.

Blazyk, J., Wiegand, R., Klein, J., Hammer, J., Epand, R. M., Epand, R. F., Maloy, W. L. and Kari, U. P. (2001). A novel linear amphipathic beta-sheet cationic antimicrobial peptide with enhanced selectivity for bacterial lipids. *The Journal of biological chemistry* **276**, 27899-27906.

Bolhassani, A. (2011). Potential efficacy of cell-penetrating peptides for nucleic acid and drug delivery in cancer. *Biochimica et biophysica acta* **1816**, 232-246.

Broughman, J. R., Shank, L. P., Prakash, O., Schultz, B. D., Iwamoto, T., Tomich, J. M. and Mitchell, K. (2002). Structural implications of placing cationic residues at either the NH2- or COOH-terminus in a pore-forming synthetic peptide. *The Journal of membrane biology* **190**, 93-103.

Bukovnik, U., Gao, J., Cook, G. A., Shank, L. P., Seabra, M. B., Schultz, B. D., Iwamoto, T., Chen, J. and Tomich, J. M. (2012). Structural and biophysical properties of a synthetic channel-forming peptide: designing a clinically relevant anion selective pore. *Biochimica et biophysica acta* **1818**, 1039-1048.

Bukovnik, U., Sala-Rabanal, M., Francis, S., Frazier, S. J., Schultz, B. D., Nichols, C. G. and Tomich, J. M. (2013). Effect of Diaminopropionic Acid (Dap) on the Biophysical Properties of a Modified Synthetic Channel-Forming Peptide. *Molecular pharmaceutics* **10**, 3959-3966.

Carmona-Ribeiro, A. M. and Carrasco, L. D. D. (2014). Novel Formulations for Antimicrobial Peptides. *International Journal of Molecular Sciences* **15**, 18040-18083.

Chen, F. Q. and Gerion, D. (2004). Fluorescent CdSe/ZnS nanocrystal-peptide conjugates for long-term, nontoxic imaging and nuclear targeting in living cells. *Nano Letters* **4**, 1827-1832.

Chen, J. H. and Tomich, J. M. (2014). Free energy analysis of conductivity and charge selectivity of M2GlyR-derived synthetic channels. *Biochimica Et Biophysica Acta-Biomembranes* **1838**, 2319-2325.

Chen, Y. J., Liu, B. R., Dai, Y. H., Lee, C. Y., Chan, M. H., Chen, H. H., Chiang, H. J. and Lee, H. J. (2012). A gene delivery system for insect cells mediated by arginine-rich cell-penetrating peptides. *Gene* **493**, 201-210.

Cohen, A. S. and Calkins, E. (1959). Electron Microscopic Observations on a Fibrous Component in Amyloid of Diverse Origins. *Nature* **183**, 1202-1203.

Cook, G. A., Prakash, O., Zhang, K., Shank, L. P., Takeguchi, W. A., Robbins, A., Gong, Y. X., Iwamoto, T., Schultz, B. D. and Tomich, J. M. (2004). Activity and structural comparisons of solution associating and monomeric channel-forming peptides derived from the glycine receptor m2 segment. *Biophys J* **86**, 1424-1435.

Copolovici, D. M., Langel, K., Eriste, E. and Langel, U. (2014). Cell-penetrating peptides: design, synthesis, and applications. *ACS nano* **8**, 1972-1994.

Cruz, J., Mihailescu, M., Wiedman, G., Herman, K., Searson, P. C., Wimley, W. C. and Hristova, K. (2013). A membrane-translocating peptide penetrates into bilayers without significant bilayer perturbations. *Biophysical journal* **104**, 2419-2428.

Delcroix, M. and Riley, L. W. (2010). Cell-Penetrating Peptides for Antiviral Drug Development. *Pharmaceuticals* **3**, 448-470.

Derossi, D., Joliot, A. H., Chassaing, G. and Prochiantz, A. (1994). The third helix of the Antennapedia homeodomain translocates through biological membranes. *The Journal of biological chemistry* **269**, 10444-10450.

Divry, P. and Florkin, M. (1927). Sur les proprietes optiques de l'amyloid. *Societe de Biologie* **97**, 180-181.

Eanes, E. D. and Glenner, G. G. (1968). X-Ray Diffraction Studies on Amyloid Filaments. *Journal of Histochemistry & Cytochemistry* **16**, 673-677.

Epand, R. F., Maloy, L., Ramamoorthy, A. and Epand, R. M. (2010). Amphipathic helical cationic antimicrobial peptides promote rapid formation of crystalline states in the presence of phosphatidylglycerol: lipid clustering in anionic membranes. *Biophysical Journal* **98**, 2564-2573.

Epand, R. M. and Epand, R. F. (2009). Lipid domains in bacterial membranes and the action of antimicrobial agents. *Biochimica et biophysica acta* **1788**, 289-294.

Eriksen, T. H., Skovsen, E. and Fojan, P. (2013). Release of antimicrobial peptides from electrospun nanofibres as a drug delivery system. *Journal of biomedical nanotechnology* **9**, 492-498.

Farkhani, S. M., Valizadeh, A., Karami, H., Mohammadi, S., Sohrabi, N. and Badrzadeh, F. (2014). Cell penetrating peptides: efficient vectors for delivery of nanoparticles, nanocarriers, therapeutic and diagnostic molecules. *Peptides* **57**, 78-94.

Fauvet, B., Mbefo, M. K., Fares, M. B., Desobry, C., Michael, S., Ardah, M. T., Tsika, E., Coune, P., Prudent, M., Lion, N., Eliezer, D., Moore, D. J., Schneider, B., Aebischer, P., El-Agnaf, O. M., Masliah, E. and Lashuel, H. A. (2012). alpha-Synuclein in central nervous system and from erythrocytes, mammalian cells, and Escherichia coli exists predominantly as disordered monomer. *The Journal of biological chemistry* **287**, 15345-15364.

Feller, S. E., Huster, D. and Gawrisch, K. (1999). Interpretation of NOESY cross-relaxation rates from molecular dynamics simulation of a lipid bilayer. *Journal of the American Chemical Society* **121**, 8963-8964.

Fleming, A. (1922). On a Remarkable Bacteriolytic Element Found in Tissues and Secretions. *Proceedings of the Royal Society of London. Series B* **93**, 306-317.

Fox, J. L. (2012). Rare-disease drugs boosted by new Prescription Drug User Fee Act. *Nature biotechnology* **30**, 733-734.

Frankel, A. D. and Pabo, C. O. (1988). Cellular uptake of the tat protein from human immunodeficiency virus. *Cell* **55**, 1189-1193.

Friedrich, N. and Kekulé, A. (1859). *Arch Pathol Anat Physiol Klin Med* **16**, 50-55.

Fuertes, G., Gimenez, D., Esteban-Martin, S., Sanchez-Munoz, O. L. and Salgado, J. (2011). A lipocentric view of peptide-induced pores. *European Biophysics Journal with Biophysics Letters* **40**, 399-415.

Futaki, S., Nakase, I., Tadokoro, A., Takeuchi, T. and Jones, A. T. (2007). Arginine-rich peptides and their internalization mechanisms. *Biochemical Society transactions* **35**, 784-787.

Futaki, S., Noshiro, D., Kiwada, T. and Asami, K. (2013). Extramembrane Control of Ion Channel Peptide Assemblies, Using Alamethicin as an Example. *Accounts of Chemical Research* **46**, 2924-2933.

Futaki, S., Suzuki, T., Ohashi, W., Yagami, T., Tanaka, S., Ueda, K. and Sugiura, Y. (2001). Arginine-rich peptides. An abundant source of membrane-permeable peptides having potential as carriers for intracellular protein delivery. *The Journal of biological chemistry* **276**, 5836-5840.

Fyles, T. M. (2007). Synthetic ion channels in bilayer membranes. *Chemical Society reviews* **36**, 335-347.

Gazit, E., Miller, I. R., Biggin, P. C., Sansom, M. S. and Shai, Y. (1996). Structure and orientation of the mammalian antibacterial peptide cecropin P1 within phospholipid membranes. *Journal of Molecular Biology* **258**, 860-870.

Glenner, G. G., Ein, D., Eanes, E. D., Bladen, H. A., Terry, W. and Page, D. L. (1971). Creation of Amyloid Fibrils from Bence Jones Proteins in-Vitro. *Science* **174**, 712-714.

Glenner, G. G. and Wong, C. W. (1984). Alzheimer's disease: initial report of the purification and characterization of a novel cerebrovascular amyloid protein. *Biochemical and Biophysical Research Communications* **120**, 885-890.

Gros, E., Deshayes, S., Morris, M. C., Aldrian-Herrada, G., Depollier, J., Heitz, F. and Divita, G. (2006). A non-covalent peptide-based strategy for protein and peptide nucleic acid transduction. *Biochimica et biophysica acta* **1758**, 384-393.

Groves, M. L., Peterson, R. F. and Kiddy, C. A. (1965). Polymorphism in Red Protein Isolated from Milk of Individual Cows. *Nature* **207**, 1007-1008.

Gudlur, S., Sukthankar, P., Gao, J., Avila, L. A., Hiromasa, Y., Chen, J., Iwamoto, T. and Tomich, J. M. (2012). Peptide nanovesicles formed by the self-assembly of branched amphiphilic peptides. *PloS one* **7**, e45374.

Habets, M. G. and Brockhurst, M. A. (2012). Therapeutic antimicrobial peptides may compromise natural immunity. *Biology letters* **8**, 416-8.

Hancock, R. E. (2001). Cationic peptides: effectors in innate immunity and novel antimicrobials. *The Lancet. Infectious diseases* **1**, 156-164.

He, J., Kauffman, W. B., Fuselier, T., Naveen, S. K., Voss, T. G., Hristova, K. and Wimley, W. C. (2013). Direct cytosolic delivery of polar cargo to cells by spontaneous membrane-translocating peptides. *The Journal of biological chemistry* **288**, 29974-29986.

Hebda, J. A. and Miranker, A. D. (2009). The Interplay of Catalysis and Toxicity by Amyloid Intermediates on Lipid Bilayers: Insights from Type II Diabetes. *Annual Review of Biophysics* **38**, 125-152.

Hebda, J. A., Saraogi, I., Magzoub, M., Hamilton, A. D. and Miranker, A. D. (2009). A Peptidomimetic Approach to Targeting Pre-amyloidogenic States in Type II Diabetes. *Chemistry & Biology* **16**, 943-950.

Heitz, F., Morris, M. C. and Divita, G. (2009). Twenty years of cell-penetrating peptides: from molecular mechanisms to therapeutics. *British journal of pharmacology* **157**, 195-206.

Herce, H. D., Garcia, A. E. and Cardoso, M. C. (2014). Fundamental molecular mechanism for the cellular uptake of guanidinium-rich molecules. *Journal of the American Chemical Society* **136**, 17459-17467.

Herrera, A. I., Al-Rawi, A., Cook, G. A., Gao, J., Iwamoto, T., Prakash, O., Tomich, J. M. and Chen, J. (2010). Structural characterization of two pore-forming peptides: consequences of introducing a C-terminal tryptophan. *Proteins* **78**, 2238-2250.

Herrera, A. I., Xiao, Y., Bommineni, Y. R., Soulages, J. L., Prakash, O. and Zhang, G. (2009). The central kink region of fowlicidin-2, an alpha-helical host defense peptide, is critically involved in bacterial killing and endotoxin neutralization. *Journal of innate immunity* **1**, 268-280.

Hilpert, K., Elliott, M. R., Volkmer-Engert, R., Henklein, P., Donini, O., Zhou, Q., Winkler, D. F. and Hancock, R. E. (2006). Sequence requirements and an optimization strategy for short antimicrobial peptides. *Chemistry & biology* **13**, 1101-1107.

Hristova, K., Selsted, M. E. and White, S. H. (1997). Critical role of lipid composition in membrane permeabilization by rabbit neutrophil defensins. *The Journal of biological chemistry* **272**, 24224-24233.

Huang, H. W. (2006). Molecular mechanism of antimicrobial peptides: the origin of cooperativity. *Biochimica et biophysica acta* **1758**, 1292-1302.

Huster, D., Feller, S. E. and Gawrisch, K. (1999). Noesy NMR crosspeaks between lipid headgroups and hydrocarbon chains - Spin diffusion or molecular disorder? *Biophysical journal* **76**, A354-A354.

Jang, H., Arce, F. T., Mustata, M., Ramachandran, S., Capone, R., Nussinov, R. and Lal, R. (2011). Antimicrobial protegrin-1 forms amyloid-like fibrils with rapid kinetics suggesting a functional link. *Biophysical journal* **100**, 1775-1783.

Jao, C. C., Hegde, B. G., Chen, J., Haworth, I. S. and Langen, R. (2008). Structure of membrane-bound alpha-synuclein from site-directed spin labeling and computational refinement. *Proceedings of the National Academy of Sciences of the United States of America* **105**, 19666-19671.

Jianquan, X., Yiyi, Y., Hao-Chih, L., Qirui, F., Winter, J. and Ge, Y. (2014). Cell penetrating peptide mediated quantum dot delivery and release in live mammalian cells. *Conference*

proceedings : ... Annual International Conference of the IEEE Engineering in Medicine and Biology Society. IEEE Engineering in Medicine and Biology Society. Annual Conference **2014**, 4260-4263.

Jones, A. T. and Sayers, E. J. (2012). Cell entry of cell penetrating peptides: tales of tails wagging dogs. *Journal of controlled release : official journal of the Controlled Release Society* **161**, 582-591.

Kayed, R., Head, E., Thompson, J. L., McIntire, T. M., Milton, S. C., Cotman, C. W. and Glabe, C. G. (2003). Common structure of soluble amyloid oligomers implies common mechanism of pathogenesis. *Science* **300**, 486-489.

Knight, J. D. and Miranker, A. D. (2004). Phospholipid catalysis of diabetic amyloid assembly. *Journal of Molecular Biology* **341**, 1175-1187.

Krittanai, C. and Panyim, S. (2004). Structural design and characterization of a channel-forming peptide. *Journal of Biochemistry and Molecular Biology* **37**, 460-465.

Langosch, D., Hartung, K., Grell, E., Bamberg, E. and Betz, H. (1991). Ion channel formation by synthetic transmembrane segments of the inhibitory glycine receptor--a model study. *Biochimica et biophysica acta* **1063**, 36-44.

Last, N. B. and Miranker, A. D. (2013). Common mechanism unites membrane poration by amyloid and antimicrobial peptides. *Proceedings of the National Academy of Sciences of the United States of America* **110**, 6382-6387.

Lear, J. D., Wasserman, Z. R. and DeGrado, W. F. (1988). Synthetic Amphiphilic Peptide Models for Protein Ion Channels. *Science* **240**, 1177-1181.

LeBeau, A. M. and Denmeade, S. R. (2014). Protease-Activated Pore-Forming Peptides for the Treatment and Imaging of Prostate Cancer. *Molecular cancer therapeutics* **14**, 659-668.

Lebleu, B., Moulton, H. M., Abes, R., Ivanova, G. D., Abes, S., Stein, D. A., Iversen, P. L., Arzumanov, A. A. and Gait, M. J. (2008). Cell penetrating peptide conjugates of steric block oligonucleotides. *Advanced drug delivery reviews* **60**, 517-529.

Lee, M. T., Chen, F. Y. and Huang, H. W. (2004). Energetics of pore formation induced by membrane active peptides. *Biochemistry* **43**, 3590-3599.

Li, Z., Yang, H., Sun, L., Qi, H., Gao, Q. and Zhang, C. (2015). Electrogenerated chemiluminescence biosensors for the detection of pathogenic bacteria using antimicrobial peptides as capture/signal probes. *Sensors and Actuators B: Chemical* **210**, 468-474.

Liu, B. R., Lin, M. D., Chiang, H. J. and Lee, H. J. (2012). Arginine-rich cell-penetrating peptides deliver gene into living human cells. *Gene* **505**, 37-45.

Lopez-Abarrategui, C., Figueroa-Espi, V., Reyes-Acosta, O., Reguera, E. and Otero-Gonzalez, A. J. (2013). Magnetic nanoparticles: new players in antimicrobial peptide therapeutics. *Current protein & peptide science* **14**, 595-606.

Madani, F., Lindberg, S., Langel, U., Futaki, S. and Graslund, A. (2011). Mechanisms of cellular uptake of cell-penetrating peptides. *Journal of biophysics* **2011**, 414729.

Magzoub, M. and Miranker, A. D. (2012). Concentration-dependent transitions govern the subcellular localization of islet amyloid polypeptide. *FASEB journal : official publication of the Federation of American Societies for Experimental Biology* **26**, 1228-1238.

Maji, S. K., Perrin, M. H., Sawaya, M. R., Jessberger, S., Vadodaria, K., Rissman, R. A., Singru, P. S., Nilsson, K. P. R., Simon, R., Schubert, D., Eisenberg, D., Rivier, J., Sawchenko, P., Vale, W. and Riek, R. (2009). Functional Amyloids As Natural Storage of Peptide Hormones in Pituitary Secretory Granules. *Science* **325**, 328-332.

Maler, L. (2013). Solution NMR studies of cell-penetrating peptides in model membrane systems. *Advanced drug delivery reviews* **65**, 1002-1011.

Marks, J. R., Placone, J., Hristova, K. and Wimley, W. C. (2011). Spontaneous membrane-translocating peptides by orthogonal high-throughput screening. *Journal of the American Chemical Society* **133**, 8995-9004.

Matsuzaki, K. and Horikiri, C. (1999). Interactions of amyloid beta-peptide (1-40) with ganglioside-containing membranes. *Biochemistry* **38**, 4137-4142.

Matsuzaki, K., Sugishita, K., Harada, M., Fujii, N. and Miyajima, K. (1997). Interactions of an antimicrobial peptide, magainin 2, with outer and inner membranes of Gram-negative bacteria. *Biochimica et biophysica acta* **1327**, 119-130.

Maurer, K., Volk, S. and Gerbaldo, H. (1997). Auguste D and Alzheimer's disease. *Lancet* **349**, 1546-1549.

Mayer, M., Semetey, V., Gitlin, I., Yang, J. and Whitesides, G. M. (2008). Using ion channel-forming peptides to quantify protein-ligand interactions. *Journal of the American Chemical Society* **130**, 1453-1465.

McLaurin, J., Franklin, T., Chakrabartty, A. and Fraser, P. E. (1998). Phosphatidylinositol and inositol involvement in Alzheimer amyloid-beta fibril growth and arrest. *Journal of Molecular Biology* **278**, 183-194.

Meyer, K., Thompson, R., Palmer, J. W. and Khorazo, D. (1934). The Nature of Lysozyme Action. *Science* **79**, 61.

Middleton, E. R. and Rhoades, E. (2010). Effects of curvature and composition on alpha-synuclein binding to lipid vesicles. *Biophysical journal* **99**, 2279-2288.

Morris, M. C., Depollier, J., Mery, J., Heitz, F. and Divita, G. (2001). A peptide carrier for the delivery of biologically active proteins into mammalian cells. *Nature biotechnology* **19**, 1173-1176.

Morris, M. C., Vidal, P., Chaloin, L., Heitz, F. and Divita, G. (1997). A new peptide vector for efficient delivery of oligonucleotides into mammalian cells. *Nucleic acids research* **25**, 2730-2736.

Moulton, H. M. (2012). Cell-penetrating peptides enhance systemic delivery of antisense morpholino oligomers. *Methods in molecular biology* **867**, 407-414.

Munoz-Morris, M. A., Heitz, F., Divita, G. and Morris, M. C. (2007). The peptide carrier Pep-1 forms biologically efficient nanoparticle complexes. *Biochemical and biophysical research communications* **355**, 877-882.

Nerelius, C., Sandegren, A., Sargsyan, H., Raunak, R., Leijonmarck, H., Chatterjee, U., Fisahn, A., Imarisio, S., Lomas, D. A., Crowther, D. C., Stromberg, R. and Johansson, J. (2009). alpha-Helix targeting reduces amyloid-beta peptide toxicity. *Proceedings of the National Academy of Sciences of the United States of America* **106**, 9191-9196.

Oiki, S., Danho, W., Madison, V. and Montal, M. (1988). M2 delta, a candidate for the structure lining the ionic channel of the nicotinic cholinergic receptor. *Proceedings of the National Academy of Sciences of the United States of America* **85**, 8703-8707.

Ordonez, S. R., Amarullah, I. H., Wubbolts, R. W., Veldhuizen, E. J. and Haagsman, H. P. (2014). Fungicidal mechanisms of cathelicidins LL-37 and CATH-2 revealed by live-cell imaging. *Antimicrobial agents and chemotherapy* **58**, 2240-2248.

Patel, L. N., Zaro, J. L. and Shen, W. C. (2007). Cell penetrating peptides: intracellular pathways and pharmaceutical perspectives. *Pharmaceutical research* **24**, 1977-1992.

Phoenix, D. A., Dennison, S. R. and Harris, F. (2013). Antimicrobial Peptides: Their History, Evolution, and Functional Promiscuity. In *Antimicrobial Peptides*, pp. 1-37. Wiley-VCH Verlag GmbH & Co. KGaA.

Planque, S. A., Nishiyama, Y., Sonoda, S., Lin, Y., Taguchi, H., Hara, M., Kolodziej, S., Mitsuda, Y., Gonzalez, V., Sait, H. B., Fukuchi, K. I., Massey, R. J., Friedland, R. P., O'Nuallain, B., Sigurdsson, E. M. and Paul, S. (2015). Specific Amyloid beta Clearance by a Catalytic Antibody Construct. *The Journal of biological chemistry*.

Prusiner, S. B. (1982). Novel Proteinaceous Infectious Particles Cause Scrapie. *Science* **216**, 136-144.

Puig, M., Moragrega, C., Ruz, L., Montesinos, E. and Llorente, I. (2014). Postinfection Activity of Synthetic Antimicrobial Peptides Against Stemphylium vesicarium in Pear. *Phytopathology* **104**, 1192-1200.

Pushpanathan, M., Gunasekaran, P. and Rajendhran, J. (2013). Antimicrobial peptides: versatile biological properties. *International journal of peptides* **2013**, 675391.

Rambaran, R. N. and Serpell, L. C. (2008). Amyloid fibrils Abnormal protein assembly. *Prion* **2**, 112-117.

Rathinakumar, R., Walkenhorst, W. F. and Wimley, W. C. (2009). Broad-spectrum antimicrobial peptides by rational combinatorial design and high-throughput screening: the importance of interfacial activity. *Journal of the American Chemical Society* **131**, 7609-7617.

Rausch, J. M., Marks, J. R., Rathinakumar, R. and Wimley, W. C. (2007). Beta-sheet pore-forming peptides selected from a rational combinatorial library: mechanism of pore formation in lipid vesicles and activity in biological membranes. *Biochemistry* **46**, 12124-11139.

Rausch, J. M., Marks, J. R. and Wimley, W. C. (2005). Rational combinatorial design of pore-forming beta-sheet peptides. *Proceedings of the National Academy of Sciences of the United States of America* **102**, 10511-10515.

Reddy, G. L., Iwamoto, T., Tomich, J. M. and Montal, M. (1993). Synthetic peptides and four-helix bundle proteins as model systems for the pore-forming structure of channel proteins. II. Transmembrane segment M2 of the brain glycine receptor is a plausible candidate for the pore-lining structure. *The Journal of biological chemistry* **268**, 14608-14615.

Ringhieri, P., Diaferia, C., Galdiero, S., Palumbo, R., Morelli, G. and Accardo, A. (2015). Liposomal doxorubicin doubly functionalized with CCK8 and R8 peptide sequences for selective intracellular drug delivery. *Journal of peptide science : an official publication of the European Peptide Society*.

Sandgren, S., Wittrup, A., Cheng, F., Jonsson, M., Eklund, E., Busch, S. and Belting, M. (2004). The human antimicrobial peptide LL-37 transfers extracellular DNA plasmid to the nuclear compartment of mammalian cells via lipid rafts and proteoglycan-dependent endocytosis. *Journal of Biological Chemistry* **279**, 17951-17956.

Schauerte, J. A., Wong, P. T., Wisser, K. C., Ding, H., Steel, D. G. and Gafni, A. (2010). Simultaneous Single-Molecule Fluorescence and Conductivity Studies Reveal Distinct Classes of A beta Species on Lipid Bilayers. *Biochemistry* **49**, 3031-3039.

Selkoe, D. J. (2003). Folding proteins in fatal ways. *Nature* **426**, 900-904.

Selsted, M. E., Harwig, S. S., Ganz, T., Schilling, J. W. and Lehrer, R. I. (1985). Primary structures of three human neutrophil defensins. *J Clin Invest* **76**, 1436-1439.

Shank, L. P., Broughman, J. R., Takeguchi, W., Cook, G., Robbins, A. S., Hahn, L., Radke, G., Iwamoto, T., Schultz, B. D. and Tomich, J. M. (2006). Redesigning channel-forming peptides: amino acid substitutions that enhance rates of supramolecular self-assembly and raise ion transport activity. *Biophys J* **90**, 2138-2150.

Shvadchak, V. V., Falomir-Lockhart, L. J., Yushchenko, D. A. and Jovin, T. M. (2011). Specificity and Kinetics of alpha-Synuclein Binding to Model Membranes Determined with Fluorescent Excited State Intramolecular Proton Transfer (ESIPT) Probe. *Journal of Biological Chemistry* **286**, 13023-13032.

Simons, M., Keller, P., De Strooper, B., Beyreuther, K., Dotti, C. G. and Simons, K. (1998). Cholesterol depletion inhibits the generation of beta-amyloid in hippocampal neurons. *Proceedings of the National Academy of Sciences of the United States of America* **95**, 6460-6464.

Singer, S. J. and Nicolson, G. L. (1972). Fluid Mosaic Model of Structure of Cell-Membranes. *Science* **175**, 720-731.

Smaoui, M. R., Orland, H. and Waldispühl, J. (2015). Probing the binding affinity of amyloids to reduce toxicity of oligomers in diabetes. *Bioinformatics*. Online advace access.

Smith, P. E., Brender, J. R. and Ramamoorthy, A. (2009). Induction of negative curvature as a mechanism of cell toxicity by amyloidogenic peptides: the case of islet amyloid polypeptide. *Journal of the American Chemical Society* **131**, 4470-4478.

Soscia, S. J., Kirby, J. E., Washicosky, K. J., Tucker, S. M., Ingelsson, M., Hyman, B., Burton, M. A., Goldstein, L. E., Duong, S., Tanzi, R. E. and Moir, R. D. (2010). The Alzheimer's disease-associated amyloid beta-protein is an antimicrobial peptide. *PloS one* **5**, e9505.

Spach, G., Merle, Y. and Molle, G. (1985). Peptides amphiphiles et canaux transmembranes. *Journal de chimie physique et de physico-chimie biologique* **82**, 719.

Stephens, J. M. and Marshall, J. H. (1962). Some Properties of an Immune Factor Isolated from Blood of Actively Immunized Wax Moth Larvae. *Canadian Journal of Microbiology* **8**, 719-725.

Sukthankar, P., Whitaker, S. K., Garcia, M., Herrera, A., Boatwright, M., Prakash, O. and Tomich, J. M. (2015). Thermally induced conformational transitions in nascent branched amphiphilic Peptide capsules. *Langmuir : the ACS journal of surfaces and colloids* **31**, 2946-2955.

Sunde, M. and Blake, C. C. (1998). From the globular to the fibrous state: protein structure and structural conversion in amyloid formation. *Quarterly reviews of biophysics* **31**, 1-39.

Tomich, J. M., Bukovnik, U., Layman, J. and Schultz, B. D. (2012). Channel Replacement Therapy for Cystic Fibrosis. In *Cystic Fibrosis - Renewed Hopes Through Research* (Sriramulu, D., ed.), pp. 291-332. InTech, Rijeka, Croatia.

Tomich, J. M., Wallace, D., Henderson, K., Mitchell, K. E., Radke, G., Brandt, R., Ambler, C. A., Scott, A. J., Grantham, J., Sullivan, L. and Iwamoto, T. (1998). Aqueous solubilization of transmembrane peptide sequences with retention of membrane insertion and function. Biophysical journal 74, 256-267.

Threat Report 2013. Center for Disease Control and Prevention. April 23, 2013.

Ueda, Y., Wei, F. Y., Hide, T., Michiue, H., Takayama, K., Kaitsuka, T., Nakamura, H., Makino, K., Kuratsu, J., Futaki, S. and Tomizawa, K. (2012). Induction of autophagic cell death of glioma-initiating cells by cell-penetrating D-isomer peptides consisting of Pas and the p53 C-terminus. *Biomaterials* **33**, 9061-9069.

Virchow, R. (1854). *Virchows Arch. Pathol. Anat. Physiol.* **6**, 135-137.

Vives, E., Schmidt, J. and Pelegrin, A. (2008). Cell-penetrating and cell-targeting peptides in drug delivery. *Biochimica et biophysica acta* **1786**, 126-138.

Wade, D., Boman, A., Wahlin, B., Drain, C. M., Andreu, D., Boman, H. G. and Merrifield, R. B. (1990). All-D Amino Acid-Containing Channel-Forming Antibiotic Peptides. *Proceedings of the National Academy of Sciences of the United States of America* **87**, 4761-4765.

Wallace, D. P., Tomich, J. M., Eppler, J. W., Iwamoto, T., Grantham, J. J. and Sullivan, L. P. (2000). A synthetic channel-forming peptide induces Cl(-) secretion: modulation by Ca(2+)-dependent K(+) channels. *Biochimica et biophysica acta* **1464**, 69-82.

Wallace, D. P., Tomich, J. M., Iwamoto, T., Henderson, K., Grantham, J. J. and Sullivan, L. P. (1997). A synthetic peptide derived from glycine-gated Cl- channel induces transepithelial Cl- and fluid secretion. *Am J Physiol* **272**, C1672-1679.

Wang, G. (2015). Improved methods for classification, prediction, and design of antimicrobial peptides. *Methods in molecular biology* **1268**, 43-66.

Wang, G., Li, X. and Wang, Z. (2009). APD2: the updated antimicrobial peptide database and its application in peptide design. *Nucleic acids research* **37**, D933-937.

Watanabe, N., Iwamoto, T., Bowen, K. D., Dickinson, D. A., Torres, M. and Forman, H. J. (2003). Bio-effectiveness of Tat-catalase conjugate: a potential tool for the identification of H2O2-dependent cellular signal transduction pathways. *Biochemical and biophysical research communications* **303**, 287-293.

Wender, P. A., Galliher, W. C., Bhat, N. M., Pillow, T. H., Bieber, M. M. and Teng, N. N. (2012). Taxol-oligoarginine conjugates overcome drug resistance in-vitro in human ovarian carcinoma. *Gynecologic oncology* **126**, 118-123.

Wender, P. A., Mitchell, D. J., Pattabiraman, K., Pelkey, E. T., Steinman, L. and Rothbard, J. B. (2000). The design, synthesis, and evaluation of molecules that enable or enhance cellular uptake: peptoid molecular transporters. *Proceedings of the National Academy of Sciences of the United States of America* **97**, 13003-13008.

Williamson, J. A., Loria, J. P. and Miranker, A. D. (2009). Helix stabilization precedes aqueous and bilayer-catalyzed fiber formation in islet amyloid polypeptide. *Journal of molecular biology* **393**, 383-396.

Wimley, W. C. (2010). Describing the Mechanism of Antimicrobial Peptide Action with the Interfacial Activity Model. *Acs Chemical Biology* **5**, 905-917.

Xiao, Y., Dai, H., Bommineni, Y. R., Soulages, J. L., Gong, Y. X., Prakash, O. and Zhang, G. (2006). Structure-activity relationships of fowlicidin-1, a cathelicidin antimicrobial peptide in chicken. *The FEBS journal* **273**, 2581-2593.

Xiong, N., Dong, X. Y., Zheng, J., Liu, F. F. and Sun, Y. (2015). Design of LVFFARK and LVFFARK-Functionalized Nanoparticles for Inhibiting Amyloid beta-Protein Fibrillation and Cytotoxicity. *ACS applied materials & interfaces* **7**, 5650-5662.

Yanagisawa, K., Odaka, A., Suzuki, N. and Ihara, Y. (1995). GM1 ganglioside-bound amyloid beta-protein (A beta): a possible form of preamyloid in Alzheimer's disease. *Nature medicine* **1**, 1062-1066.

Yip, C. M., Elton, E. A., Darabie, A. A., Morrison, M. R. and McLaurin, J. (2001). Cholesterol, a modulator of membrane-associated A beta-fibrillogenesis and neurotoxicity. *Journal of Molecular Biology* **311**, 723-734.

Zaat, S. A. (2014). BALI beating biofilms, *4th International Meeting on Antimicrobial Peptides*. September 29-30 2014. Graz, Austria.

Zanetti, M., Gennaro, R. and Romeo, D. (1995). Cathelicidins: a novel protein family with a common proregion and a variable C-terminal antimicrobial domain. *FEBS Lett* **374**, 1-5.

Zasloff, M. (1987). Magainins, a class of antimicrobial peptides from Xenopus skin: isolation, characterization of two active forms, and partial cDNA sequence of a precursor. *Proc Natl Acad Sci U S A* **84**, 5449-5453.

Zasloff, M. (2002). Antimicrobial peptides of multicellular organisms. *Nature* **415**, 389-395.

Zatsepin, T. S., Turner, J. J., Oretskaya, T. S. and Gait, M. J. (2005). Conjugates of oligonucleotides and analogues with cell penetrating peptides as gene silencing agents. *Current pharmaceutical design* **11**, 3639-3654.

Zhang, Y. T., Sukthankar, P., Tomich, J. M. and Conrad, G. W. (2012). Effect of the Synthetic NC-1059 Peptide on Diffusion of Riboflavin across an Intact Corneal Epithelium. *Investigative Ophthalmology & Visual Science* **53**, 2620-2629.

Chapter 2 - Structural characterization and consequences of introducing a C-terminal tryptophan to a Monomeric Channel-Forming Peptide Derived from the Glycine Receptor M2 Segment

Introduction

Membrane ion channels are transmembrane proteins that allow the flow of ions following their electrochemical gradient across the membranes of cells and organelles, this flow generates an electrical current that is required for the modulation of membrane potential and the regulation of multiple cellular activities, like signal transduction, neurotransmission, hormone secretion, motility, and regulation of extracellular conditions (Kim, 2014). Defective ion channels have been implicated in many human diseases collectively known as channelopathies. This diseases affect different systems, including the nervous system (generalized epilepsy with febrile seizures, familial hemiplegic migraine, episodic ataxia), the cardiovascular system (Brugada syndrome, catecholaminergic polymorphic ventricular tachycardia), the respiratory system (cystic fibrosis), the endocrine system (neonatal diabetes mellitus, familial hyperinsulinemic hypoglycemia, familial hyperaldosteronism), the urinary system (Bartter syndrome, nephrogenic diabetes insipidus, autosomal-dominant polycystic kidney disease), and the immune system (myasthenia gravis, neuromyelitis optica, Isaac syndrome) (Cannon, 2007;Jentsch et al., 2002;Kim, 2014;Welsh and Smith, 1993). Cystic fibrosis is cause by suboptimal synthesis, folding, transport, or gating of the Cystic Fibrosis Transmembrane Conductance Regulator (CFTR); an ATP-gated anion channel. Defects in the CFTR are caused by various genotypes (Tomich et al., 2012).

Epithelia, one of the tissues potentially affected by channelopathies act as regulated barriers to the movement between body compartments of small molecules including ions and drugs. Defective ion channels disrupt the proper function and regulation of the epithelial surfaces casing the disease states. Most ions cross the epithelial apical and basolateral membranes via tightly regulated ion-specific transporters and channels. Peptide-based channel replacement therapy has been proposed as a treatment modality for correcting genetically based channelopathies (Tomich et al., 1998;Wallace et al., 2000;Wallace et al., 1997). A particularly attractive strategy is to deliver an aqueous soluble monomeric membrane-active channel forming peptide to the apical surface of affected epithelia. Channel forming peptides have the ability to spontaneously insert and undergo supramolecular assembly to form functioning homo-oligomeric ion-conducting pores upon interaction with the apical cell membrane. As a treatment for the symptomatology found in the airways of individuals with cystic fibrosis, the potential therapeutic peptide sequence should make up for the lost function of the CFTR, with high anion conduction rates and high chloride selectivity. For effective delivery of a therapeutic peptide, high aqueous solubility with minimal solution aggregation is essential. With the purpose of finding an optimal amino acid sequence for the cystic fibrosis therapeutic peptide, a series of channel forming peptides derived from the second transmembrane domain of the α1-subunit of the glycine receptor (M2GlyR) were designed, synthesized and tested over recent years (Broughman et al., 2004;Broughman et al., 2001;Broughman et al., 2002a;Broughman et al., 2002b;Bukovnik et al., 2012;Bukovnik et al., 2013;Cook et al., 2004;Gao et al., 2001;Herrera et al., 2010;Shank et al., 2006;Wallace et al., 2000). The NK_4-M2GlyR-p22 sequence (KKKKP ARVGL GITTV LTMTT QS) has been determined to be a good candidate, in that it has high solubility in physiological buffers, controls the orientation of the inserted sequence, and at the same time, has assembled

channel properties similar to the full length M2GlyR segment (Broughman et al., 2002b). In the open state, the channels formed by NK_4-M2GlyR-p22 peptides are able to sustain anion transport rates across Madin–Darby canine kidney (MDCK) epithelial monolayers with a maximum short circuit current (I_{max}) of 23.7 ± 5.6 μA cm^{-2}. However, NK_4-M2GlyR-p22 peptide forms soluble associations that greatly reduce the concentration of membrane active monomer, requiring a concentration of 210 ± 70μM to reach one-half I_{max} ($K_{1/2}$). Whole cell patch clamp measurements of the current-voltage relation revealed inward rectification at positive voltages, (Shank et al., 2006) suggesting that the assembled channel has a substantial degree of structural flexibility and can undergo conformational changes at different voltages. A later designed modification of the peptide intended to define the lipid-water boundary of the peptide by replacing serine residue 22 with a membrane anchoring tryptophan (NK_4-M2GlyR-p22 S22W) eliminates nonproductive solution assemblies and decreases the peptide concentration required for channel activity. For this substituted peptide pore formation can occur at a lower peptide concentration with a $K_{1/2}$ of 45 ± 6 μM (Tomich et al., 2012). However, there is a substantial decrease of the ion current across the membrane (I_{max}=13.0 ± 1.0 μA cm^{-2}) at saturating peptide concentrations (Figure 2-1) (See Chapter 3 Materials and Methods for experimental determination details), and the inward rectification observed for NK_4-M2GlyR-p22 is abolished, possibly because the membrane anchoring by the tryptophan residue at the C-terminus is as expected restricting certain conformational states (and flexibility) of the assembled channel.

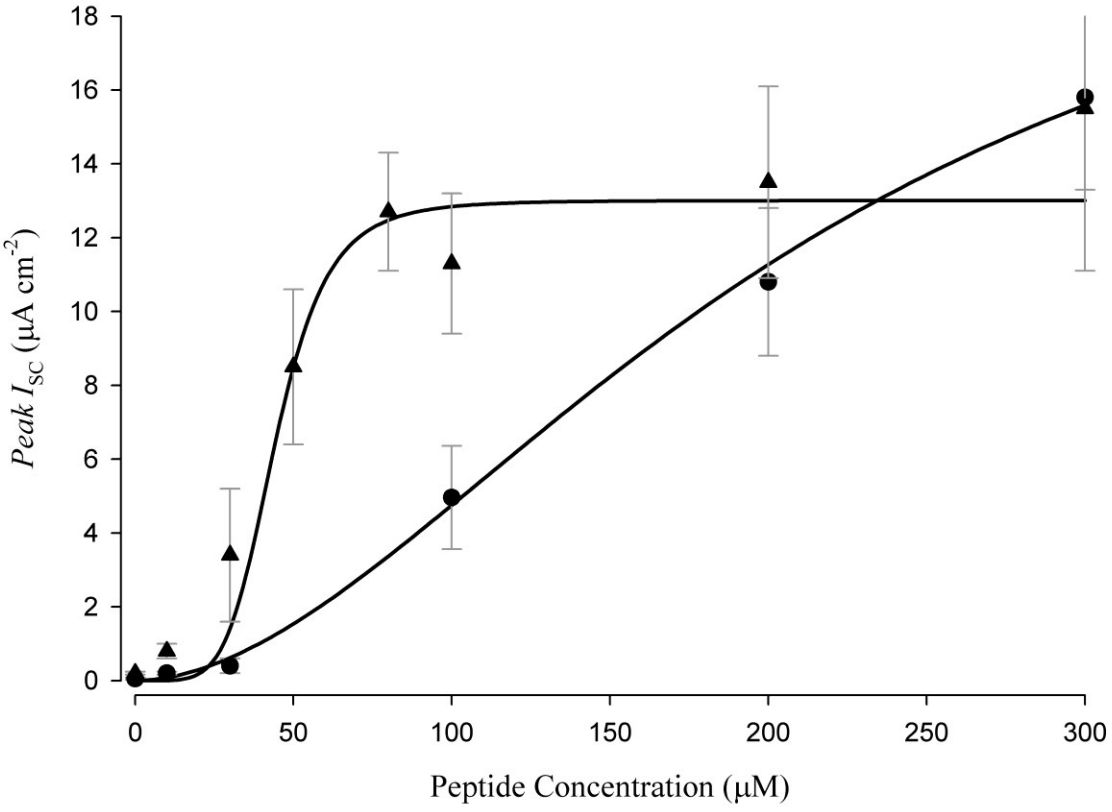

Figure 2-1. Concentration-dependence of I_{sc} induced by NK_4-M2GlyR-p22 and NK_4-M2GlyR-p22 S22W on MDCK epithelial monolayers. NK_4-M2GlyR-p22 (●), NK_4-M2GlyR-p22 S22W (▲). Data from (Cook et al., 2004)

Interestingly M2GlyR-derived peptides do not appear to cause immune or inflammatory responses at clinically relevant doses (van Ginkel et al., 2008). However, a drawback shared by both NK_4-M2GlyR-p22 and NK_4-M2GlyR-p22 S22W is that the enhanced ion conductivity seems to be accomplished at the cost of much weaker anion permselectivity compared with channels formed by the full length M2GlyR segment (Shank et al., 2006). This represents an important limitation for any potential therapeutic applications of such peptides. Further understanding of the consequences that sequence substitution has onto the overall peptide

structure, both in solution and in the membrane environment, is needed to improve the design of a monomeric channel-forming peptide with therapeutic application.

In our efforts to determine the monomeric structures of the M2GlyR peptides in solution we used proton (^{1}H) Nuclear Magnetic Resonance (NMR) spectroscopy, which has been considered as one of the most powerful experimental techniques for the investigation of molecular structures at the atomic level in solution and membrane like environments (Wüthrich, 1986). The one-dimensional (1D) ^{1}H NMR spectra of peptides are often complex due to the large number of signals from the abundant hydrogen atoms. Although, important structural information is contained in these NMR spectra, that information is crammed into a relatively small frequency range, making assignment of the peaks impractical and most of the time impossible. The first step required for the interpretation of ^{1}H NMR spectra is the identification of the molecular groupings that give rise to the proton resonances. This step has been made possible for peptides and other biological macromolecules with the development of multi-dimensional NMR techniques, that separate all the resonances detected from the molecules being studied into multiple frequency dimensions corresponding to the type of nuclei that generate the signal (^{1}H, ^{13}C, ^{15}N, etc..), or the type of interaction between the nuclei (through bond, through space).

The molecular weight of the M2GlyR peptides is within the experimental range that allows the use of a combination of two-dimensional (2D) proton-proton NMR techniques without the need of a complex expression and purification methodology for isotope enrichment (^{15}N, ^{13}C) like the one required for the study of larger proteins. For NMR signal assignments we use 2D NMR experiments, determining through bond connectivities such as 2D homonuclear spin correlated

spectroscopy (COSY) (Bax and Freeman, 1981) and 2D Total Correlation Spectroscopy (TOCSY) (Bax and Davis, 1985) followed by 2D NMR experiments determining through space connectivities such as 2D proton - proton nuclear Overhauser effect spectroscopy (NOESY) (Kumar et al., 1980). Since the different secondary structure elements in a peptide, protein and macromolecule produce different NOESY signal patterns (Billeter et al., 1982), therefore, NOESY spectra analyses can lead to the identification of secondary structure. The quantitative analysis of NOESY data is used to estimate proton - proton distance constraints with the help of isolated spin pair approximation method. For the calculation of the 3D structure of M2GlyR derived peptides on the basis of the experimental constraints, we use a computational approach developed by Clore et al., which combines distance geometry algorithms (Braun and Go, 1985;Havel et al., 1983), dynamical simulated annealing (Nilges et al., 1988a;Nilges et al., 1988b) and restrained molecular dynamics (Clore and Gronenborn, 1989). Computer programs: CNS, MOLMOL and VMD were used for structure calculations and molecular graphics (Brunger et al., 1998;Humphrey et al., 1996;Koradi et al., 1996).

For NK_4-M2GlyR-p22 peptide the resonance assignments were performed mainly by the analysis of a TOCSY experiment spectrum. The pulse sequence for the TOCSY experiment contains a 90° pulse, two trim pulses and a MLEV-17 composite pulse. The trim pulse defocuses magnetization transverse to the x-axis and allows easy phasing of the 2D spectrum in the absorption mode. The MLEV-17 sequence consist of the following: ABBA BBAA BAAB AABB, where A and B are the composite pulses of $(90°_{-y}\ 180°_{x}\ -90°_{-y})$ and $(90°_{y}\ 180°_{-x}\ -90°_{y})$. An integer number *n* repetitions of MLEV-17 are used to transfer magnetization between homonuclear coupled spins (Bax and Davis, 1985). Cross peaks in a TOCSY spectrum connect

protons within a coupled spin network, making the TOCSY experiment ideal for extracting connectivities between protons belonging to the same spin system, in this case belonging to the same amino acid residue.

Information extracted from the spectra of NOESY experiments is used to stablish sequential connectivities that allow for the differentiation of resonances belonging to residues that are repeated in the sequence (K2, K3, K4, V8, V15, G9, G11, L10, L16, T13, T14, T17, T19, T20). In the basic NOESY experiment the frequency-labeled magnetization is transferred from one proton to another during the mixing time via through-space dipolar spin relaxation interactions (Kumar et al., 1980). The NOESY spectra contain a main diagonal and cross peaks which represent dipole-dipole couplings between nuclei which are at 5 Å or less from each other, allowing for the detection of sequential cross peaks between the protons of neighbor amino acid residues like the ones presented in Figure 2-2, that contribute to the assignment of ambiguous spin systems.

The bulk of the structural information used during the structure calculations is also derived from the NOESY spectra, cross peaks identified in these spectra not only come from amino acid residues adjacent in the peptide sequence, but are produced by any pair of protons that come within a distance of 5 Å due to the molecular conformation. The intensity of the NOESY cross peak is related to the distance *r* between interacting protons by the following proportion:

$$NOE \propto f_{(\tau_C)} * \frac{1}{r^6}$$

Where $f_{(\tau_C)}$ is a function of the rotational correlation time (τ_C), and represents the influence of the motion of the molecule on the observed NOE. The rotational correlation time τ_C can be defined as the average time it takes a particular molecule to rotate one radian (McNaught and Wilkinson, 1997). The correlation time of a molecule in solution will be affected by the molecular size, temperature, and viscosity of the solution.

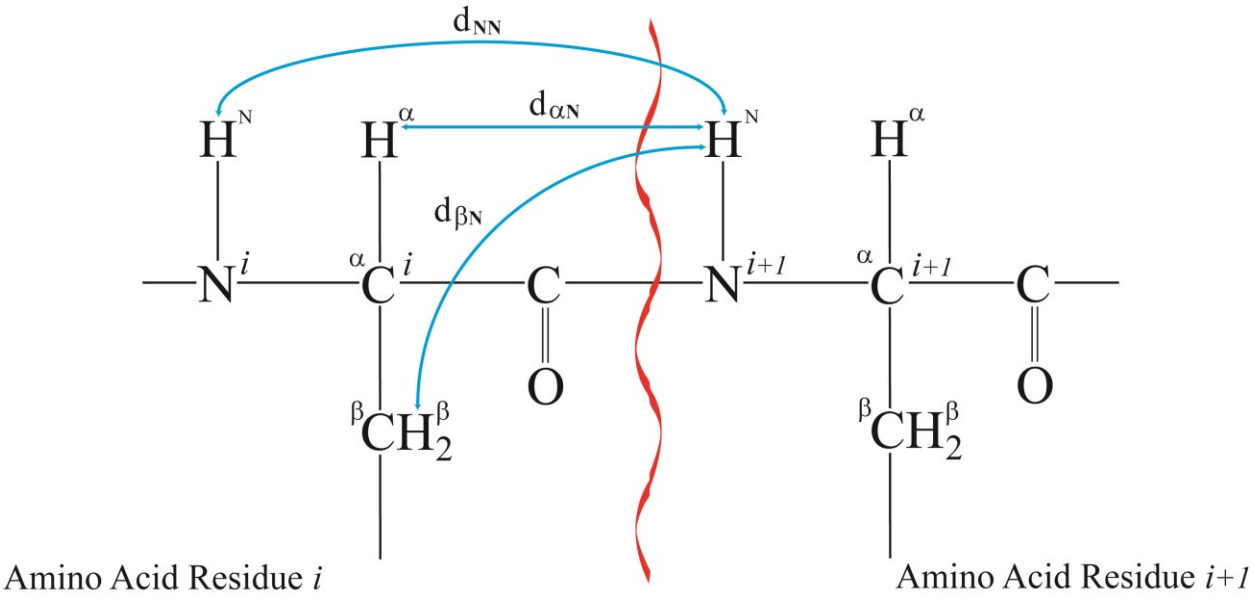

Figure 2-2. Notation of sequential proton-proton distances in peptide chains

Concurrently with the analysis of the TOCSY and NOESY spectra, the spectrum obtained from a 2D double-quantum-filtered correlation spectroscopy (DQF-COSY) experiment was also used in the completion of the resonance assignments. In a DQF-COSY experiment a first 90° pulse flips the magnetization into the transverse plane, and the various magnetization components are labeled during the evolution time (t_1). A second 90° pulse excites multiple quantum coherences, and is followed by a third 90° pulse after a delay of several microseconds that allows time for

phase shifting of the radiofrequency between the second and third pulses. Appropriate phase cycling is used to select specific multiple-quantum coherence transfer pathways. For a double-quantum filter, the phase is cycled through the values of 0°, 90°, 180° and 270° (Bax and Freeman, 1981). A DQF-COSY spectrum provides information on the J-connectivities between protons linked via two or three bonds in the covalent structure, the same way a COSY spectrum does, however in a DQF-COSY spectrum, both cross diagonal and cross peaks have absorption line shapes in both dimensions. This characteristic makes the cross peaks near the diagonal observable because the intensity of the tails of the diagonal peaks are reduced by the elimination of the dispersive character of the diagonal peaks, also singlets are suppressed by the double-quantum filer, making the DQF version of the COSY experiment preferable for resonance assignments of peptides.

From the assigned DQF-COSY spectrum it is possible to obtain coupling constant (^3J) values. Based on the Karplus equation it is possible to calculate the torsion angles in the protein or peptide (Karplus, 1959). The coupling constants of the H^N-H^α region are used to determine the ϕ angles that make up the peptide backbone. From ^3J values it is possible to predict the secondary structure based on the hertz difference of peak splitting. Extremes of the Karplus scale, which ranges from 3 to10, can indicate helix formation (<6 Hz) or the presence of β strand (>8 Hz) in the conformation (Nanzer et al., 1994). Coupling constants residing within these extremes can represent a turn, loop or an average of different secondary structures. The dihedral angle constraints derived from the DQF-COSY spectrum were used during the structural calculations.

Using the two dimensional NMR experimental techniques discussed above the monomeric solution structures of peptides NK_4-M2GlyR-p22 and NK_4-M2GlyR-p22 S22W were reported in a 2,2,2-trifluoroethanol (TFE):water solvent system (Cook et al., 2004). The structure of peptide NK_4-M2GlyR-p22 S22W was later calculated in a Sodium Dodecyl Sulfate (SDS) micelle environment, while the determination of the structure of peptide NK_4-M2GlyR-p22 in SDS micelles had remained elusive due to technical challenges in the sample preparation and experimental optimization. Here the monomeric solution structure determination using 2D NMR methodology in SDS micelles and the 3D structure calculations of NK_4-M2GlyR-p22 using molecular dynamics simulations are presented. The obtained 3D structure has been compared to the 3D structure obtained for the same peptide in the TFE:water environment. Furthermore, a comparison between solution structures of NK_4-M2GlyR-p22 and NK_4-M2GlyR-p22 S22W in the membrane like environment is also discussed.

The NMR structural information on NK_4-M2GlyR-p22 and NK_4-M2GlyR-p22 S22W, existing biophysical data, and molecular modeling were combined to construct atomistic models of the putative pentameric channels of these peptides. Molecular dynamics (MD) simulations were performed to refine and validate these structural models. These studies help in the rationalization of the functional consequences of introducing a single C-terminal tryptophan, and the availability of these structural models paves the way for future studies to rationally modify and improve M2GlyR-derived peptides toward potential peptide-based channel replacement therapy. The details about the simulations methodology and results are discussed in the Appendix A - Chapter 2.

Materials and Methods

Peptide Synthesis and Purification

Peptides NK_4-M2GlyR-p22 (NH2-KKKKPARVGLGITTVLTMTTQS-CONH2; MW = 2356.9 Da) and NK_4-M2GlyR-p22 S22W (NH2-KKKKPARVGLGITTVLTMTTQW-CONH2; MW = 2456.0 Da) were chemically synthesized by solid phase peptide synthesis methodology on an Applied Biosystems model 431A peptide synthesizer (Applied Biosystems, Foster City, CA) using 9-fluorenylmethoxycarbonyl (Fmoc) chemistry at a synthesis scale of 0.1-0.2 mmol, CLEAR amide resin (0.3 mmol/g) purchased from Peptides International Inc. (Louisville, KY) was preloaded with the first amino acid and N^{α}-Fmoc amino acids were purchased from Anaspec (Fremont, CA), Bachem Inc. (Torrance, CA), and Peptides International Inc. (Louisville, KY) (Tomich et al., 1998). All peptides were purified using a Phenomenex (Torrance, CA) reversed-phase C-18 column on a System Gold HPLC system (Beckman Instruments Inc., Fullerton, CA). Peptides were eluted from the column using a linear gradient of 3.0% min^{-1} of 10–90% acetonitrile containing 0.1% trifluoroacetic acid (TFA) at 1 mL/min. HPLC-purified peptides were characterized by matrix-assisted-laser desorption time-of-flight mass spectroscopy (MALDI-TOF/TOF) using a Bruker Ultraflex II mass spectrometer (Bruker Instruments Inc., Billerica, MA). After characterization, peptides were lyophilized and stored as dry powders until used. The purity of the samples and connectivity of amino acid residues in NK_4-M2GlyR-p22 and NK_4-M2GlyR-p22 S22W were further indicated by the complete analysis of the TOCSY and NOESY NMR spectra of each peptide.

NMR Sample Preparation

Lyophilized peptide was dissolved in 1.0 mL of a (1:1) mixture of 1,1,1,3,3,3-hexafluoro-2-propanol:TFE. The solution was transferred to a glass test tube and dried with a stream of nitrogen gas in order to dry the peptide into a thin film on the wall of the test tube. Once the peptide was considered dry by visual inspection, the test tube containing the peptide was put in a lyophilizer overnight to remove any remaining solvent and moisture. The following day, the peptide was dissolved in 250µl of 1 M SDS-d_{25} in water. Once the peptide appeared dissolved, 250µl of an 80%H_2O:20% D_2O mixture was added (Cambridge Isotope Labs, Andover, MA), for a final SDS-d_{25} concentration of 500mM in 90%H_2O-10% D_2O and a peptide concentration of 2.5 mM.

NMR Spectroscopy

Initial 2D ^{1}H-^{1}H TOCSY experiments were performed with the 11.75 tesla 500 MHz Varian VNMRS spectrometer (Varian now Agilent Inc., Palo Alto, CA), running VNMRj version 2.3 at the Biomolecular NMR facility of the Biochemistry and Biophysics Department at Kansas State University, using a room temperature 3mm (sample tube diameter) inverse detection Penta probe. The obtained spectra did not have the needed quality for resonance analysis due to signal broadening. The prepared peptide sample was sent to the Biomolecular NMR laboratory at the University of Kansas (Lawrence, KS); there 2D ^{1}H-^{1}H TOCSY, ^{1}H-^{1}H DQF-COSY and 2D ^{1}H-^{1}H NOESY spectra were recorded with a 18.8 tesla Bruker Avance 800 MHz NMR spectrometer (Bruker Instruments, Billerica, MA) equipped with an inverse detection TCI cryoprobe running

Topspin 1.3. Experiments were performed at 45°C, the elevated data acquisition temperature was chosen to reduce the molecular tumbling time and improve spectral quality, CD measurements show minimal structural differences with the temperature increase (Tomich et al., 1998). Raw NMR data obtained from the 800 MHz instrument was processed using NMRPipe (Delaglio et al., 1995) and analyzed with Sparky software (Goddard and Kneller, 2004) using a Dell Precision 690 workstation (Round Rock, TX). NOE cross peaks were classified as strong, medium, weak and very weak based on the observed number of contour lines. Spin-lock time of 100 ms at B1 field strength of 7 KHz was used for 2D ^{1}H-^{1}H TOCSY experiments using MLEV-17 pulse sequence (Bax and Davis, 1985), and mixing times of 300 and 400 ms were used for 2D ^{1}H-^{1}H NOESY experiments. For all 2D experiments 1024 complex data points were collected in the direct dimension and 256 in the indirect dimension. Linear prediction and zero filling were used during NMR data processing; the suppression of the solvent peak was achieved using the WATERGATE pulse scheme during acquisition (Piotto et al., 1992) and the residual water peak (4.61 ppm) was used as reference for chemical shift values.

NMR Structure Calculations

A previously established protocol was used for structure calculations (Cook et al., 2004). Unambiguously identified NOE cross peaks were converted into inter-proton distance upper bounds using the following classifications: strong (2.7 Å), medium (3.5 Å), weak (4.0 Å), and very weak (5.0 Å) (Wüthrich et al., 1983). Upper distance limits for NOEs involving methyl protons and nonstereo specifically assigned methylene protons, were corrected appropriately for center averaging by adding 1 Å to the maximum distance constraint (Wüthrich et al., 1983).

Backbone dihedral angle restraints were derived from the distance restraints and $^{3}J_{\alpha HNH}$ coupling constants using the program HABAS (Guntert et al., 1989). The obtained distance and dihedral restraints were used to calculate peptide structures using the crystallography and NMR system (CNS) software version 1.1, (Brunger et al., 1998). The protocol involved combined simulated annealing in torsional space and MD refinement in Cartesian space to produce structures with minimal restraint violations (Stein et al., 1997). A total of 100 accepted structures were subjected to energy minimization in the AMBER force field (Cornell et al., 1995;D.A. Case, 2002) using SYBYL 7.1 (Tripos Inc., St. Louis, MO). The minimized structures were then clustered based on mutual heavy-atom root mean square deviation (RMSD). The resulting structures were evaluated with the program Procheck v.3.5.4 (European Bioinformatics Institute, Cambridge, UK). The cluster of 10 structures with no restraint violation and the lowest energies were selected as the representative NMR structures.

Results and Discussion

NMR Data Analysis

Several unsuccessful attempts to acquire good quality data of NK_4-M2GlyR-p22 peptide in SDS micelles using the 500 MHz NMR instrument located at the Biomolecular NMR facility of the Biochemistry and Biophysics Department at Kansas State University were performed. These failures were attributed to a combination of instrumental limitations along with challenges on proper NMR sample preparation in SDS micelles. Optimization of the NMR sample preparation procedure to maximize peptide solubility, micelle formation and peptide insertion into the

micelles are described in the methods section of this chapter. When we tried to acquire 2D NMR ^{1}H-^{1}H TOCSY spectrum on the NK_4-M2GlyR-p22 sample in SDS micelles using the 500 MHz NMR instrument equipped with a room temperature probe, the spectrum showed broadening of NMR peaks. Figure 2-3 A shows the H^{N}- H^{α} finger print region of the TOCSY spectrum displaying severe overlapping due to broadening of most of the cross peaks.

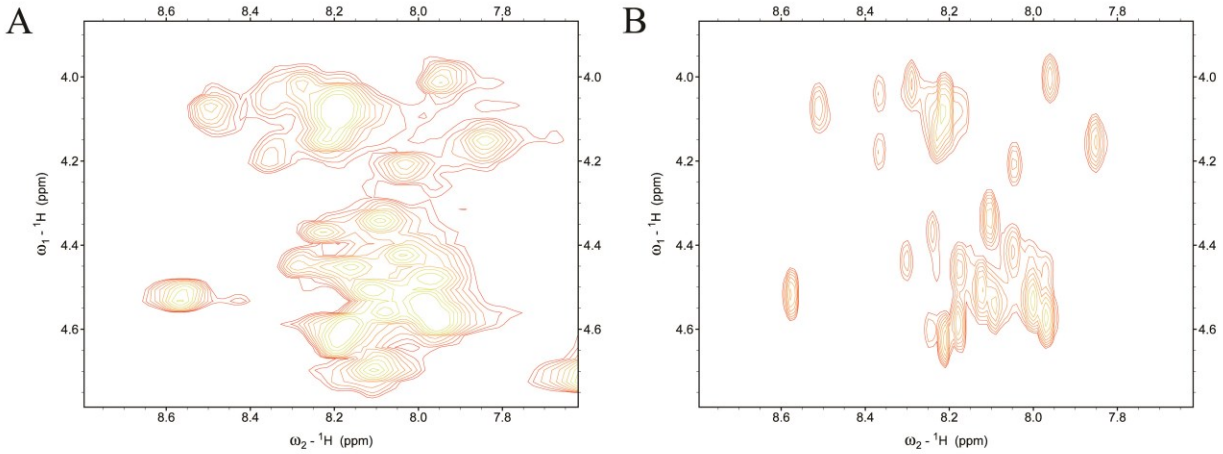

Figure 2-3. Finger print region (H^{N}- H^{α}) of TOCSY spectra collected on (A) 500 MHz room temperature probe and (B) 800 MHz cryogenic probe

The signal broadening found in the spectrum is not expected for a peptide of the size of NK_4-M2GlyR-p22 (MW = 2356.9 Da), it is the consequence of the slow tumbling caused by the effective particle size present in the sample. The aggregation number (AN) of SDS in pure water at room temperature has been reported to be around 62, and expected to increase in the presence of impurities (Bales et al., 1998). In another report the temperature effect on the aggregation of SDS micelles was studied using solutions in D_2O at different concentrations, according to this report the AN for a 500 mM solution of SDS at 45 °C is around 90 (Hammouda, 2013). With a diameter of the SDS micelles reported to be of at least 34 Å, and a concentration of micelles in

the sample of at least twice the peptide concentration (SDS concentration /AN), we assumed that the majority of micelles is the sample have one inserted peptide at the most. These considerations make the molecular weight of the particles in the samples to be at least 25,000 Da, and the observed proton linewidths more consistent with that of a 25 kDa protein. To overcome this limitation, 2D NMR spectra were acquired using a higher magnetic field spectrometer, where the signals are spread over a larger frequency range (normalized in the ppm scale for comparison). Figure 2-3 B shows the same spectral region as in part A, of a TOCSY spectrum collected at the Biomolecular NMR laboratory at the University of Kansas using a Bruker Avance 800 MHz NMR spectrometer, reduction of the signal overlapping allowed the interpretation of the spectra. Additional gain in spectral quality was obtained from the use of a cryogenically refrigerated NMR probe, these probes use a closed refrigeration helium system to cool the electronics of the probe (coils, pre-amplifiers) to a temperate near 25K (while keeping the sample at the desired experimental temperature). Decreasing the thermal vibrations responsible for most of the noise in the NMR signal increases the signal to noise ratio of the acquired signal up to 10 times compared with the signal to noise of a room temperature probe. The full 2D ^{1}H-^{1}H TOCSY spectrum after processing of NK_4-M2GlyR-p22 in SDS micelles, acquired with an 800 MHz spectrometer is shown in Figure 2-4. In similar fashion 2D ^{1}H-^{1}H DQF-COSY (Figure 2-5) and 2D ^{1}H-^{1}H NOESY with 300 and 400 ms mixing times were collected and processed.

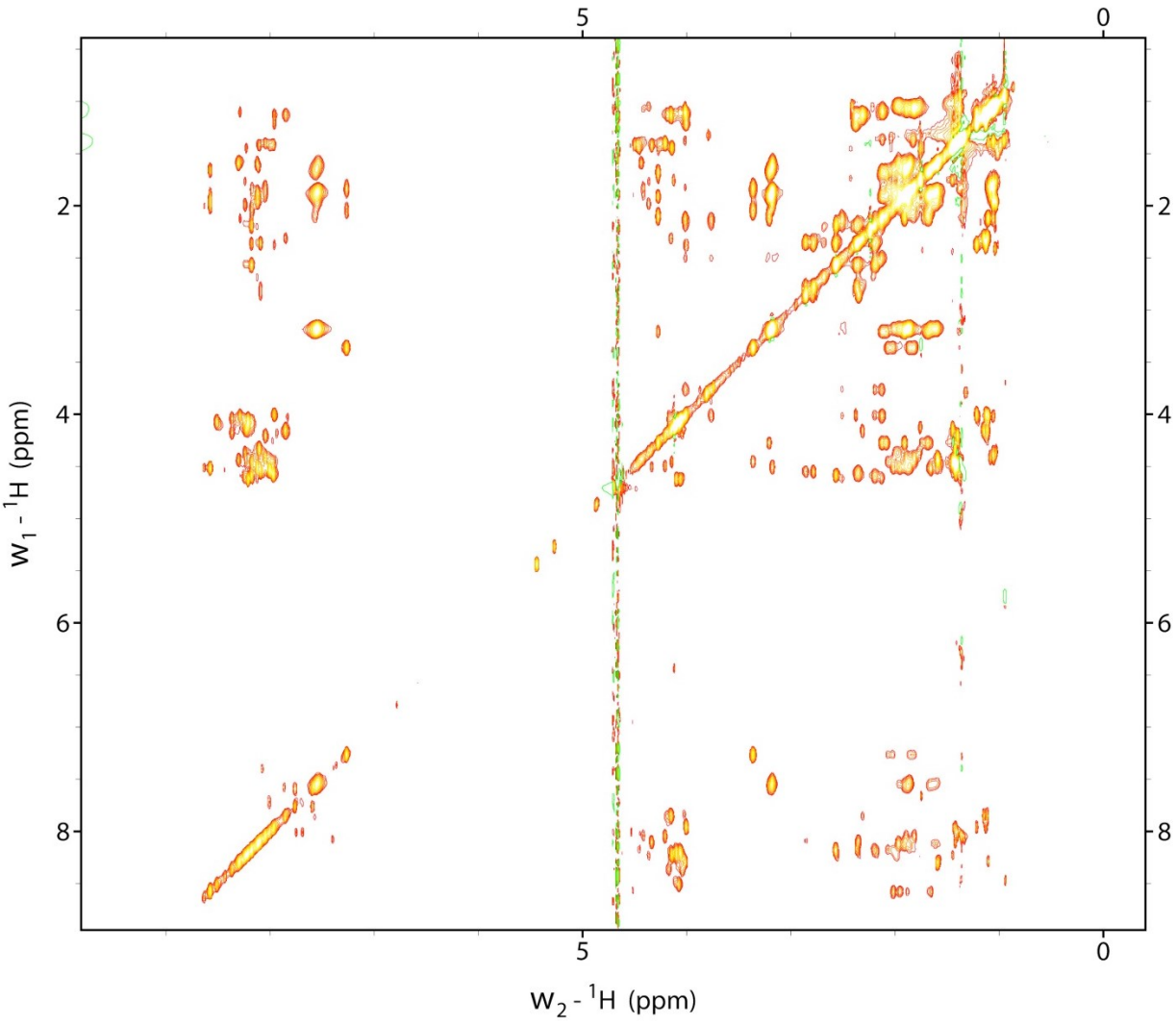

Figure 2-4. 2D ^{1}H-^{1}H TOCSY Spectrum of NK_4-M2GlyR-p22 in SDS micelles

Proton chemical shift assignments were made by standard techniques (Wüthrich, 1986) using 2D ^{1}H-^{1}H DQF-COSY and 2D ^{1}H-^{1}H TOCSY spectra for intra-residue spin systems assignment and 2D ^{1}H-^{1}H NOESY for inter residue spin system connectivities. The H^N- H^α/and sidechain proton fingerprint region of TOCSY spectrum was used to identify and assign H^N- H^α, H^N- H^β, H^N- H^γ, and H^N- H^δ intra-residue spin connectivity which was used to determine residue type in the peptide. Figure 2-6 shows H^N- H^α, H^N- H^β, H^N- H^γ, and H^N- H^δ cross peak assignments in the

finger print region of the TOCSY spectrum used for residue identification. In the same way the finger print region containing H^N- H^α cross peaks in 2D NOESY spectra were used to identify $d_{\alpha N}(i,i+1)$ proton connectivity for sequential assignments and differentiation of repeated amino acid residues (e.g. K 1-4 T 13, 14, 17, 19, 20). The resulting chemical shift values for the unambiguously assigned proton resonances are presented in Table 2-1.

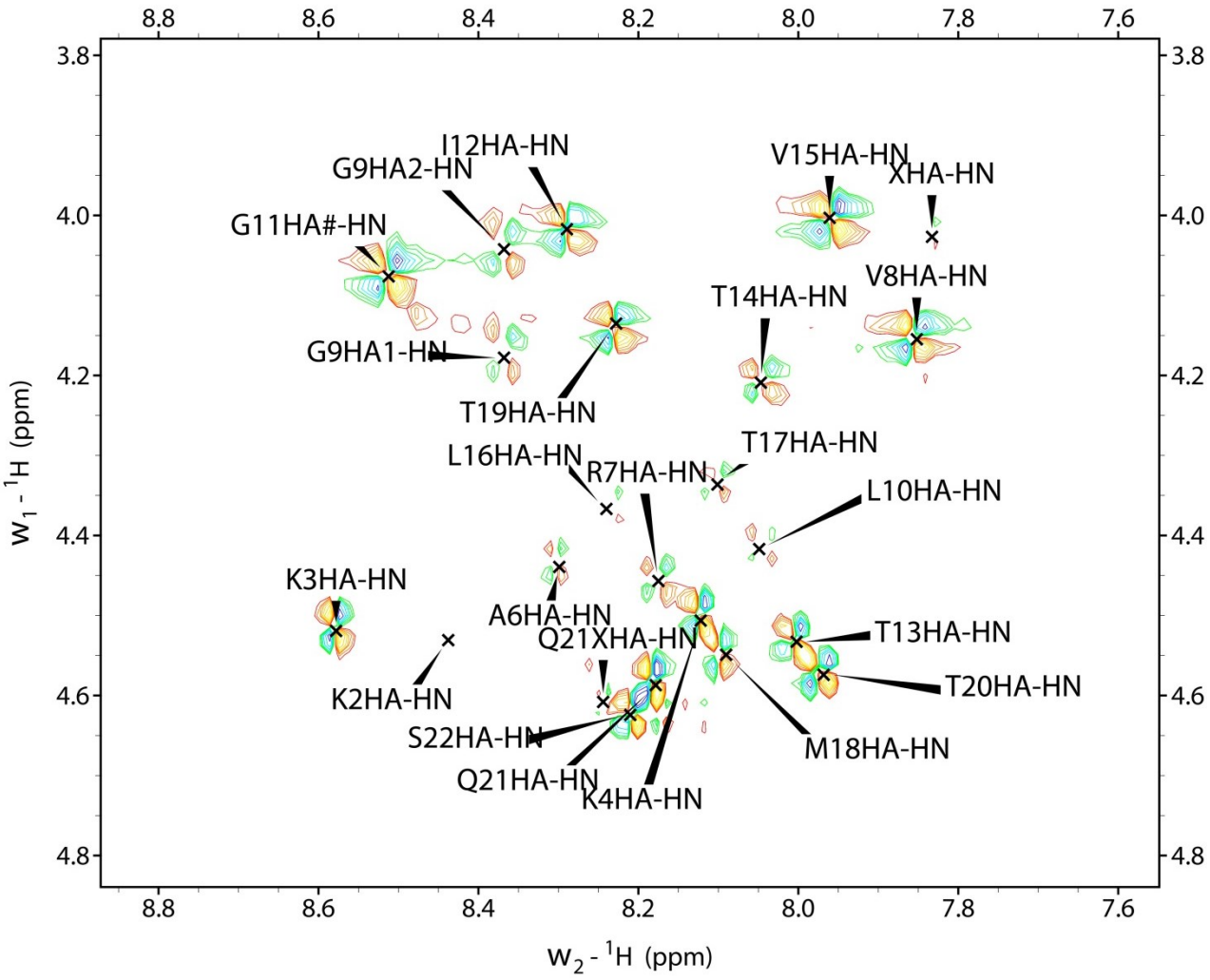

Figure 2-5. Finger print (H^N- H^α) region of 2D ^{1}H-^{1}H DQF-COSY spectrum of NK_4-M2GlyR-p22. Showing labeled assignments. All assigned spectra are labeled using X-PLOR nomenclature (HA=H^α, HN=H^N, HB=H^β, HG=H^γ, HG=H^ε)

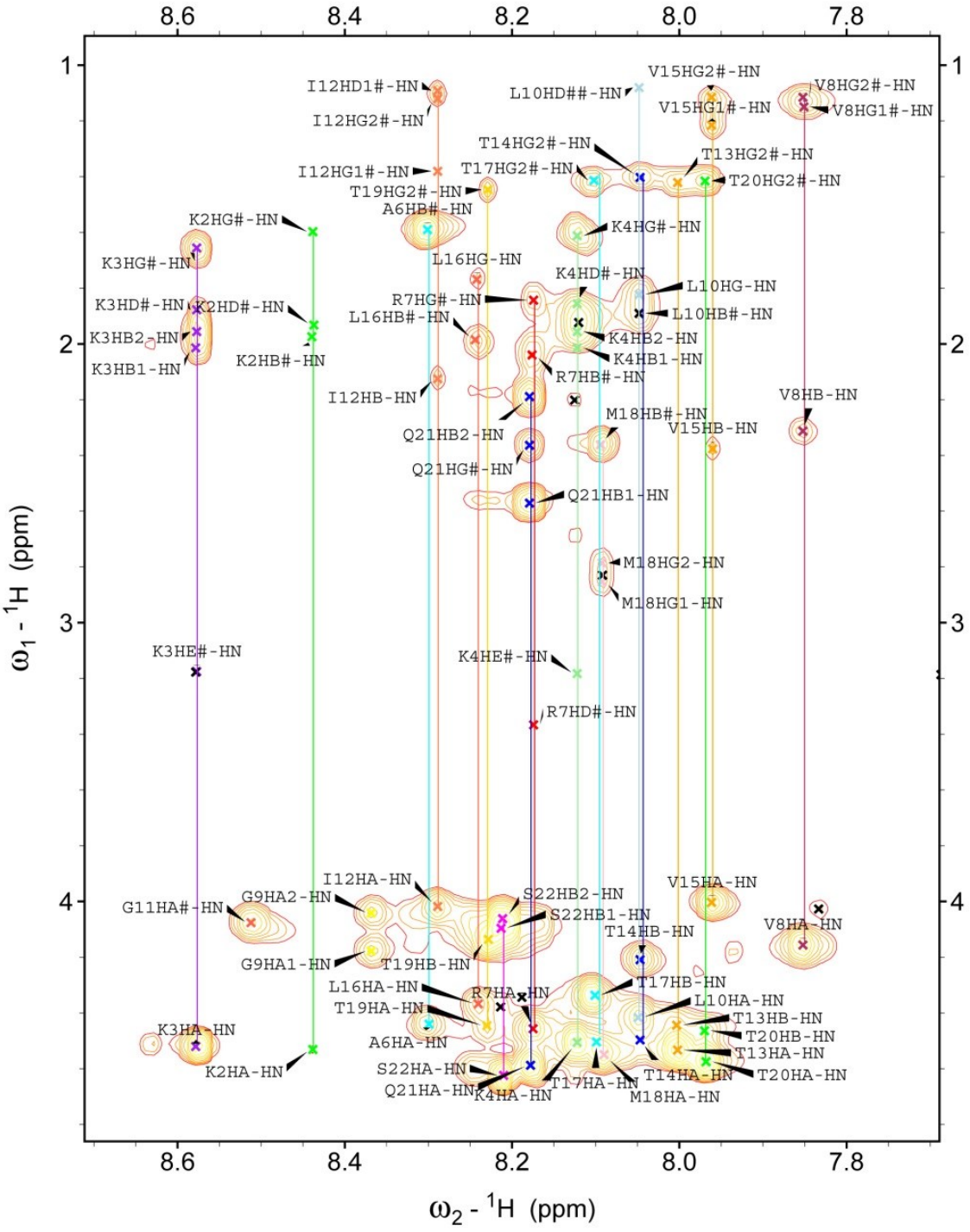

Figure 2-6. 2D ^{1}H-^{1}H TOCSY finger print (H^N- H^α and side chain protons) spectral region for NK_4-M2GlyR-p22. Showing individual amino acid spin systems connected with a vertical line and labeled assignments

Table 2-1. Chemical Shift Values (ppm) for NK_4-M2GlyR-p22 in SDS micelles

Residue	*Chemical Shift (ppm)*				
	H^N	H^α	H^β	H^γ	*Others*
K1			2.12 2.08	1.69	δ 1.91 ε 3.19
K2	8.44	4.53	1.97	1.60	δ 1.93
K3	8.58	4.51	2.01 1.96	1.66	δ 1.88 ε 3.18
K4	8.12	4.50	2.02	1.96	δ 1.86 ε 3.18
P5		4.62	2.51 2.19	2.12	δ 4.01 3.76
A6	8.30	4.44	1.59		
R7	8.18	4.46	2.04	1.84	δ 3.37 NεH 7.26
V8	7.85	4.15	2.31	1.15 1.11	
G9	8.37	4.11			
L10	8.05	4.42	1.89	1.82	δ 1.08
G11	8.51	4.07			
I12	8.29	4.02	2.12	1.38 1.12	δ 1.09
T13	8.00	4.53	4.44	1.42	
T14	8.05	4.21	4.50	1.41	
V15	7.96	4.00	2.37	1.21 1.12	
L16	8.24	4.37	1.99	1.77	
T17	8.10	4.34	4.50	1.41	
M18	8.09	4.55	2.36	2.85 2.78	
T19	8.23	4.14	4.45	1.45	
T20	7.97	4.57	4.46	1.42	
Q21	8.18	4.59	2.57 2.19	2.36	
S22	8.21	4.62	4.1 4.06		

Chemical shift dispersion for the H^N and H^α protons indicate a folded structure for the peptide in the micelle environment. The nature of the parent sequence as well as the previously determined

structure of the NK_4-M2GlyR-p22 S22W make the overall structure of NK_4-M2GlyR-p22 expected to be of mostly helical nature in SDS micelles. The Chemical Shift Index (CSI) was calculated based on the shifted H^{α} resonances as the difference in chemical shift compared to the random coil values reported by Wishart et al. (Wishart and Nip, 1998). A negative CSI value (<-0.10 ppm, upfield shift) suggests a turn in the structure and several consecutive residues with negative CSI values indicate a presence of a helix. A series of positive CSI values (>0.10 ppm, downfield shift) suggest the presence of a β-strand. Since the random coil chemical shifts used are reported for an aqueous solution at 25°C, a more pertinent source of references values was selected, the new values were calculated based on the peptide sequence with a sequence-dependent correction and a temperature correction as well, (Kjaergaard et al., 2011;Kjaergaard and Poulsen, 2011) the resulting corrected CSI values are reported in Table 2-2. The resulting CSI plot for NK_4-M2GlyR-p22 H^{α} protons is shown in Figure 2-7.

Table 2-2. Chemical Shift Index Values for NK_4-M2GlyR-p22 H^{α} protons

Residue	*H^{α} Experimental (ppm)*	*H^{α} Corrected Reference (ppm)*	*CSI (ppm)*
K2	4.53	4.29	0.24
K3	4.51	4.31	0.20
K4	4.50	4.60	-0.09
P5	4.62	4.41	0.21
A6	4.44	4.29	0.15
R7	4.46	4.39	0.07
V8	4.15	4.11	0.04
G9	4.11	4.02	0.09
L10	4.42	4.37	0.05

G11	4.07	4.03	0.04
I12	4.02	4.27	-0.26
T13	4.53	4.48	0.06
T14	4.21	4.40	-0.19
V15	4.00	4.14	-0.14
L16	4.37	4.44	-0.07
T17	4.34	4.36	-0.02
M18	4.55	4.61	-0.06
T19	4.14	4.45	-0.31
T20	4.57	4.38	0.19
Q21	4.59	4.42	0.16
S22	4.62	4.43	0.20

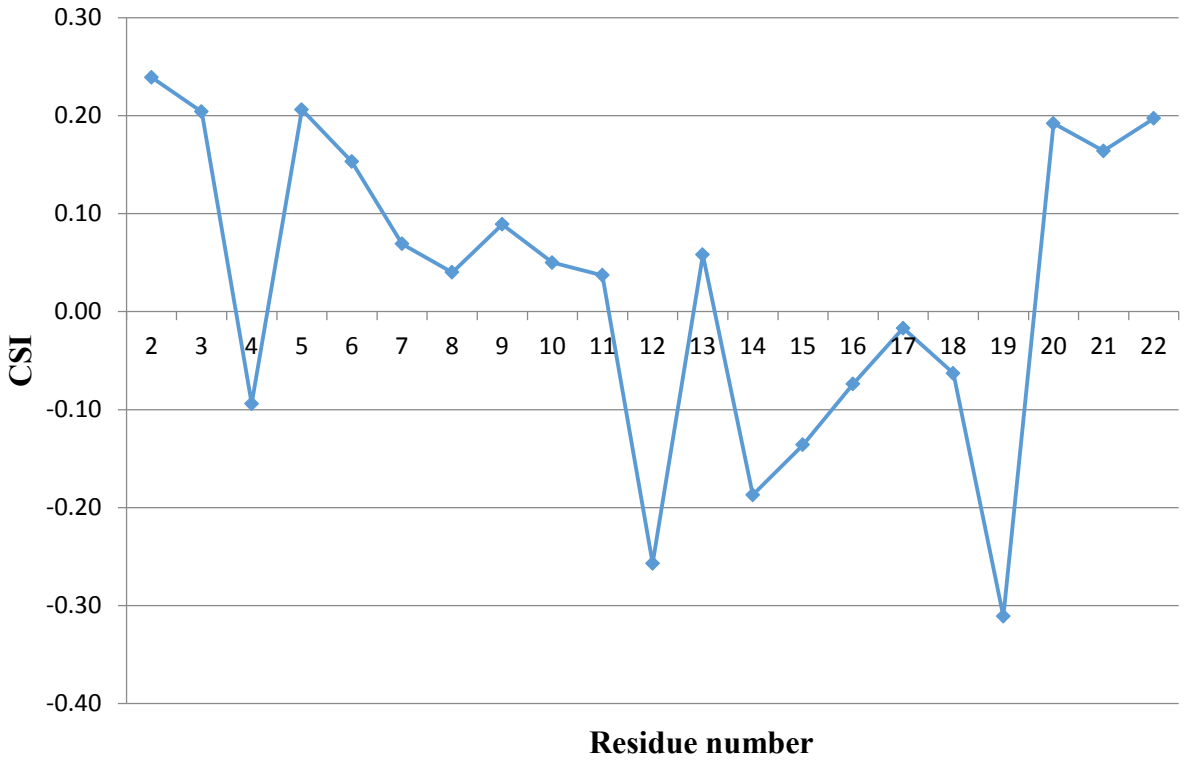

Figure 2-7. Chemical Shift Index (CSI) plot for H^{α} protons of NK_4-M2GlyR-p22 calculated using temperature and sequence corrected values

Most of the calculated CSI values have an absolute value under 0.1 making them not suitable for a prediction of secondary structure. The residues with CSI absolute value greater than 0.1 (2-3, 5-6, 2, 14-15, 19, 20-22) are in short stretches of mostly 1 or 2 residues, also making any prediction of secondary structure for this residues unreliable. The calculation of the CSI was not able to provide the prediction of secondary structure that was expected, and has been reported during the structure calculations of M2GlyR derived peptides before (Cook et al., 2004).

Detailed analysis of the NOESY data, by concurrently evaluating the 300 ms and 400 ms mixing time spectra (to confirm or reject ambiguous NOESY peaks) revealed short and medium range connectivities including, $d_{\alpha N}(i, i+1)$, $d_{\beta N}(i, i+1)$, $d_{NN}(i, i+1)$, $d_{\alpha N}(i, i+2)$ and $d_{\alpha N}(i, i+3)$ that are consistent with a helical conformation (Wüthrich, 1986). An example of NOESY spectra showing inter-residue as well as intra-residue cross peaks including sequential and medium range connectivities is presented in Figure 2-8 overlaid with the TOCSY spectrum in order to highlight the presence of pure NOESY peaks. Cross peaks corresponding to $d_{NN}(i, i+1)$ connectivities indicative of helical conformation are shown in Figure 2-9. A graphic summary of all sequential and medium range NOE connectivity for NK_4-M2GlyR-p22 in SDS micelles is presented in Figure 2-10. NOE characteristic of helical conformation are observed from residues alanine 6 to threonine 20.These results suggest a continuous stretch of helical conformation for NK_4-M2GlyR-p22 in SDS micelles.

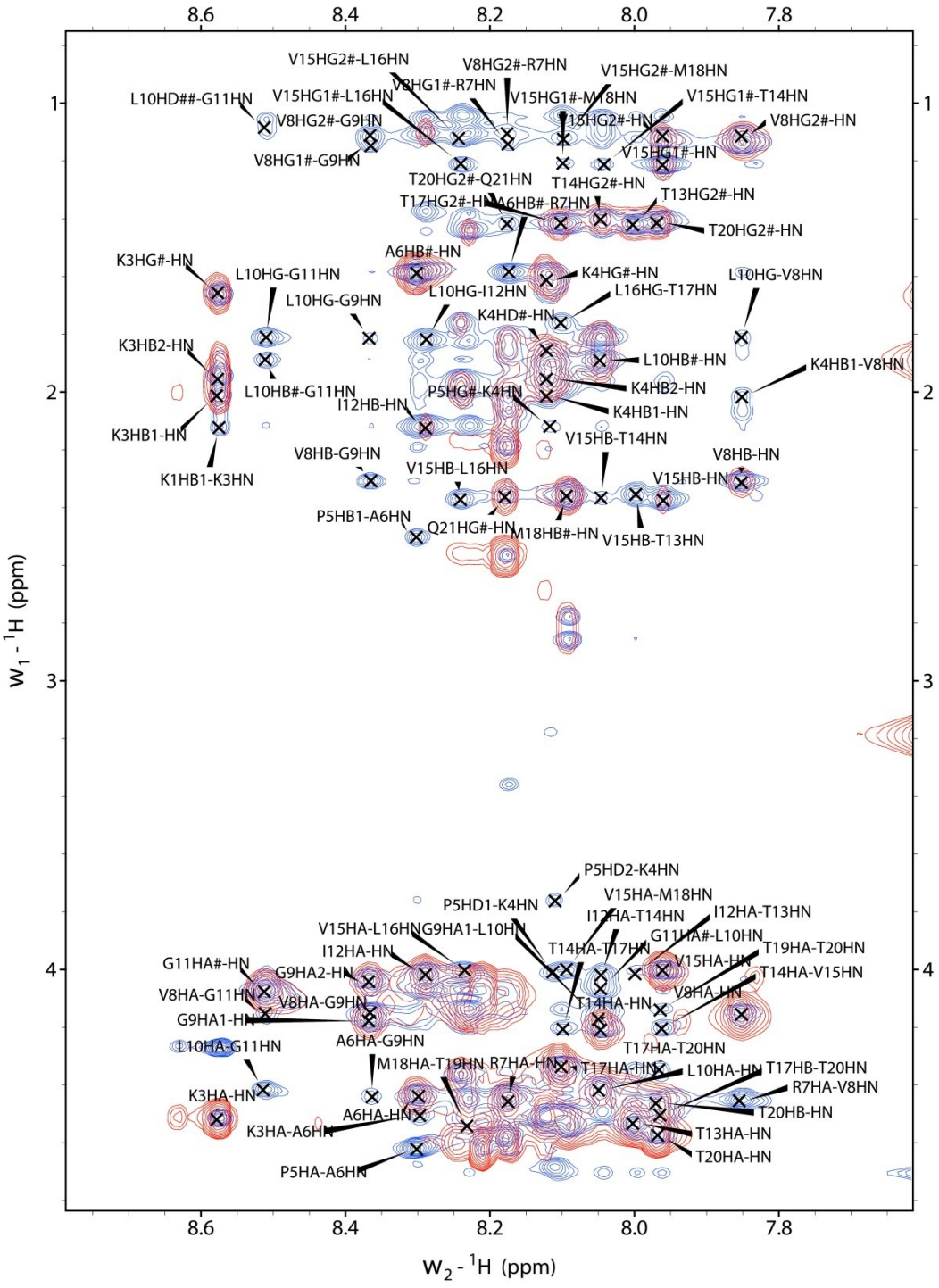

Figure 2-8. Overlay of 2D ^{1}H-^{1}H NOESY spectrum (blue) over 2D ^{1}H-^{1}H TOCSY spectrum (red), finger print spectral region (H^{N}- H^{α} and side chain protons) for NK_4-M2GlyR-p22

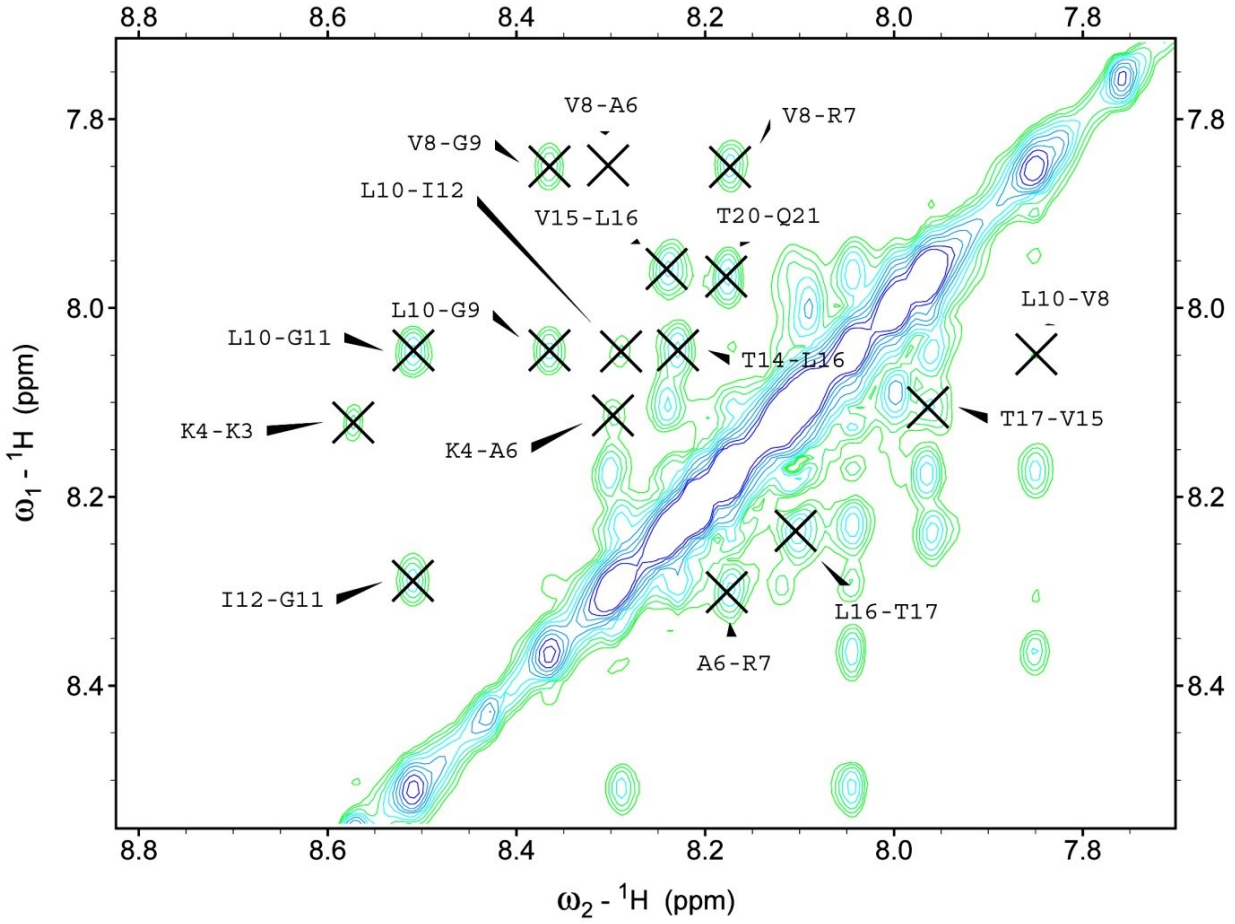

Figure 2-9. H^N-H^N region of 2D ^{1}H-^{1}H NOESY spectrum acquired with 400ms mixing time, showing $d_{NN}(i,i+1)$ connectivities

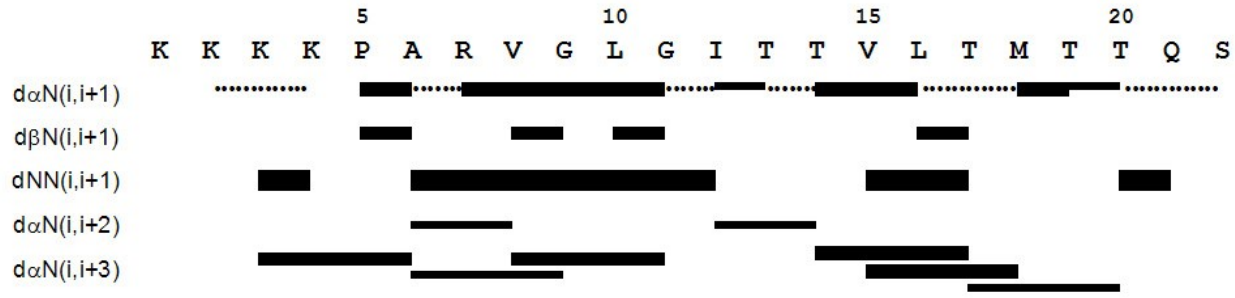

Figure 2-10: Summary of NOE connectivity for peptide NK_4-M2GlyR-p22 in SDS micelles. Line thickness indicates peak intensity, and dotted line indicates ambiguity due to peak overlapping

NMR Structure Calculations

For the structure calculations unambiguously assigned NOE cross peaks, from both the 400 ms and the 300 ms 2D ^{1}H-^{1}H NOESY spectra, were classified as: intra-residue, sequential, medium range (between protons from four or less, but more than two residues apart), and long range (between proton from more than four residues apart); and converted into a total of 117 distance constraints as described in the methods section. Among the distance constraints generated, 38 were intra-residue, 53 sequential, and 26 were medium range. From the 2D ^{1}H-^{1}H DQF-COSY spectrum 18 dihedral angle constraints were obtained. The generated distance and dihedral angle constraints summarized in Table 2-3 were used to calculate structure ensembles with help of CNS software. The cluster of 10 structures with the lowest total energies, and no distance violation >0.5 Å or dihedral violation >5° for NK_4-M2GlyR-p22 in SDS micelles is shown in Figure 2-11.The backbone ψ and φ angles distribution of the calculated energy-minimized structures were evaluated against the Ramachandran Plot values using the PROCHECK program (Laskowski et al., 1996). More than 99% of the ψ and φ angles of the peptide backbone cluster were found to reside within the allowed regions; these results are also summarized in Table 2-3. The average structure of NK_4-M2GlyR-p22 after molecular dynamics refinement in implicit membrane is shown in Figure 2-12a. This refined monomer structure was used as the starting point to construct putative pentameric channels as described in the appendix section of this chapter.

Table 2-3. Structural Statistics for peptide NK_4-M2GlyR-p22 in SDS micelles

Experimental NMR Constraints	
NOE Distance Constraints	
Intra-residue	38
Sequential	53
Medium Range	26
Long Range	0
Angle Constraints	18
Energy (kcal/mol^{-1})	
E_{total}	-52.9±16.08
RMSD from the mean structure (Å)	
Backbone of the helical segment (residues 6-20)	0.46 ± 0.12
Ramachandran statistics	
Residues in allowed regions	> 99%
Residues in generously allowed regions	< 1%
Residues in disallowed regions	0

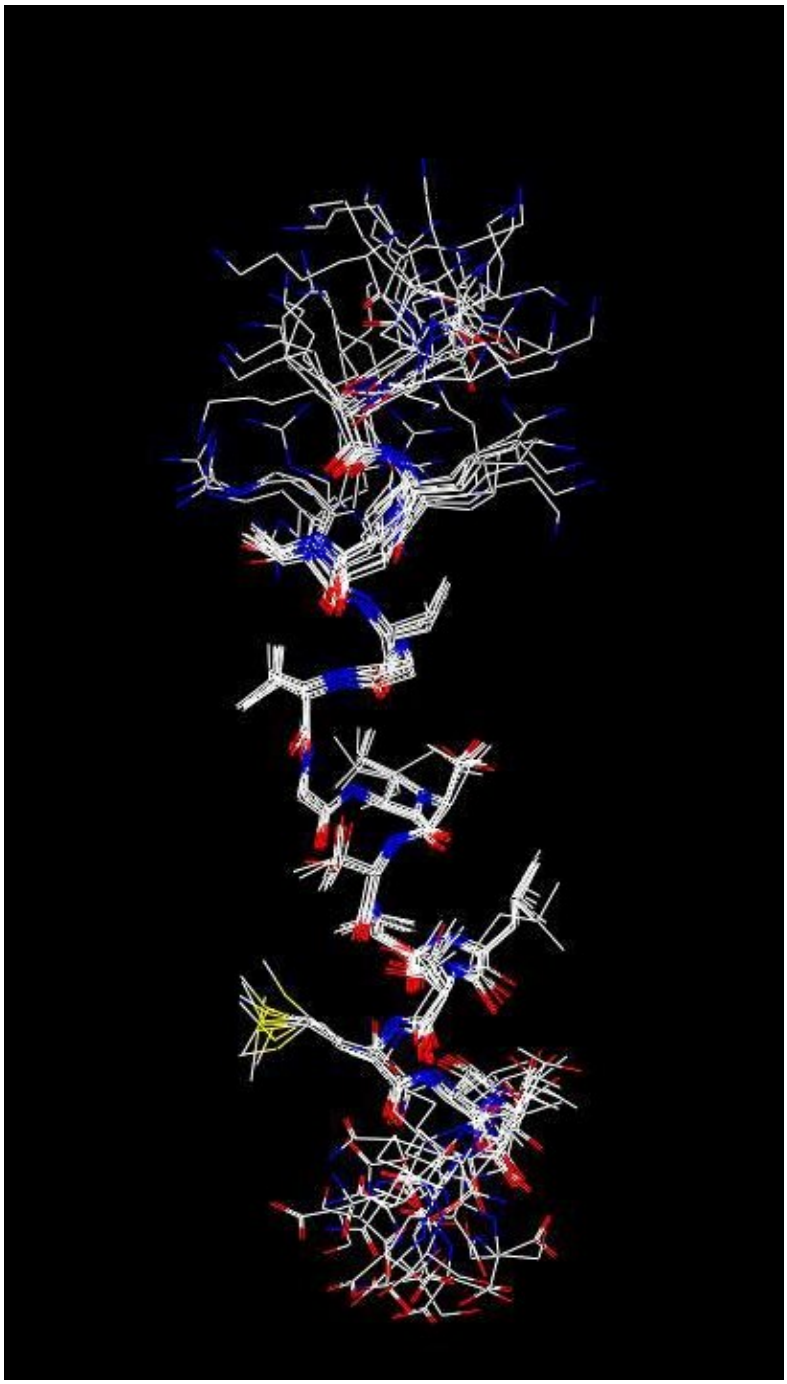

Figure 2-11. Solution monomeric structure of peptide NK_4-M2GlyR-p22 in SDS micelles. Cluster of the 10 calculated structures with the lowest energies superimposed

Discussion and Analysis

The determined NMR structure for NK_4-M2GlyR-p22 peptide in SDS micelles clearly shows a linear and mostly helical conformation from residues 6-20. The N-terminal lysine residues are largely unstructured and flexible. The hydrophobic and hydrophilic side chains of the residues in the helix are segregated to different sides of the helix, as expected for a channel forming transmembrane segment. The average structure of NK_4-M2GlyR-p22 in SDS micelles has the same characteristics (unstructured N-terminus, amphipathic helix) as the solution structure previously determined in a 40% TFE solution (Cook et al., 2004). The structure in micelles appears better defined for residues proline 5 to arginine 7 when compared with the 40% TFE structure, potentially due to a more restrictive environment found in the interior of the micelles. The whole structure in micelles is better defined, as the calculated structures in TFE solution showed a RMSD to the mean structure for residues 9-20 of 1.95± 0.6 Å (Cook et al., 2004), whereas the cluster of structures in SDS micelles showed a RMSD to the mean structure (residues 6-20) of 0.46 ± 0.12 Å.

Although the structure determined in SDS micelles has the expected conformation, the CSI calculation was not able to predict it even when the best available reference chemical shifts for random coil were used. The prediction of secondary structure by calculation of the CSI is based on a statistical analysis of calculated structures and comparison of their corresponding residue assignments with the chemical shift values found for extended peptides in a simple solvent system (Mielke and Krishnan, 2004). This method has been found useful even in solid-state NMR, but the results presented here show that a prediction cannot always be made for a compartmentalized solution system like micelles in an aqueous solution.

The average structure for peptide NK_4-M2GlyR-p22 in SDS micelles also shows resemblance to the average structure calculated for peptide NK_4-M2GlyR-p22 S22W (Figure 2-12b) in a similar environment (Herrera et al., 2010). Figure 2-12 shows the two average structures side by side, with the backbone as a blue tube. In the average structures it can be visualized that both peptides have a similar helical conformation on most of the length (residue 6-20) of the peptide. The NK_4-M2GlyR-p22 S22W shows a convexity while NK_4-M2GlyR-p22 has a more linear axis in the central portion of the structure. For both peptides a relative unstructured state of the N-terminal lysines is observed, that is more pronounced for the NK_4-M2GlyR-p22 sequence. These lysines are predicted to be out of the micelle exposed to the aqueous environment and/or interacting with the sulfate groups from the SDS molecules, the C-terminus of NK_4-M2GlyR-p22 also shows greater variability compared with NK_4-M2GlyR-p22 S22W possibly due to lacking the anchoring tryptophan residue. As mentioned in the methods section, the acquisition of the spectra for NK_4-M2GlyR-p22 was particularly challenging, as the spectra suffered from peak broadening and decreased signal to noise ratio (compared to the same peptide in TFE:water solution and NK_4-M2GlyR-p22 S22W in SDS micelles); this could be due to a greater flexibility or freedom for NK_4-M2GlyR-p22 compared with NK_4-M2GlyR-p22 S22W in the membrane-like environment.

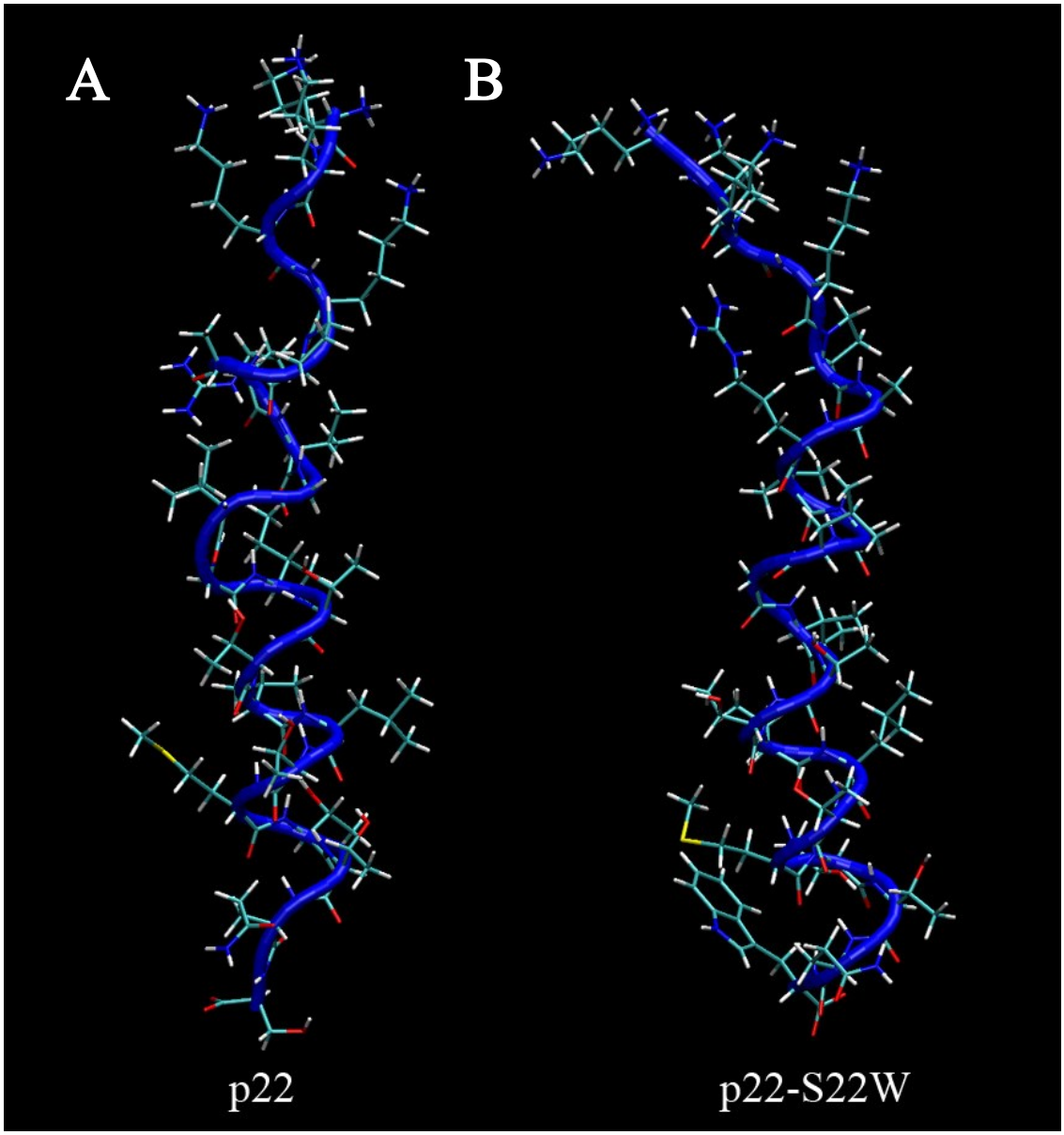

Figure 2-12. Average monomeric solution structures in SDS micelles for peptides: (A) NK_4-M2GlyR-p22; (B) NK_4-M2GlyR-p22 S22W

The flexibility found in the N-terminus as well as in the C-terminal residues is consistent with the findings of the whole cell patch clamp measurements of the current-voltage relation that showed inward rectification at positive voltages, (Shank et al., 2006) as this flexibility can play a role in allowing the channel assembly the required conformational changes at different

transmembrane voltages. Furthermore the higher peptide concentration required by NK_4-M2GlyR-p22 compared with NK_4-M2GlyR-p22 S22W to reach one-half I_{max} on epithelial monolayers (210 ± 70 μM for NK_4-M2GlyR-p22 to 45 ± 6 μM for NK_4-M2GlyR-p22 S22W) , (Figure 2-1) could be attributed not only to the soluble associations formed by the peptide in the aqueous environment, but also to the higher conformational flexibility in the membrane environment, that may negatively impact the stability of the assembled ion channel.

Appendix A - Chapter 2 describes the computational assemblies and molecular dynamics simulations performed on the ion channels formed by NK_4-M2GlyR peptides, based on the calculated NMR solution structures. Computational studies refine and validate NMR structural models, and characterize the structural and dynamic properties of the channel in fully solvated model membrane bilayers. A key validation is to examine how a single S22W mutation impacts the channel characteristics and subsequently membrane insertion efficacy, assembly and channel properties.

In summary, the determined NMR structures of NK_4-M2GlyR-p22 in SDS micelles and in TFE solution show many similarities. However the NMR structure of NK_4-M2GlyR-p22 in SDS micelles shows some similarities to the structure determined for the NK_4-M2GLYR-p22 S22W peptide, but with notable differences that can help explain the physical and biological differences found between the two peptides. These results serve to better understand the determining factors for the desired characteristics of an optimized therapeutic peptide. The structural characterization supports the initial postulation that the S22W mutation helps in anchoring the pore to the membrane and reduces the flexibility of the whole assembly. The implied increased stability of

the NK_4-M2GlyR-p22 S22W channel explains the steeper short circuit current-concentration slope measured experimentally (Figure 2-1). Furthermore, according to the simulations, the introduction of the C-terminal tryptophan appears to lead to global changes of the channel structure.

References

Bales, B. L., Messina, L., Vidal, A., Peric, M. and Nascimento, O. R. (1998). Precision relative aggregation number determinations of SDS micelles using a spin probe. A model of micelle surface hydration. *Journal of Physical Chemistry B* **102**, 10347-10358.

Bax, A. and Davis, D. G. (1985). Mlev-17-Based Two-Dimensional Homonuclear Magnetization Transfer Spectroscopy. *Journal of Magnetic Resonance* **65**, 355-360.

Bax, A. and Freeman, R. (1981). Investigation of Complex Networks of Spin-Spin Coupling by Two-Dimensional Nmr. *Journal of Magnetic Resonance* **44**, 542-561.

Billeter, M., Braun, W. and Wuthrich, K. (1982). Sequential resonance assignments in protein 1H nuclear magnetic resonance spectra. Computation of sterically allowed proton-proton distances and statistical analysis of proton-proton distances in single crystal protein conformations. *Journal of molecular biology* **155**, 321-346.

Braun, W. and Go, N. (1985). Calculation of protein conformations by proton-proton distance constraints. A new efficient algorithm. *Journal of molecular biology* **186**, 611-626.

Brooks, B. R., Brooks, C. L., 3rd, Mackerell, A. D., Jr., Nilsson, L., Petrella, R. J., Roux, B., Won, Y., Archontis, G., Bartels, C., Boresch, S., Caflisch, A., Caves, L., Cui, Q., Dinner, A. R., Feig, M., Fischer, S., Gao, J., Hodoscek, M., Im, W., Kuczera, K., Lazaridis, T., Ma, J., Ovchinnikov, V., Paci, E., Pastor, R. W., Post, C. B., Pu, J. Z., Schaefer, M., Tidor, B., Venable, R. M., Woodcock, H. L., Wu, X., Yang, W., York, D. M. and Karplus, M. (2009). CHARMM: the biomolecular simulation program. *Journal of computational chemistry* **30**, 1545-1614.

Brooks, B. R., Bruccoleri, R. E., Olafson, B. D., States, D. J., Swaminathan, S. and Karplus, M. (1983). CHARMM: A program for macromolecular energy, minimization, and dynamics calculations. *Journal of Computational Chemistry* **4**, 187-217.

Broughman, J. R., Brandt, R. M., Hastings, C., Iwamoto, T., Tomich, J. M. and Schultz, B. D. (2004). Channel-forming peptide modulates transepithelial electrical conductance and solute permeability. *American journal of physiology. Cell physiology* **286**, C1312-1323.

Broughman, J. R., Mitchell, K. E., Sedlacek, R. L., Iwamoto, T., Tomich, J. M. and Schultz, B. D. (2001). NH(2)-terminal modification of a channel-forming peptide increases capacity for epithelial anion secretion. *American journal of physiology. Cell physiology* **280**, C451-458.

Broughman, J. R., Shank, L. P., Prakash, O., Schultz, B. D., Iwamoto, T., Tomich, J. M. and Mitchell, K. (2002a). Structural implications of placing cationic residues at either the NH2- or COOH-terminus in a pore-forming synthetic peptide. *The Journal of membrane biology* **190**, 93-103.

Broughman, J. R., Shank, L. P., Takeguchi, W., Schultz, B. D., Iwamoto, T., Mitchell, K. E. and Tomich, J. M. (2002b). Distinct structural elements that direct solution aggregation and membrane assembly in the channel-forming peptide M2GlyR. *Biochemistry* **41**, 7350-7358.

Brunger, A. T., Adams, P. D., Clore, G. M., DeLano, W. L., Gros, P., Grosse-Kunstleve, R. W., Jiang, J. S., Kuszewski, J., Nilges, M., Pannu, N. S., Read, R. J., Rice, L. M., Simonson, T. and Warren, G. L. (1998). Crystallography & NMR system: A new software suite for macromolecular structure determination. *Acta Crystallogr D Biol Crystallogr* **54 (Pt 5)**, 905-921.

Bukovnik, U., Gao, J., Cook, G. A., Shank, L. P., Seabra, M. B., Schultz, B. D., Iwamoto, T., Chen, J. and Tomich, J. M. (2012). Structural and biophysical properties of a synthetic channel-forming peptide: designing a clinically relevant anion selective pore. *Biochimica et biophysica acta* **1818**, 1039-1048.

Bukovnik, U., Sala-Rabanal, M., Francis, S., Frazier, S. J., Schultz, B. D., Nichols, C. G. and Tomich, J. M. (2013). Effect of Diaminopropionic Acid (Dap) on the Biophysical Properties of a Modified Synthetic Channel-Forming Peptide. *Molecular pharmaceutics* **10**, 3959-3966.

Cannon, S. C. (2007). Physiologic principles underlying ion channelopathies. *Neurotherapeutics* **4**, 174-183.

Clore, G. M. and Gronenborn, A. M. (1989). Determination of three-dimensional structures of proteins and nucleic acids in solution by nuclear magnetic resonance spectroscopy. *Crit Rev Biochem Mol Biol* **24**, 479-564.

Cook, G. A., Prakash, O., Zhang, K., Shank, L. P., Takeguchi, W. A., Robbins, A., Gong, Y. X., Iwamoto, T., Schultz, B. D. and Tomich, J. M. (2004). Activity and structural

comparisons of solution associating and monomeric channel-forming peptides derived from the glycine receptor m2 segment. *Biophys J* **86**, 1424-1435.

Cornell, W. D., Cieplak, P., Bayly, C. I., Gould, I. R., Merz, K. M., Ferguson, D. M., Spellmeyer, D. C., Fox, T., Caldwell, J. W. and Kollman, P. A. (1995). A 2nd Generation Force-Field for the Simulation of Proteins, Nucleic-Acids, and Organic-Molecules. *Journal of the American Chemical Society* **117**, 5179-5197.

D.A. Case, D. A. P., J.W. Caldwell, T.E. Cheatham III, J. Wang, W.S. Ross, C.L. Simmerling, T.A. Darden, K.M. Merz, R.V. Stanton, A.L. Cheng, J.J. Vincent, M. Crowley, V. Tsui, H. Gohlke, R.J. Radmer, Y. Duan, J. Pitera, I. Massova, G.L. Seibel, U.C. Singh, P.K. Weiner and P.A. Kollman (2002). AMBER 7.

Darden, T., York, D. and Pedersen, L. (1993). Particle Mesh Ewald - an N.Log(N) Method for Ewald Sums in Large Systems. *Journal of Chemical Physics* **98**, 10089-10092.

Delaglio, F., Grzesiek, S., Vuister, G. W., Zhu, G., Pfeifer, J. and Bax, A. (1995). NMRPipe: a multidimensional spectral processing system based on UNIX pipes. *J Biomol NMR* **6**, 277-293.

Gao, L., Broughman, J. R., Iwamoto, T., Tomich, J. M., Venglarik, C. J. and Forman, H. J. (2001). Synthetic chloride channel restores glutathione secretion in cystic fibrosis airway epithelia. *Am J Physiol Lung Cell Mol Physiol* **281**, L24-30.

Goddard, T. D. and Kneller, D. G. (2004). SPARKY 3. University of California, San Francisco.

Guntert, P., Braun, W., Billeter, M. and Wuthrich, K. (1989). Automated Stereospecific H-1-Nmr Assignments and Their Impact on the Precision of Protein-Structure Determinations in Solution. *Journal of the American Chemical Society* **111**, 3997-4004.

Hammouda, B. (2013). Temperature Effect on the Nanostructure of SDS Micelles in Water. *Journal of Research of the National Institute of Standards and Technology* **118**, 151-167.

Han, G. W., Deng, Y. F., Glimm, J. and Martyna, G. (2007). Error and timing analysis of multiple time-step integration methods for molecular dynamics. *Computer Physics Communications* **176**, 271-291.

Havel, T. F., Kuntz, I. D. and Crippen, G. M. (1983). The combinatorial distance geometry method for the calculation of molecular conformation. I. A new approach to an old problem. *Journal of theoretical biology* **104**, 359-381.

Herrera, A. I., Al-Rawi, A., Cook, G. A., Gao, J., Iwamoto, T., Prakash, O., Tomich, J. M. and Chen, J. (2010). Structural characterization of two pore-forming peptides: consequences of introducing a C-terminal tryptophan. *Proteins* **78**, 2238-2250.

Humphrey, W., Dalke, A. and Schulten, K. (1996). VMD: visual molecular dynamics. *J Mol Graph* **14**, 33-8, 27-28.

Im, W., Feig, M. and Brooks, C. L., 3rd. (2003). An implicit membrane generalized born theory for the study of structure, stability, and interactions of membrane proteins. *Biophysical journal* **85**, 2900-2918.

Jentsch, T. J., Stein, V., Weinreich, F. and Zdebik, A. A. (2002). Molecular structure and physiological function of chloride channels. *Physiological reviews* **82**, 503-568.

Jo, S., Kim, T. and Im, W. (2007). Automated builder and database of protein/membrane complexes for molecular dynamics simulations. *PloS one* **2**, e880.

Jo, S., Kim, T., Iyer, V. G. and Im, W. (2008). CHARMM-GUI: a web-based graphical user interface for CHARMM. *Journal of computational chemistry* **29**, 1859-1865.

Karplus, M. (1959). Contact Electron-Spin Coupling of Nuclear Magnetic Moments. *Journal of Chemical Physics* **30**, 11-15.

Kim, J. B. (2014). Channelopathies. *Korean journal of pediatrics* **57**, 1-18.

Kjaergaard, M., Brander, S. and Poulsen, F. M. (2011). Random coil chemical shift for intrinsically disordered proteins: effects of temperature and pH. *Journal of biomolecular NMR* **49**, 139-149.

Kjaergaard, M. and Poulsen, F. M. (2011). Sequence correction of random coil chemical shifts: correlation between neighbor correction factors and changes in the Ramachandran distribution. *Journal of biomolecular NMR* **50**, 157-165.

Koradi, R., Billeter, M. and Wuthrich, K. (1996). MOLMOL: a program for display and analysis of macromolecular structures. *Journal of molecular graphics* **14**, 51-5, 29-32.

Kumar, A., Ernst, R. R. and Wuthrich, K. (1980). A Two-Dimensional Nuclear Overhauser Enhancement (2d Noe) Experiment for the Elucidation of Complete Proton-Proton Cross-Relaxation Networks in Biological Macromolecules. *Biochemical and Biophysical Research Communications* **95**, 1-6.

Laskowski, R. A., Rullmannn, J. A., MacArthur, M. W., Kaptein, R. and Thornton, J. M. (1996). AQUA and PROCHECK-NMR: programs for checking the quality of protein structures solved by NMR. *Journal of biomolecular NMR* **8**, 477-486.

Lee, J. and Im, W. (2008). Transmembrane helix tilting: Insights from calculating the potential of mean force. *Physical Review Letters* **100**.

McNaught, A. D. and Wilkinson, A. (1997). IUPAC. Compendium of Chemical Terminology, 2nd ed. (the "Gold Book"). Blackwell Scientific Publications.

Mielke, S. P. and Krishnan, V. V. (2004). An evaluation of chemical shift index-based secondary structure determination in proteins: influence of random coil chemical shifts. *Journal of biomolecular NMR* **30**, 143-153.

Montal, M. and Opella, S. J. (2002). The structure of the M2 channel-lining segment from the nicotinic acetylcholine receptor. *Biochimica Et Biophysica Acta-Biomembranes* **1565**, 287-293.

Nanzer, A. P., Poulsen, F. M., Vangunsteren, W. F. and Torda, A. E. (1994). A Reassessment of the Structure of Chymotrypsin Inhibitor-2 (Ci-2) Using Time-Averaged Nmr Restraints. *Biochemistry* **33**, 14503-14511.

Nilges, M., Clore, G. M. and Gronenborn, A. M. (1988a). Determination of three-dimensional structures of proteins from interproton distance data by hybrid distance geometry-dynamical simulated annealing calculations. *FEBS letters* **229**, 317-324.

Nilges, M., Gronenborn, A. M., Brunger, A. T. and Clore, G. M. (1988b). Determination of three-dimensional structures of proteins by simulated annealing with interproton distance restraints. Application to crambin, potato carboxypeptidase inhibitor and barley serine proteinase inhibitor 2. *Protein engineering* **2**, 27-38.

Phillips, J. C., Braun, R., Wang, W., Gumbart, J., Tajkhorshid, E., Villa, E., Chipot, C., Skeel, R. D., Kale, L. and Schulten, K. (2005). Scalable molecular dynamics with NAMD. *J Comput Chem* **26**, 1781-1802.

Piotto, M., Saudek, V. and Sklenar, V. (1992). Gradient-Tailored Excitation for Single-Quantum Nmr-Spectroscopy of Aqueous-Solutions. *Journal of Biomolecular Nmr* **2**, 661-665.

Reddy, G. L., Iwamoto, T., Tomich, J. M. and Montal, M. (1993). Synthetic peptides and four-helix bundle proteins as model systems for the pore-forming structure of channel proteins. II. Transmembrane segment M2 of the brain glycine receptor is a plausible candidate for the pore-lining structure. *The Journal of biological chemistry* **268**, 14608-14615.

Ryckaert, J. P., Ciccotti, G. and Berendsen, H. J. C. (1977). Numerical-Integration of Cartesian Equations of Motion of a System with Constraints - Molecular-Dynamics of N-Alkanes. *Journal of Computational Physics* **23**, 327-341.

Shank, L. P., Broughman, J. R., Takeguchi, W., Cook, G., Robbins, A. S., Hahn, L., Radke, G., Iwamoto, T., Schultz, B. D. and Tomich, J. M. (2006). Redesigning channel-forming peptides: amino acid substitutions that enhance rates of supramolecular self-assembly and raise ion transport activity. *Biophys J* **90**, 2138-2150.

Stein, E. G., Rice, L. M. and Brunger, A. T. (1997). Torsion-angle molecular dynamics as a new efficient tool for NMR structure calculation. *Journal of magnetic resonance* **124**, 154-164.

Tomich, J. M., Bukovnik, U., J., L. and Schultz, B. D. (2012). Channel Replacement Therapy for Cystic Fibrosis. In *Cystic Fibrosis - Renewed Hopes Through Research* (Sriramulu, D., ed.). InTech.

Tomich, J. M., Wallace, D., Henderson, K., Mitchell, K. E., Radke, G., Brandt, R., Ambler, C. A., Scott, A. J., Grantham, J., Sullivan, L. and Iwamoto, T. (1998). Aqueous solubilization of transmembrane peptide sequences with retention of membrane insertion and function. *Biophysical journal* **74**, 256-267.

van Ginkel, F. W., Iwamoto, T., Schultz, B. D. and Tomich, J. M. (2008). Immunity to a self-derived, channel-forming peptide in the respiratory tract. *Clinical and vaccine immunology : CVI* **15**, 260-266.

Wallace, D. P., Tomich, J. M., Eppler, J. W., Iwamoto, T., Grantham, J. J. and Sullivan, L. P. (2000). A synthetic channel-forming peptide induces Cl(-) secretion: modulation by Ca(2+)-dependent K(+) channels. *Biochimica et biophysica acta* **1464**, 69-82.

Wallace, D. P., Tomich, J. M., Iwamoto, T., Henderson, K., Grantham, J. J. and Sullivan, L. P. (1997). A synthetic peptide derived from glycine-gated Cl- channel induces transepithelial Cl- and fluid secretion. *Am J Physiol* **272**, C1672-1679.

Welsh, M. J. and Smith, A. E. (1993). Molecular mechanisms of CFTR chloride channel dysfunction in cystic fibrosis. *Cell* **73**, 1251-1254.

White, S. H. and von Heijne, G. (2005). Transmembrane helices before, during, and after insertion. *Current Opinion in Structural Biology* **15**, 378-386.

Wishart, D. S. and Nip, A. M. (1998). Protein chemical shift analysis: a practical guide. *Biochemistry and cell biology = Biochimie et biologie cellulaire* **76**, 153-163.

Wüthrich, K. (1986). *NMR of proteins and nucleic acids*. The George Fisher Baker non-resident lectureship in chemistry at Cornell University, Wiley, New York.

Wüthrich, K., Billeter, M. and Braun, W. (1983). Pseudo-structures for the 20 common amino acids for use in studies of protein conformations by measurements of intramolecular proton-proton distance constraints with nuclear magnetic resonance. *J Mol Biol* **169**, 949-961

Appendix A - Chapter 2

The work described in this section was performed by Drs. Chen and Al-Rawi in the Department of Biochemistry and Molecular Biophysics at Kansas State University. The purpose of these studies was to construct, characterize, and validate initial high-resolution structural models of the putative pentameric channels formed by peptides NK_4-M2GlyR-p22 and NK_4-M2GlyR-p22 p22-S22W.

The initial step was the further refinement of the average structures from the ensembles calculated by CNS based on the NMR data, using the GBSW implicit membrane model (Im et al., 2003) in CHARMM (Brooks et al., 2009;Brooks et al., 1983). Distortions to covalent geometry due to averaging were corrected by short energy minimization while harmonic positional restrains on heavy atoms. These refinements might be particularly useful to remove potential structural distortions due to difference between micelle and bilayer membrane environments, which facilitates subsequent assembly of monomer structures into channels. The refinement protocol involves 100 ps restrained molecular dynamics simulation at 300 K followed by energy minimization. Default GBSW implicit membrane parameters were used with a hydrophobic membrane thickness of 35 Å. All NMR restraints were imposed with force constants of 50 kcal/mol/$Å^2$ for NOE distances and 100 kcal/mol/$Å^2$ for dihedral angles during MD refinement. The force constants of NOE distances were increased to 100 kcal/mol/$Å^2$ during the final energy minimization.

Starting from refined monomer NMR structures, the peptides structures were assembled into pentamers using CHARMM based on the following experimental and theoretical considerations: First, previous experimental work indicate that this family of peptides spontaneously assembled into pentameric structures when inserted into synthetic bilayers or cell membranes (Reddy et al., 1993). Second, cysteine-scanning experiments on a related peptide sequence (NK_4-M2GlyR p22-T19R/S22W) have identified residues A6, L10, T13, and T17 as pore lining residues (Bukovnik et al., 2012). Third, solid-state NMR and free-energy calculations suggest that transmembrane helix tilt angles most likely fall in the range 10°–15° (Lee and Im, 2008;Montal and Opella, 2002) for peptides of similar length, as a result of balance between helix procession entropy and peptide-membrane interactions. Fourth, when the monomers are aligned to form the pentamer, the adjacent peptides should be in contact with each other while maintaining a pore cavity sufficiently large for ions to traverse.

Multiple initial models were generated for each sequence with different handiness of helix packing. The assembled channels were subject to energy minimization in presence of harmonic positional restraints on all heavy atoms and then solvated in a pre-equilibrated POPC bilayer membrane using the CHARMM-GUI automated Membrane Builder (Jo et al., 2007;Jo et al., 2008). A six-cycle equilibration protocol was applied to equilibrate the system at 303 K using CHARMM, during equilibration, two cycles of NVT simulation (constant volume and temperature) were performed for 25 ps each, followed by three cycles of NPT simulation (constant pressure and temperature) of 25– 100 ps. A final NPT equilibration cycle was performed for 100 ps where only the protein backbone atoms were held with weak harmonic positional restraints. SHAKE was used to fix the length of hydrogen-attaching bonds (Ryckaert

et al., 1977) to allow for a two femtosecond (fs) dynamic time step during cycles 4–6. Periodic boundary conditions were enforced. Particle Mesh Ewald (PME) (Darden et al., 1993) was used for treatment of long-range electrostatic interactions, and van der Waals interactions were smoothly switched off from 10 to 12 Å. The fluctuations in temperature, volume, and energy were examined, and all were within reasonable ranges. The protein, water, and lipids were monitored during the equilibration to ensure that the water did not penetrate the lipid bilayer.

The final structure from the CHARMM equilibration simulation was used in the NAMD software package (Phillips et al., 2005) for the production simulation. Another 100 ps equilibration with weak harmonic positional restraints on protein backbone atoms (k=0.1 kcal mol^{-1} $Å^{-2}$) in the NAMD simulations was used to suppress potential strains during subtle differences between CHARMM and NAMD. Setups equivalent or identical to those described above were used, unless otherwise noted below. Electrostatic interactions were evaluated based on a multiple-time-stepping algorithm (Han et al., 2007) implemented in NAMD, where bonded interactions were updated every time step, short-range non-bonded electrostatic and van der Waals interactions every two steps, and long-range interactions every four steps. After the system was equilibrated, all restraints were released. A NPAT (constant pressure and membrane area) production simulation was carried out for 20 nanoseconds for each structural model, with the coordinates saved every 1 ps.

The channel structures are stable in the POPC membrane bilayers within the 20 ns NAMD production simulations, the whole channel drifts upward relative to the membrane, presumably to allow better solvent exposure of the charged N-terminal lysines. The positively charged lysine

side chains also interact extensively with lipid phosphate groups. The drift results in substantial distortions in the local membrane environment, particularly, thinning of the bilayer adjacent to the channel. The helical segments of all five peptides are stable (at the secondary structure level). In fact, the peptide structures become more helical compared with the monomeric NMR structures in SDS micelles, reaching ~75%. The increase in helicity is due primarily to the formation of more regular helices within residues 6–20. The averaged helix tilt angles with respect to the membrane normal (computed using residues 6–20) increase to ~25°. This tilt angle is larger than expected for short helices, repulsion among positively charged side chains (K1–4 and R7), coupled with unstructured N-termini and local membrane thinning, is likely the main driving force for the large helix tilt angle.

To directly test that the membrane-anchoring tryptophan residue at the C-terminus of peptide NK_4-M2GlyR-p22 S22W increases the channel stability and rigidity, the whole channel C_α root mean square fluctuation (RMSF) was calculated using the last 5 ns of the production simulation. As it is shown in Figure A-1(a), the results support that the NK_4-M2GlyR-p22 pore is more flexible than NK_4-M2GlyR-p22 S22W. The presence of the C-terminal tryptophan not only reduces the channel flexibility near the C-terminus, but also leads to a global reduction of flexibility including the unstructured N-termini. Figure A-1 (b, c) shows how the C-terminal tryptophan mainly restricts the translational motion along the membrane normal and might thus enhance the overall integrity of the channel assembly. Tryptophan residues might also contribute further to the channel stability by restricting rotation around the helix principle axis (White and von Heijne, 2005). Although reduced flexibility does not necessarily reflect increased stability, these two properties are often positively correlated. An increased stability of the NK_4-M2GlyR-

p22 S22W channel as suggested by reduced flexibility is consistent with the difference in concentration dependence of short circuit current induced by NK_4-M2GlyR-p22 and NK_4-M2GlyR-p22 S22W measured in MDCK cell monolayers (Figure 2-1).

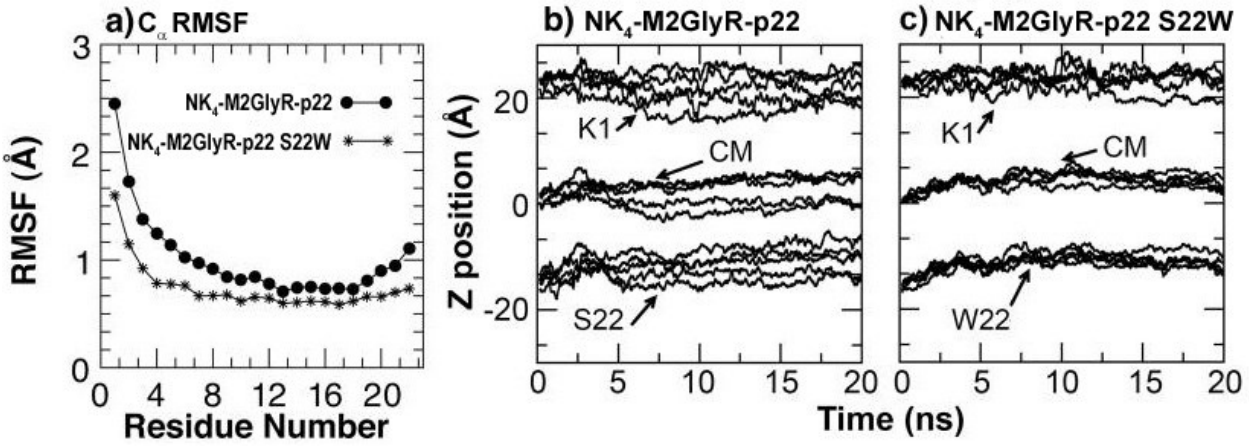

Figure A-1. a) Cα RMSF of NK_4-M2GlyR channels. b,c) Position of N-terminus, C-terminus and center of mass as a function of time during simulation

During the course of the simulations, several incidences of spontaneous Cl^- diffusion through the channels were observed. This is probably due to substantial local Cl^- concentration enrichment at the N-terminal opening of the channels due to the presence of large number of lysine residues. This observation allows us to qualitatively understand the nature of chloride conduction and possible mechanism of anion selectivity of these synthetic channels. Figure A-2 shows the time evolution of the position of a single Cl^- along the membrane normal during an incidence of its spontaneous diffusion through the NK_4-M2GlyR-p22 channel, together with a snapshot where this particular Cl^- locates inside the channel around the narrowest point (near Thr17). Cl^- ions remain highly solvated throughout the diffusion process, in fact, both p22 and p22-S22W pores remain solvated throughout the simulations

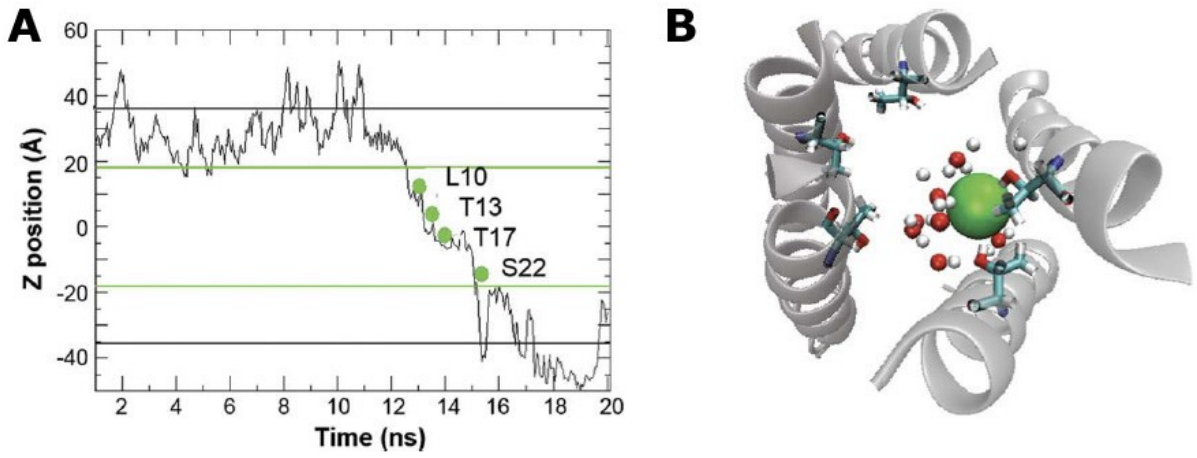

Figure A-2. A) Position of Cl^- as a function of simulation time during diffusion through the NK_4-M2GlyR-p22 channel B) Snapshot of the interactions between Cl^- and water molecules with Thr17 hydroxyl side chains inside the channel

Chapter 3 - Structural and functional characterization of a shorter length (20 amino acid residues) membrane spanning Channel-Forming Peptide derived from the Glycine Receptor M2

Introduction

The analysis of the structural and physiological characteristics of 22 residues containing peptides NK_4-M2GlyR-p22 and NK_4-M2GlyR-p22 S22W (Cook et al., 2004;Herrera et al., 2010) showed that the substitution of tryptophan residue 22 for a serine residue was advantageous due to the reduction in the concentration required to reach one-half I_{max}, but since the actual I_{max} was reduced compared with the unsustituted sequence, new modificationes that would restore I_{max} were explored. The next step in the pursue of find an optimal channel forming peptide, derived from the M2GlyR sequence, that would be functional as a potential cystic fibrosis therapeutic was to introduce a second substitution, with a charged amino acid, near the C-terminus. Out of the many tested posibilities the substitution of threonine 19 for an arginie residue was found to be the position that gave the best results (Shank et al., 2006). The structural and biophysical properties of peptide NK_4-M2GlyR-p22 T19R S22W were extensively characterized (Bukovnik et al., 2012), notably this peptide induces an I_{max} of 33.7 ± 1.3 μA/cm^2 across MDCK epithelial monolayers with a concentration of 71 ±5 μM to reach one-half I_{max} ($K_{1/2}$) (See Table 4-2 and Figure 4-2). Monomeric structures determined by NMR, together with a cysteine scanning study suggested that threonine residues at positions 13, 17, and 20 line the pore of the assembled channel of NK_4-M2GlyR-p22 T19R S22W peptides (Bukovnik et al., 2012).

One direction explored subsequently for improving the channel forming sequence's performance was making the peptide sequences shorter, effectively making the ion conduction path shorter, and the synthesis of the peptide easier and more economical. In order to preserve the membrane anchoring effect of the C-terminal residues and the spacial distribution of the pore lining side chains, the sequence was modified by eleminating the first two residues after the four N-terminal lysines namely proline 5 and alanine 6. Sequences shorter than 20 residues were previously found to be inefective in forming ion channels (Broughman et al., 2002). The resulting peptide sequence was: KKKKR VGLGI TTVLT MRTQW and it was named NK_4-M2GlyR-p20 T17R S20W, a comparison of this amino acid sequence with other M2GlyR derived channel forming peptides can be seen in Figure 3-1.

NK_4-M2GlyR-p22	K K K K P A R V G L G I T T V L T M T T Q S
NK_4-M2GlyR-p22 S22W	K K K K P A R V G L G I T T V L T M T T Q W
NK_4-M2GlyR-p22 T19R S22W	K K K K P A R V G L G I T T V L T M R T Q W
NK_4-M2GlyR-p20 T17R S20W	K K K K R V G L G I T T V L T M R T Q W

Figure 3-1. M2GlyR-p20 T17 S20W peptide sequence compared to other M2GlyR derived channel forming peptides

This chapter presents the efforts in the determination of an atomic level monomeric structure by multidimensional NMR methodology in two different solvent systems and the characterization of the ion conductance of NK_4-M2GlyR-p20 T17R S20W channels across MDCK epithelial monolayers. The results obtained from the shorter peptide NK_4-M2GlyR-p20 T17R S20W showed an improvement in ion conductance over the sequences previous reported.

Dissolving peptides in 2,2,2-trifluoroethanol (TFE) solutions has been used by several investigators for the structural study of peptides and proteins as a way of mimicking the hydrophobic environment of the membrane (Cammers-Goodwin et al., 1998;Jasanoff and Fersht, 1994;MacPhee et al., 1997). TFE:water mixtures often stabilize secondary structural elements of peptides including α-helices. The TFE molecules displace water molecules by clustering around the peptide. This displacement of water molecules prevents hydrogen bonding of the CO and NH groups of the peptide backbone to water molecules providing a low dielectric environment which encourages the formation of intramolecular hydrogen bonds that stabilize the secondary structure of the peptide (Roccatano et al., 2002).

The low dielectric environment in the TFE solution homogeneously surrounds the peptide, which limits the applicability of the determined structures, since a protein containing a transmembrane segment experiences at least three surrounding environments, one for the bulk of the solution, akin of a water solution, one for the hydrophobic interior of the cellular membrane, and one for the membrane-solution interface where the charged or hydrophilic head groups of the phospholipids reside. Detergents like Sodium Dodecyl Sulfate (SDS) have been used to better mimic membrane environments in order to acquire structure information of membrane spanning segments of proteins or peptides (Arseniev et al., 1985;Pervushin et al., 1991;Rizo et al., 1993). Detergent molecules in an aqueous solution at the critical micelle concentration or higher will assemble to form micelles with the polar head groups on the outside and the hydrophobic tails on the inside providing a compartmentalized environment similar to that of a membrane bilayer. For NMR experiments additional consideration should be taken to the micelle size because fast

tumbling of the peptide-SDS micelles, which is a requirement for rapid isotropic motions, is needed for good quality of the generated NMR spectra.

In order to test the presence of secondary structure for the peptide monomers in the solvent systems to be used, before running lengthy NMR experiments, the peptide was dissolved in both TFE:water and SDS micelles and analyzed by circular dichroism (CD) spectroscopy

Materials and Methods

Peptide Synthesis and Purification

Peptide NK_4-M2GlyR-p20 T17R S20W (NH_2-KKKKRVGLGITTVLTMRTQW-$CONH_2$; MW = 2344.9 Da) was chemically synthesized at the Biotechnology Core Facility of Kansas State University by solid phase peptide synthesis methodology on an Applied Biosystems model 431A peptide synthesizer (Foster City, CA) using 9-fluorenylmethoxycarbonyl (Fmoc) chemistry as described in Chapter 2 (Tomich et al., 1998). CLEAR amide resin (0.3 mmol/g) was purchased from Peptides International Inc. (Louisville, KY) and N^{α}-Fmoc amino acids were purchased from Anaspec (Fremont, CA), Bachem Inc. (Torrance, CA), and Peptides International Inc.(Louisville, KY). The peptide was purified using a Phenomenex, (Torrance, CA) reversed-phase C-18 column on a System Gold HPLC system (Beckman Instruments Inc., Fullerton, CA). The peptide was eluted from the column using a linear gradient of 3.0% min^{-1} of 5–90% acetonitrile containing 0.1% trifluoroacetic acid (TFA) at 1 mL/min. HPLC-purified peptide was characterized by matrix-assisted-laser desorption time-of-flight mass spectroscopy (MALDI-

TOF/TOF) using a Bruker Ultraflex II mass spectrometer (Bruker Instruments Inc., Billerica, MA). After characterization, the peptide was lyophilized and stored as dry powder until used.

Transepithelial ion transport measurements

For the transepithelial ion transport measurements Madin-Darby canine kidney (MDCK) epithelial cells cultured from parental cells that were a generous gift of Dr. Lawrence Sullivan (KUMC, Kansas City, KS) were used. Cells were maintained as sub-confluent monolayers in a 1:1 mixture of Dulbecco's modified Eagle medium and Ham's F-12 nutrient mixture (DMEM/F-12) (Life Technologies, Carlsbad, CA), supplemented with 5% fetal bovine serum (FBS) (BioWhittaker, Walkersville, MD), and 105 units/L penicillin and 100 mg/L streptomycin (P/S) (Life Technologies, Grand Island, NY), cells were allowed to propagate until they were harvested under 5% CO_2 and 37°C conditions. MDCK cells (2.5 x 10^5 cells) were plated onto permeable culture support wells (Snapwell, 12 mm diameter. CoStar, Cambridge, MA). Snapwell supports were placed in a six-well plate with DMEM/F-12 plus P/S and FBS, monolayers of MDCK cells were used 7-14 days after reaching confluency. Transepithelial ion transport was evaluated with the use of a modified Ussing chambers (Model DCV9, Navicyte, San Diego, CA). Confluent MDCK cells in the Snapwells were mounted vertically in the Ussing chambers. Apical and basolateral surfaces of the monolayers were bathed in a modified Ringer solution (120 mM NaCl, 25 mM $NaHCO_3$, 3.3 mM KH_2PO_4, 0.8 mM K_2HPO4, 1.2 mM $MgCl_2$, and 1.2 mM $CaCl_2$), which was prepared daily, all components were purchased from Sigma-Aldrich (St. Louis, MO). The solution bathing the monolayers was kept at 37 °C and continuously bubbled with 5% CO_2/ 95% O_2 to maintain pH, provide aeration and guarantee

rapid mix of the fluids in the chambers. 1-ethyl-2-benzimidazolinone (1-EBIO; Acros, Morris Plains, NJ) was prepared as a 1 M stock solution in dimethyl sulfoxide (DMSO). (Grantham et al., 1989;Wallace et al., 1997) Experiments were conducted on monolayers with a resistance of at least 800 Ohms cm^2. The transepithelial voltage was measured with glass capillary probe tubes containing a plug of 5% agar in 3 M KCl and Ag-AgCl electrodes. The electrodes were situated near the apical and the basolateral surfaces of the cell monolayers, the transepithelial membrane potential (V_{TE}) was clamped to 0 mV and the short-circuit current (I_{SC}; the current necessary to clamp the voltage to zero) measured continuously with a voltage clamp apparatus (Model 558C, University of Iowa, Department of Bioengineering, Iowa City, IA).

MDCK monolayers mounted into the Ussing chambers were treated with 300 μM 1-EBIO 10 minutes prior to addition of the peptide solution. 1-EBIO activates of Ca^{2+} dependent basolateral K^+ channels, which hyperpolarizes the cell (Devor et al., 1996) thus increasing the electrochemical driving force for Cl^- conductance through any open channels capable of chloride transport in the apical membrane (Broughman et al., 2001). The increase in endogenous transepithelial ion current induced by the EBIO serves as a baseline correction to the currents induced by the tested peptide solutions. Corresponding volumes of stock peptide solution in water were added to the apical bath to obtain NK_4-M2GlyR-p20 T17R S20W peptide concentrations of: 10, 30, 60, 100, 200, 300 and 500 μM in the apical bathing solution. Data acquisition was performed at 1 Hz with a Macintosh computer (Apple Computers, Cuppertino, CA) using Aqknowledge software (ver. 3.2.6, BIOPAC Systems, Santa Barbara, CA) with an MP100A-CE interface. The raw I_{SC} data correspond to steady-state flux levels. At the end of the experimental run 1 μL of forskolin from 10 mM stock solution is added to the apical and basolateral sides of the MDCK monolayer to indicate that cells at the end of the experiment are

still intact and responsive. Forskolin is an adenylyl cyclase activator that catalyzes the conversion of ATP to cAMP, thereby activating protein kinase A. This in turn activates components of active ion transport pathways, such as CFTR, and results in increased anion secretion (Carlin et al., 2006). Also forskolin is known to drive the uptake of chloride via $Na^+/K^+/^{Cl-}$-cotransporter (D'Andrea-Winslow et al., 2001). The data points reported in Figure 3-3 for each peptide concentration represent the mean peak I_{SC} stimulated by the peptide at that concentration; bars indicate the standard error of the mean. Continuous lines presented in the figure represent the best fit of the data to the modified Hill equation:

$$I_{SC} = I_{MAX}\left(\frac{X^n}{K_{1/2}^n + X^n}\right)$$

Where $K_{1/2}$ is the concentration of peptide that provides a half maximal I_{SC} , I_{MAX} the maximal current induced and n represents the Hill coefficient.

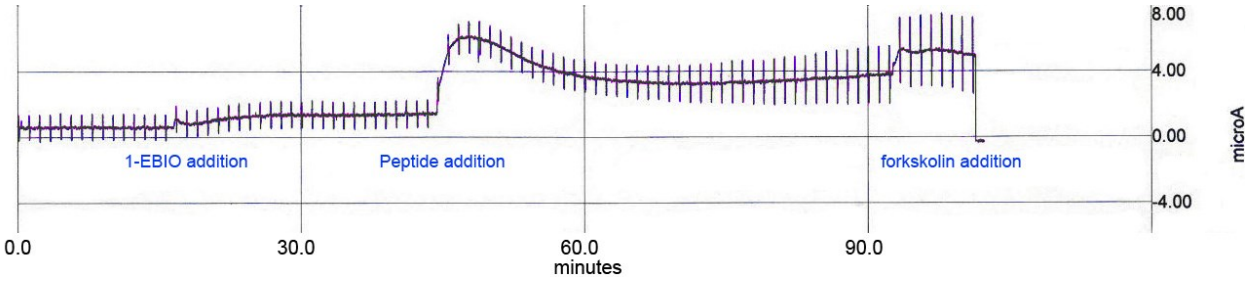

Figure 3-2. Typical Ussing chamber experimental run with peptide NK_4-M2GlyR-p20 T17R S20W

Figure 3-2 shows the data trace for an individual channel/chamber during a typical Ussing chamber experimental run with peptide NK_4-M2GlyR-p20 T17R S20W (30μM). The changes in I_{SC} due to the addition of 1-EBIO, peptide solution, and forkskolin to the media can be appreciated at the indicated times as sudden perturbations of the trace.

Circular Dichroism

To obtain a first indication of peptide secondary structure in TFE-water solutions and SDS micelles in water, CD spectroscopy measurements were performed on a Jasco J-815 spectropolarimeter (Jasco Inc., Tokyo, Japan) using a 0.1 mm path length cylindrical quartz cuvette (Fisher Scientific, Waltham, MA). All spectra were recorded from 260 to 190 nm using a 1.0 nm spectral bandwidth, 0.2 nm step resolution, 20 nm/min scan speed, and 2 second response time. Also a baseline measurement was performed at the beginning of every run to check instrument stability. The CD spectra presented for the peptide solutions are an average of eight scans with background subtraction. Peptide stock solution was prepared to a concentration of 1 mM in water, stock solution concentration was determined using fluorescence at 278 nm, and final peptide concentration in all CD samples was 50 μM. Bovine serum albumin (BSA) served as the protein standard. The DI-distilled H_2O peptide sample (0% TFE) was prepared by diluting 50 μL peptide stock solution with 950 μL DI H_2O. TFE-water peptide samples were prepared by vortexing 50 μL peptide stock solution with calculated volumes of TFE (Sigma-Aldrich, St. Louis, MO) and DI-distilled H_2O to produce a final TFE concentration of 25% and 50% by volume. The SDS micelles peptide sample was prepared by adding 50 μL of peptide stock solution with two minute sonication to calculated volumes to yield 10 mM SDS, 10 mM NaCl, and 10 mM phosphate buffer at pH 7.0 concentrations.

NMR Sample Preparation

For the preparation of the NMR sample in TFE:water solvent system, 4 mg of purified lyophilized peptide was added to 300 µL of a solvent mixture containing 50% Deuterated TFE (TFE-d_3 Cambridge Isotope Labs, Andover, MA), and 50% H_2O (by volume) followed by one minute sonication to prepare an NMR sample with peptide concentration of 5.7 mM. For the preparation of the NMR samples in SDS micelles, the lyophilized peptide was dissolved in 1.0 mL solvent mixture of 1,1,1,3,3,3-hexafluoro-2-propanol:TFE (1:1). The solution was transferred to a glass test tube and a stream of nitrogen gas was passed into the solution to dry the peptide into a thin film on the wall of the test tube. Once the peptide was seen dried by visual inspection, the test tube containing the peptide was put in a lyophilizer overnight to remove any remaining solvent and moisture. The following day, the peptide was dissolved in 250µL of 1 M SDS-d_{25} solution in water. Once the peptide appeared dissolved, 250µL of an 80% H_2O:20% D_2O solvent mixture was added (Cambridge Isotope Labs, Andover, MA), for a final SDS-d_{25} concentration of 500 mM in 90% H_2O:10% D_2O and a peptide concentration of 2.5 mM.

NMR Spectroscopy

Experiments on the NMR samples of peptide in TFE solution were performed with a 11.75 tesla 500 MHz Varian UNITYplus spectrometer (Varian now Agilent Inc., Palo Alto, CA), running VNMR version 6.1C at the Biomolecular NMR facility of the Biochemistry and Biophysics Department at Kansas State University, with a 3-mm triple-resonance inverse detection probe. 2D ^{1}H-^{1}H TOCSY and 2D ^{1}H-^{1}H NOESY experiments were performed at 15°C. Water peak suppression was obtained by low-power irradiation of the H_2O resonance. A total of 256

increments of 4K data points were recorded for all the 2D experiments. All data sets were obtained in hyper complex phase-sensitive mode. 2D ^{1}H-^{1}H TOCSY spectra were recorded by using MLEV-17 for isotropic mixing for 100 ms at a B1 field strength of 8 KHz. 2D ^{1}H-^{1}H NOESY experiments were performed with 200, 300, and 400 ms mixing times. The residual TFE methylene peak was used as reference for the chemical shift values. Varian software VNMR 6.1C on a Silicon Graphics Octane workstation (Mountain View, CA) was used for data processing, data analysis was performed with Sparky software (Goddard and Kneller, 2004) using a Dell Precision 690 workstation (Round Rock, TX).

The peptide sample dissolved in SDS micelles was sent to the Biomolecular NMR laboratory at the University of Kansas (Lawrence, KS) for high-resolution NMR data collections. The NMR spectra were recorded with the 18.8 tesla Bruker Avance 800 MHz NMR spectrometer (Bruker Instruments Inc., Billerica, MA) equipped with an inverse detection TCI cryoprobe running Topspin 1.3. Experiments were performed at 25°C. The NMR data obtained from 800 MHz instrument was processed using NMRPipe (Delaglio et al., 1995) and analyzed with Sparky software (Goddard and Kneller, 2004) using a Dell Precision 690 workstation (Round Rock, TX). Spin-lock time of 100 ms at B1 field strength of 7 KHz was used for 2D ^{1}H-^{1}H TOCSY experiments, and mixing times of 300 and 400 ms were used for 2D ^{1}H-^{1}H NOESY experiments. For all 2D experiments, 1024 complex data points were collected in the direct dimension and 256 in the indirect dimension. Linear prediction and zero filling were used during processing. The suppression of the solvent peak was achieved using the WATERGATE pulse scheme during acquisition (Piotto et al., 1992), and the residual water peak (4.74 ppm) was used as reference for chemical shift assignments.

NMR Structure Calculations

The protocol described in Chapter 2 was also used for the structure calculations (Cook et al., 2004;Kirnarsky et al., 2000). NOESY cross peaks were classified as strong, medium, weak and very weak based on the observed relative intensity and volume integration of the corresponding peaks. Unambiguously identified NOESY cross peaks were converted into inter-proton distance upper bounds using the following classifications: strong, medium, weak, and very weak. Upper distance limits for NOEs involving methyl protons and nonstereo specifically assigned methylene protons, were corrected appropriately for center averaging by adding 0.5-1 Å to the maximum distance constraint for center averaging (Wüthrich et al., 1983). The obtained distance restraints were used to calculate peptide structures using the crystallography and NMR system (CNS) version 1.1, (Brunger et al., 1998). The protocol combines simulated annealing in torsional angle space and MD refinement in Cartesian space to produce structures with minimal restraint violations (Stein et al., 1997). A total of 100 accepted structures were subjected to energy minimization in the AMBER force field (Cornell et al., 1995;D.A. Case, 2002) using SYBYL 7.1 (Tripos Inc. St. Louis, MO). The minimized structures were then clustered based on mutual heavy-atom root mean square deviation (RMSD). The cluster of 15 structures with no restraint violation and the lowest energies were selected as the representative NMR structures. The procedure was performed independently for each sample condition (TFE solution sample and SDS micelle sample).

Results and Discussion

Transepithelial ion transport measurements

Experiments with an Ussing chamber instrument were performed to evaluate the concentration dependence of the I_{SC} induced on monolayers of MDCK epithelial cells by aqueous solutions of NK_4-M2GlyR-p20 T17R S20W peptide, Table 3-1 shows the peak current measured for peptide concentrations ranging from 10 μM to 500μM with 4 repetitions for each concentration; the average peak I_{SC} and the standard error of the mean is also reported in the table.

Table 3-1. I_{SC} induced by NK_4-M2GlyR-p20 T17R S20W peptide in MDCK cells

Concentration (μM)	*Peak Current (μA cm^{-2})*				*Average* I_{SC}	*Standard Error*
	1	2	3	4		
10	2.50	3.28	2.12	3.87	2.94	0.39
30	11.60	7.15	7.63	12.98	9.84	1.81
60	24.53	18.33	18.70	20.26	20.45	1.42
100	36.39	37.43	32.59	33.15	34.89	1.19
200	36.34	39.96	38.18	37.74	38.06	0.75
300	35.77	33.33	42.44	42.85	38.60	2.39
500	42.23	47.66	44.61	48.18	45.67	1.39

In Figure 3-3 the average peak I_{SC} induced by the NK_4-M2GlyR-p20 T17R S20W peptide on MDCK epithelial monolayers is plotted against the concentration of the peptide in the apical bathing solution after peptide addition, in the presence of 1-EBIO. The continuous line is the best fit to the data to a modified Hill equation as detailed in the methods section. From the fitted data an I_{MAX} of 43.8 ± 2.8 μA/cm^2 and $K_{1/2}$ of 58μM ± 8 (Hill Coefficient n=1.8) were determined for NK_4-M2GlyR-p20 T17R S20W peptide channels in MDCK epithelial cell monolayers.

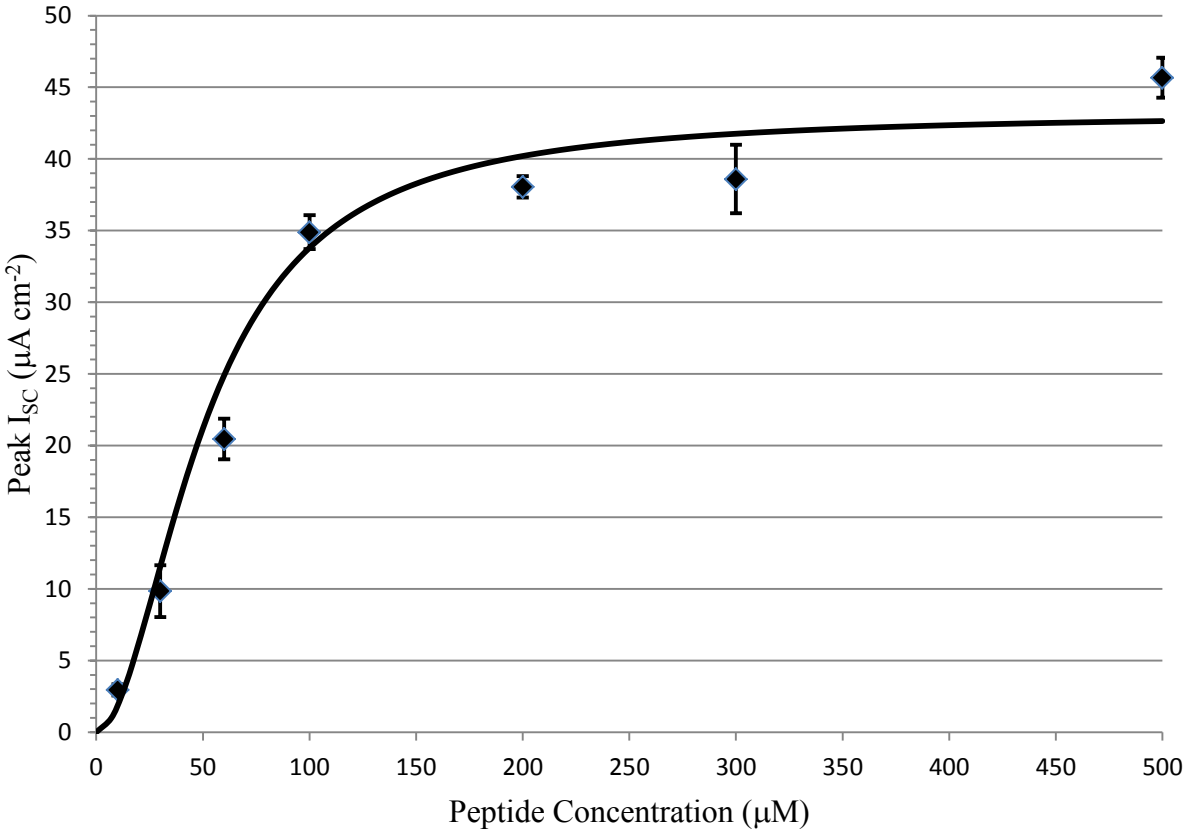

Figure 3-3. Concentration dependence of I_{SC} induced by NK_4-M2GlyR-p20 T17R S20W peptide on monolayers of epithelial MDCK cells, when applied to the apical membrane in the presence of 1-EBIO

Circular Dichroism

The CD spectra of peptide NK_4-M2GlyR-p20 T17R S20W were recorded as a function of TFE concentration. Figure 3-4 shows the CD spectra of this peptide in 0% TFE:water, 25% TFE:water, and 50% TFE:water. The shape of the CD spectrum in 0% TFE:water is similar to the spectrum reported for peptide NK_4-M2GlyR-p22 S22W at the same conditions (Cook et al., 2004) suggesting that in 100% water the NK_4-M2GlyR-p20 T17R S20W peptide is partially or

transiently structured. The spectrum in 0% TFE has a minimum at ~195nm, which is a hallmark for random coil. However it is missing the random coil's characteristic positive minimum at 215 nm. The negative band near ~195 that is observed in the absence of TFE arises from π to π^* electronic transition. As TFE concentration increases, the band shifts to 208nm and an additional shoulder appears around 220nm as a result of the n to π^* electronic transition. A strong positive band appears around 192 nm with increasing TFE concentration in the CD sample. The CD spectra of NK_4-M2GlyRp20 T17R S20W peptide collected at increasing concentrations of TFE showed the characteristics for α-helix with double minima at 208 and 222 nm, and maximum at ~192 nm. The extracted information provided confidence that the NK_4-M2GlyR-p20 T17R S20W peptide is structured in the TFE:water solution and suitable for NMR studies for determination of the solution structure.

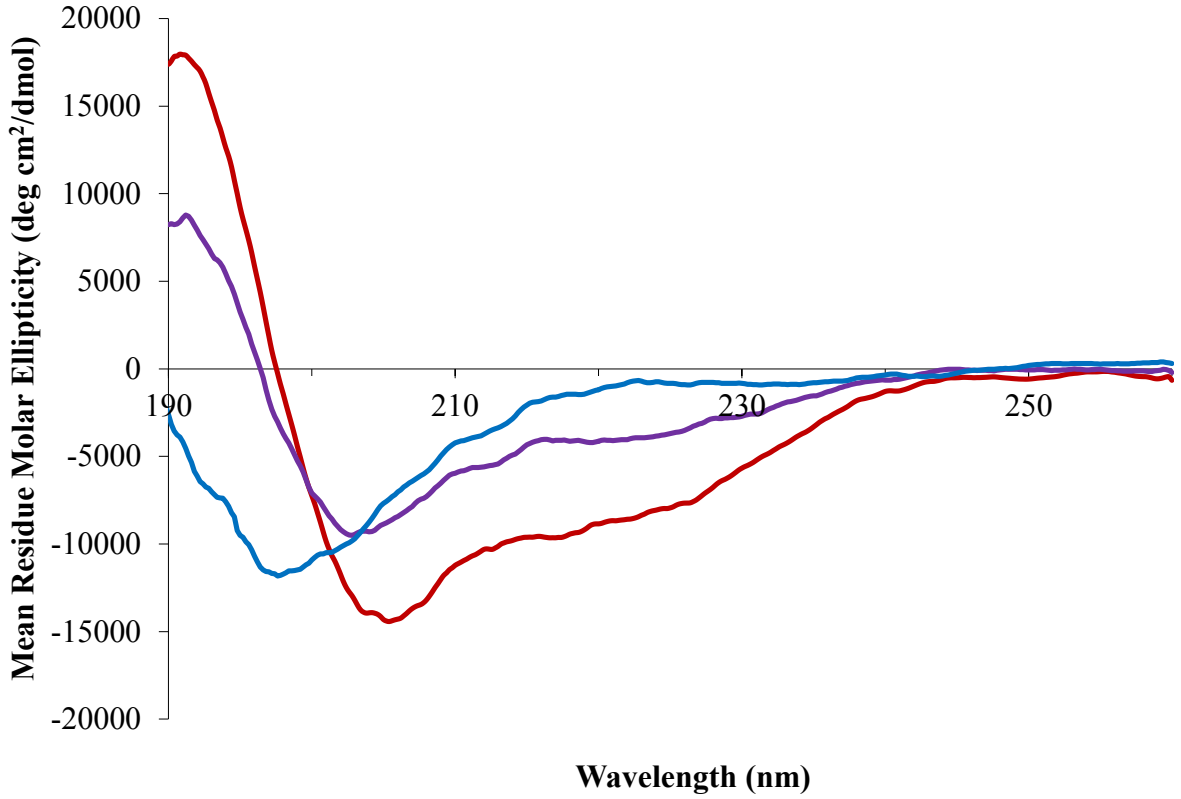

Figure 3-4. Circular dichroism spectra of peptide NK_4-M2GlyR-p20 T17R S20W in TFE. (—) 0% TFE (—) 25% TFE (—) 50% TFE

The CD spectrum of peptide NK_4-M2GlyR-p20 T17R S20W in 10mM SDS solution, presented in Figure 3-5 is similar to the spectrum for the same peptide in 50% TFE:water, shows the characteristics of α-helix (double minima at 208 and 222 nm, and maximum at ~192 nm). These results suggest that the peptide NK_4-M2GlyR-p20 T17R S20W in SDS micelles is structured as well, and the NMR SDS micelle sample will be suitable for further structure studies. Advanced analysis of CD spectra, like spectra deconvolution, was not performed because these analyses have not been accurate for M2GlyR peptides in the past (Cook et al., 2004), where a predicted β-strand content has not been detected in the determined structures, and since a detailed structure was to be calculated by NMR it was consider unnecessary.

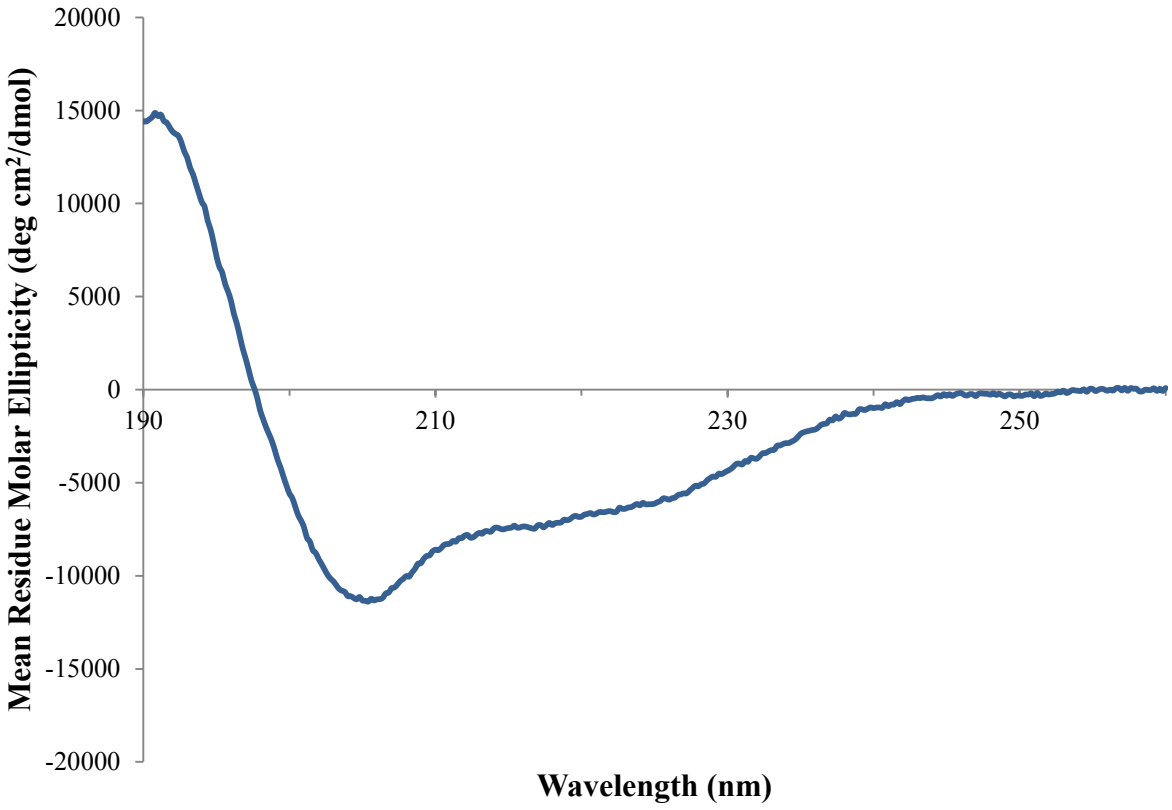

Figure 3-5. Circular dichroism spectra of peptide NK_4-M2GlyR-p20 T17R S20W in 10 mM SDS Micelles

NMR Data Analysis

Figure 3-6 shows the acquired 2D ^{1}H-^{1}H TOCSY spectrum of peptide NK_4-M2GlyR-p20 T17R S20W in 50 % TFE-d3:water.This spectrum has signals with low resolution in the side chain–side chain and H^N-H^α regions. As discussed before in Chapter 2, the proton chemical shift assignments were made by standard techniques (Wüthrich, 1986) using the 2D ^{1}H-^{1}H TOCSY spectrum for intra-residue spin systems identification and 2D ^{1}H-^{1}H NOESY for inter-residue connectivity. The finger-print regions (H^N-H^α + H^N-Side chain) in the TOCSY spectrum were

used for identification and assignment of H^N- H^α, H^N- H^β, H^N- H^γ, and H^N- H^δ intra-residue spin connectivity and eventually to determine residue type. Where the spectral resolution did not allow for unambiguous assignment in TOCSY spectrum simultaneous analysis with the 2D ^{1}H-^{1}H NOESY was necessary. The assignment of pure NOESY cross peaks due to sequential $d_{\alpha N}$ (i,i+1) proton connectivity aided in completing the assignment of every amino acid residue spin system as well as with the differentiation of repeated amino acid. Figure 3-7 shows the assignment of cross peaks in the H^N-H^α figure-print region of 2D ^{1}H-^{1}H NOESY spectrum acquire with 200 ms mixing time for the 50% TFE sample. The assignments of cross peaks in the TOCSY finger print region and identification of residue type are presented in Figure 3-8. The chemical shift values in ppm for NK_4-M2GlyR-p20 T17R S20W in 50% TFE-d3 are presented in Table 3-2.

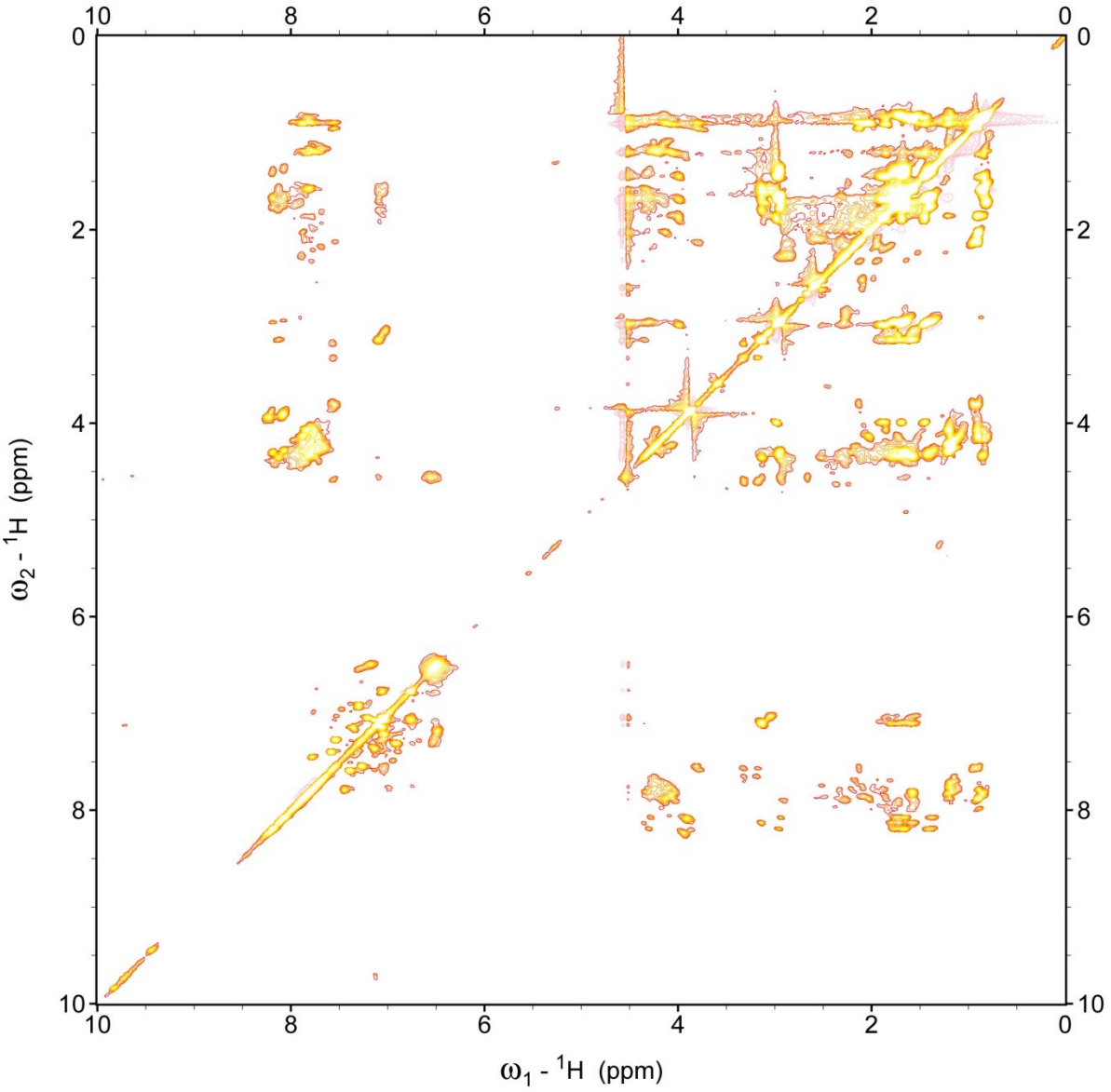

Figure 3-6. Full 2D ^{1}H-^{1}H TOCSY Spectrum of NK$_4$-M2GlyR-p20 T17R S20W in 50% TFE-d3. Acquired on a 500 MHz NMR instrument

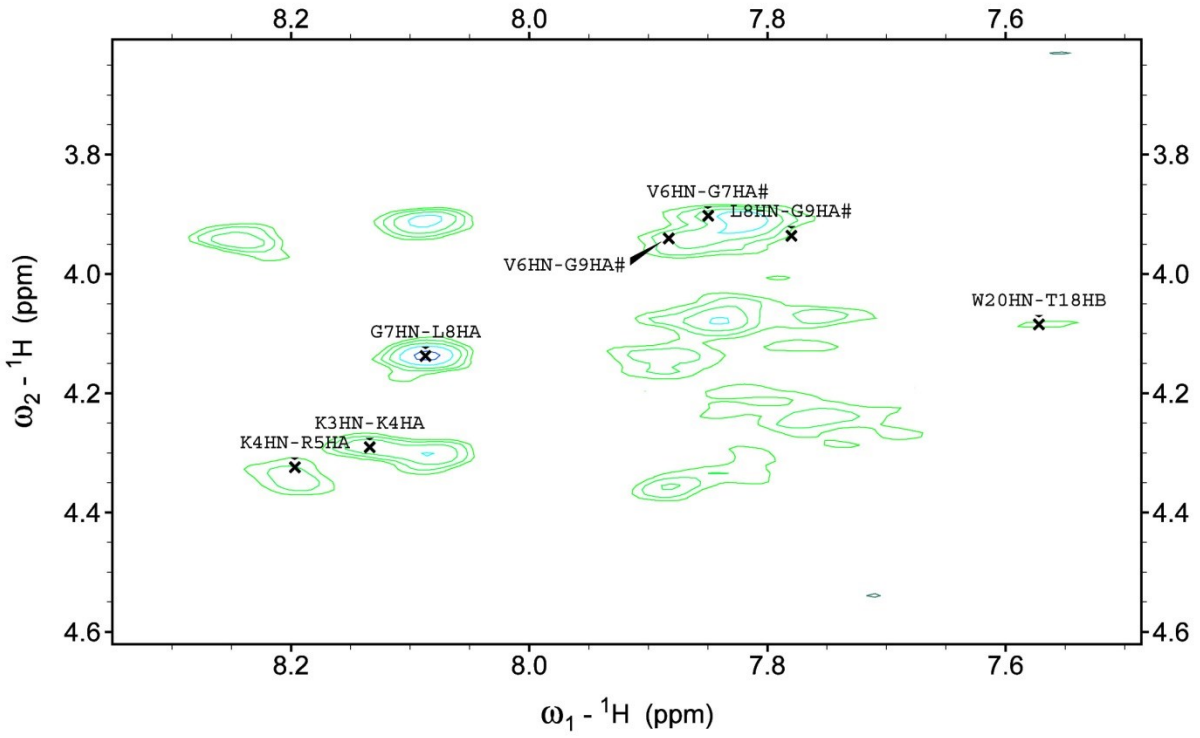

Figure 3-7. The H^N-H^α finger-print region of 2D ^{1}H-^{1}H NOESY spectrum for NK_4-M2GlyR-p20 T17R S20W in 50% TFE-d3 sample, acquired with 200 ms mixing time on a 500 MHz NMR instrument

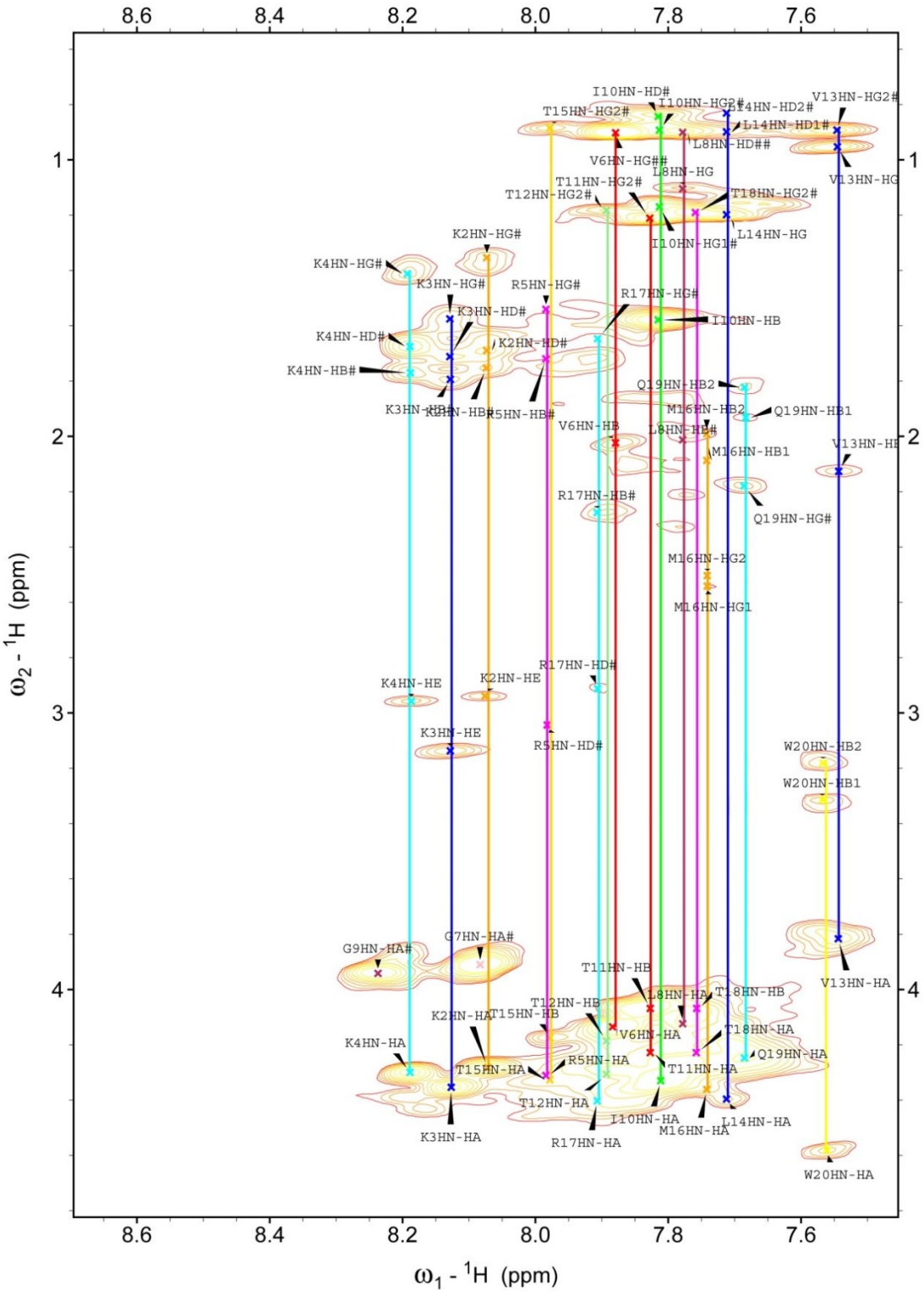

Figure 3-8. 2D ^{1}H-^{1}H TOCSY finger print region for NK$_4$-M2GlyR-p20 T17R S20W in 50% TFE-d3 acquired on a 500 MHz NMR instrument. Showing individual amino acid spin systems connected with a vertical line and labeled assignments of the cross peaks

Table 3-2. Chemical Shift Values (ppm) for NK_4-M2GlyR-p20 T17R S20W in 50% TFE-d3

Residue	*Chemical Shift (ppm)*				
	H^N	H^α	H^β	H^γ	*Others*
K1		3.99	1.87 1.69	1.22	δ 1.45 ε 2.99
K2	8.07	4.28	1.75	1.35	δ 1.69 ε 2.94
K3	8.13	4.35	1.79	1.58	δ 1.71 ε 3.14
K4	8.19	4.30	1.77	1.41	δ 1.68 ε 2.96
R5	7.98	4.32	1.72	1.54	δ 3.04
V6	7.88	4.14	2.03	0.91	
G7	8.09	3.91			
L8	7.78	4.13	2.01	1.11	δ 0.90
G9	8.24	3.94			
I10	7.81	4.33	1.58	1.17 0.89	δ 0.84
T11	7.83	4.23	4.07	1.21	
T12	7.89	4.31	4.19	1.18	
V13	7.55	3.82	2.13	0.95 0.89	
L14	7.71	4.40		1.20	δ 0.90 0.83
T15	7.98	4.33	4.18	0.89	
M16	7.74	4.36	2.09 1.99	2.54 2.50	
R17	7.91	4.40	2.28	1.65	δ 2.91
T18	7.76	4.23	4.08	1.19	
Q19	7.69	4.25	1.93 1.82	2.18	
W20	7.57	4.58	3.32 3.18		

A simultaneous analysis of 2D ^1H-^1H NOESY spectra (with 200 ms, 300 ms, and 400 ms mixing times) acquired for NK_4-M2GlyR-p20 T17R S20W in 50% TFE-d3, was performed for characterization of cross peaks due to dipole-dipole couplings between protons in spatial proximity. Several cross peaks indicative of $d_{\alpha N}(i, i+1)$, $d_{\beta N}(i, i+1)$, $d_{NN}(i, i+1)$, $d_{\alpha N}(i, i+2)$ and

$d_{\alpha N}(i, i+3)$ connectivity, which are consistent with a helical conformation (Wüthrich, 1986), were identified among other short and medium range connectivities. Figure 3-9 shows the H^N-H^N finger-print region of the 200 ms 2D ^{1}H-^{1}H NOESY spectrum with cross peak assignments. The observed NOEs are summarized graphically Figure 3-10.

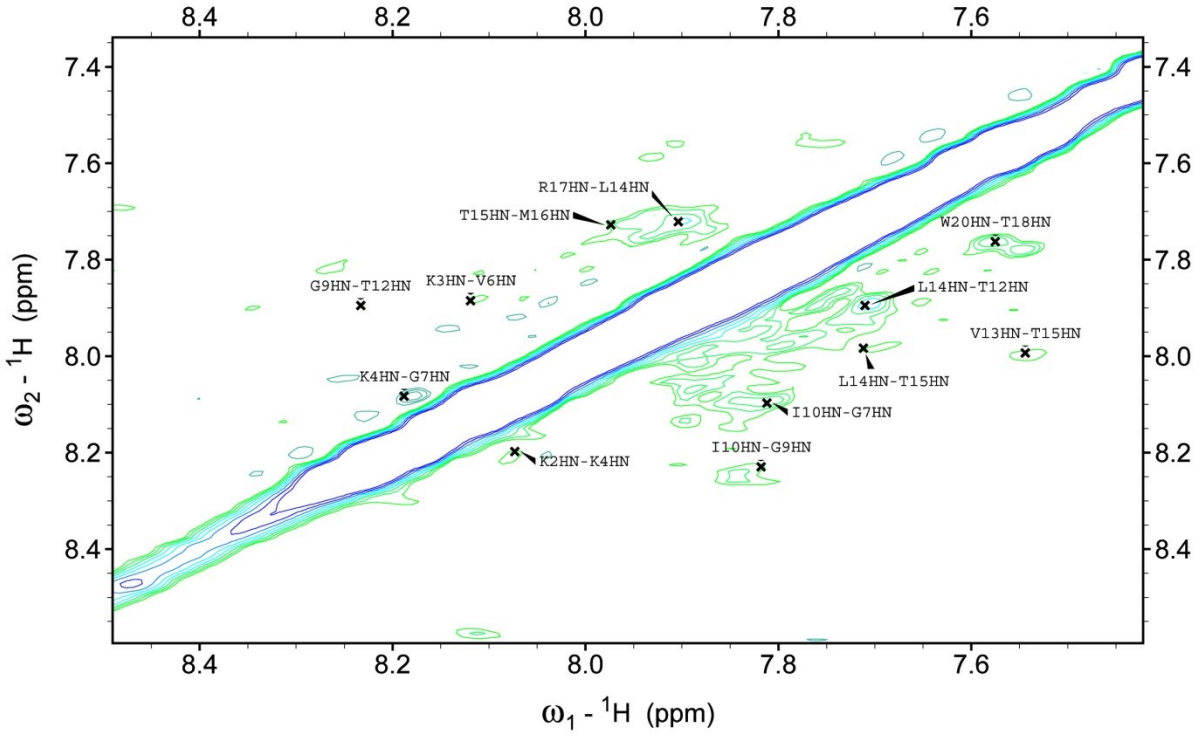

Figure 3-9. H^N-H^N finger-print region of 2D ^{1}H-^{1}H NOESY spectrum for NK_4-M2GlyR-p20 T17R S20W in 50% TFE-d3. The spectrum was acquired with 200 ms mixing time on a 500 MHz NMR instrument. The H^N-H^N connectivities are indicated by one letter amino-acid letter codes

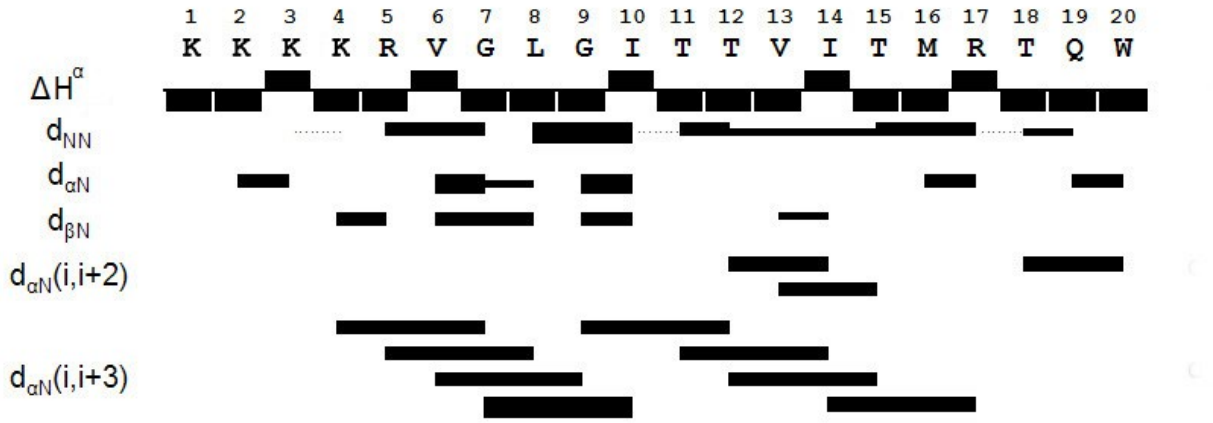

Figure 3-10. H^{α} Chemical Shift Index and summary of NOE connectivity for peptide NK_4-M2GlyR-p20 T17R S20W in 50% TFE-d3. The thickness of the lines is in proportion to the relative NOE intensities and dotted lines indicate ambiguity due to peak overlapping

The analysis of the NMR data collected for peptide NK_4-M2GlyR-p20 T17R S20W in SDS micelles followed the same procedure as describe above for the spectra from the 50% TFE-d3 sample. Notably the 2D ^1H-^1H TOCSY spectrum for the sample in SDS micelles (Figure 3-11) displays broader peaks and inefficient water suppression (~4.7 ppm). As expected and discussed in Chapter 2, it may be due to an increase in particle size. The analysis of the spectra acquired in SDS micelles sample was performed independently from spectra acquired in 50% TFE-d3, considering that the conditions of the two samples differ substantially and errors in interpretation could be introduced by assuming similar chemical shifts for both conditions.

Figure 3-12 shows the TOCSY spectral "finger print" region (H^N-H^{α}/side chain protons), for peptide NK_4-M2GlyR-p20 T17R S20W in SDS micelles. The individual amino acid spin systems are connected with a vertical line and labeled with residue one letter code and sequence

number. The chemical shift values for the unambiguously assigned resonances of this peptide sample in SDS micelles are presented in Table 3-3.

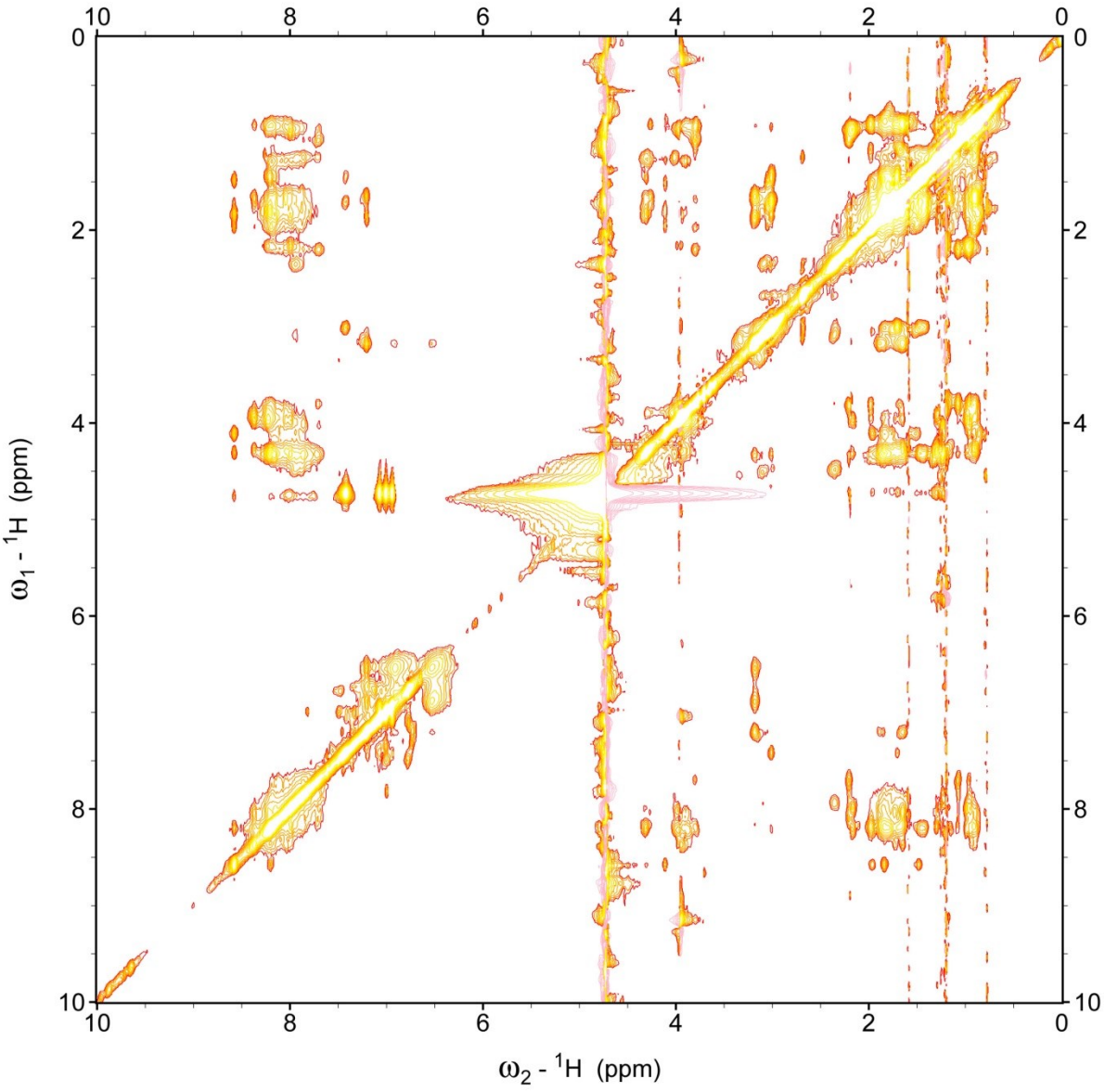

Figure 3-11. Full 2D ^{1}H-^{1}H TOCSY Spectrum of NK_4-M2GlyR-p20 T17R S20W in SDS micelles acquired on an 800 MHz NMR instrument

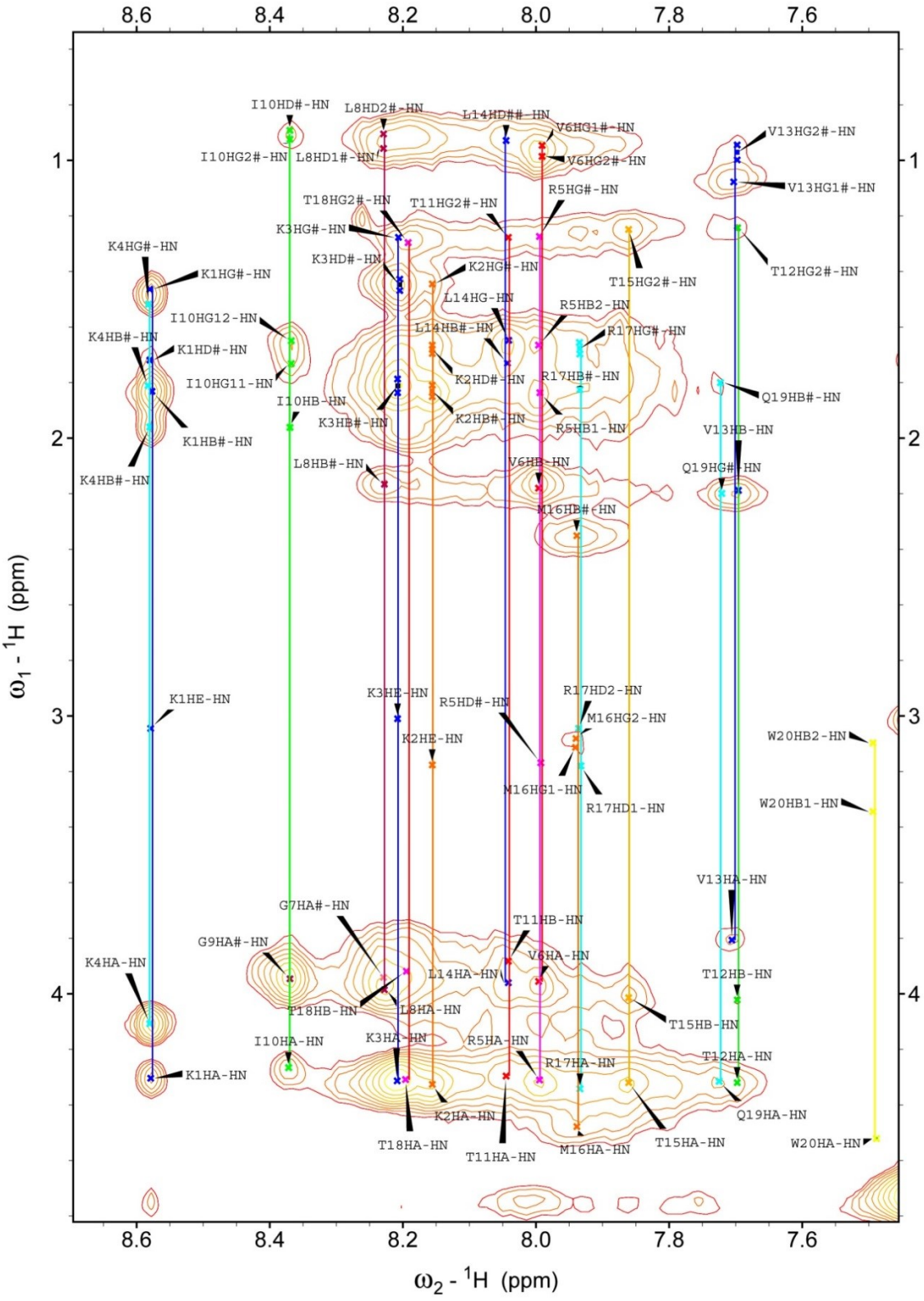

Figure 3-12. ^{1}H-^{1}H TOCSY finger print region for NK_4-M2GlyR-p20 T17R S20W in SDS micelles acquired on an 800 MHz NMR instrument

Table 3-3. Chemical Shift Values (ppm) for NK_4-M2GlyR-p20 T17R S20W in SDS micelles

Residue	*Chemical Shift (ppm)*				
	H^N	H^α	H^β	H^γ	*Others*
K1	8.58	4.30	1.83	1.47	δ 1.71 ε 3.05
K2	8.16	4.33	1.83	1.43	δ 1.68 ε 3.18
K3	8.21	4.31	1.81	1.28	δ 1.45 ε 3.02
K4	8.58	4.12	1.89	1.52	
R5	7.99	4.31	1.84 1.67	1.27	δ 3.16
V6	8.00	3.95	2.18	0.95 0.98	
G7	8.23	3.94			
L8	8.25	3.99	2.17		δ 0.96 0.91
G9	8.37	3.94			
I10	8.36	4.26	1.96	1.73 1.65	δ 0.87
T11	8.04	4.29	3.88	1.28	
T12	7.69	4.32	4.03	1.22	
V13	7.70	3.81	2.19	0.97 1.08	
L14	8.04	3.96	1.73	1.65	δ 0.93
T15	7.86	4.32	4.01	1.25	
M16	7.94	4.48	2.35	3.11 3.08	
R17	7.93	4.35	1.83	1.68	δ 3.19 3.05
T18	8.19	4.31	3.92	1.30	
Q19	7.72	4.34	1.80	2.20	
W20	7.50	4.52	3.35 3.10		

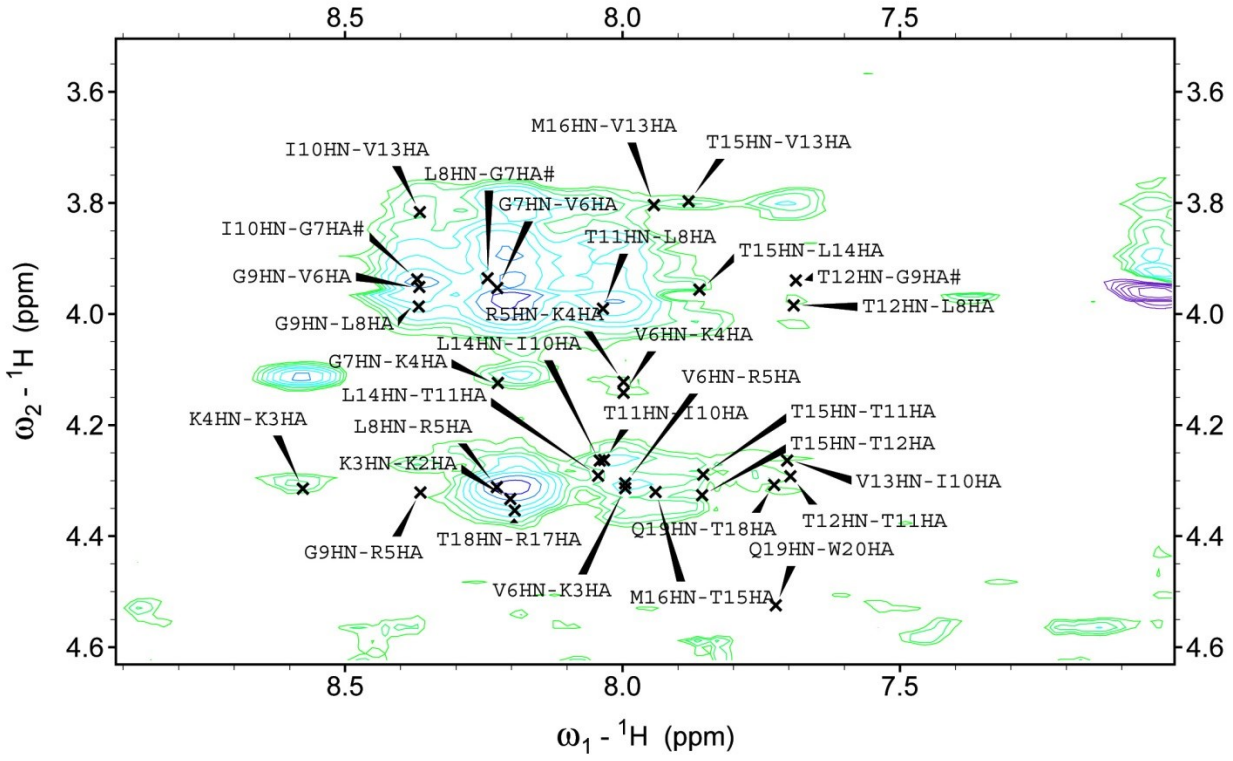

Figure 3-13. H^N-H^α finger-print region of 2D ^1H-^1H NOESY spectrum for NK_4-M2GlyR-p20 T17R S20W in SDS micelles, acquired with 400 ms mixing time on an 800 MHz NMR instrument, showing $d_{\alpha N}$ connectivities

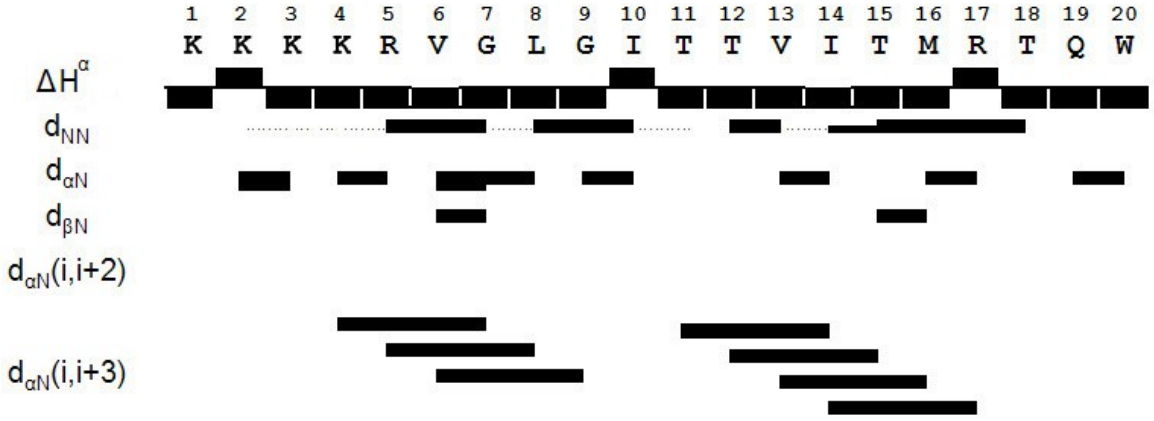

Figure 3-14. H^α Proton chemical shift index and summary of NOE connectivity for peptide NK_4-M2GlyR-p20 T17R S20W in SDS micelles. Line thickness indicates relative NOE peak intensity, and dotted lines indicate ambiguity due to peak overlapping

2D ^{1}H-^{1}H NOESY spectra collected with 300 ms and 400 ms mixing times for NK_4-M2GlyR-p20 T17R S20W in SDS micelles were analyzed simultaneously. The observation of sequential cross peaks corresponding to $d_{\alpha N}(i, i+1)$, $d_{\beta N}(i, i+1)$, $d_{NN}(i, i+1)$ connectivities and also the presence of cross peaks related to $d_{\alpha N}(i, i+3)$ connectivity suggested a continuous stretch of backbone ϕ and ψ angle values in the helical region of conformational space (Figure 3-13). Several other NOESY cross peaks were identified as short and medium range connectivities in other spectral regions, including the H^N-H^N region. A graphic summary of the NOE connectivities found for NK_4-M2GlyR-p20 T17R S20W in the SDS micelles sample is presented in Figure 3-14.

NMR Structure Calculations

The NMR structures were calculated from extended backbone conformations as starting models using the program CNS (Brunger et al., 1998). Unambiguously assigned NOE cross peaks from the 2D ^{1}H-^{1}H NOESY spectra (200 ms, 300 ms, and 400 ms for the 50% TFE sample and 300 ms and 400 ms for the SDS micelles sample) were classified as: intra-residue, sequential (i-j=1), and medium range (1< i-j<=4), however no long range connectivities (i-j>4) were found for either sample. NOE-derived inter-proton distance restraints were classified into approximate distance ranges of 1.8-2.5 Å; 1.8-3.5 Å, 1.8-5.0 Å, 1.8-5.0 Å and 1.8-6.0 Å corresponding to strong, medium, weak and very weak NOE cross peaks; an additional 0.5-1.0 Å was added to the upper distance bound of distance restraints involving methyl groups. A total of 112 distance constraints for the 50% TFE sample and 146 distance constraints for the SDS micelles sample

were derived from corresponding NOE data. For the 50% TFE sample we observed 22 intra-residue, 44 sequential, and 46 medium range constraints; while the SDS micelles sample showed 22 were intra-residue, 56 sequential, and 68 medium range constraints.

Table 2-3 summarizes the distance constrains used during the structure calculations for peptide NK_4-M2GlyR-p20 T17R S20W in 50% TFE and SDS micelles. The NMR structure calculations were performed independently for each of sample conditions as described in the methods section.

Figure 3-15 shows the cluster of 15 calculated structures of peptide NK_4-M2GlyR-p20 T17R S20W in 50% TFE with lowest average energy. These 15 structures are superimposed and clustered by root mean square deviation (RMSD) of the backbone atoms and may be considered a representation of the predominant conformation for peptide NK_4-M2GlyR-p20 T17R S20W in TFE solution. These structures show a well-defined α-helix in the central part of the peptide (spanning from residues arginine 5 to methionine 16) with segregation of the hydrophobic and hydrophilic side chains to different sides of the helix. The four N-terminal lysines seem to be unstructured with a less defined conformation. The four C-terminal residues (arginine 17, threonine 18, glutamine 19, and tryptophan 20) appear to have a bend or turn, a similar distortion from a purely helical structure was reported for peptide NK_4-M2GlyR-p22 S22W in the structure calculated by NMR in TFE solution (Cook et al., 2004).

Table 3-4. Structural Statistics for peptide NK_4-M2GlyR-p20 T17R S20W in 50% TFE and in SDS Micelles

	50% TFE	SDS Micelles
Experimental NMR Constraints		
NOE Distance Constraints		
Intra-residue	22	22
Sequential	44	56
Medium Range	46	68
Long Range	0	0
Energy (kcal/mol^{-1})		
E_{total}	-104.32 ±18.3	-58.00 ±12.9
RMSD from the mean structure (Å)		
Backbone atoms (residues 1-20)	1.21 ± 0.51	1.45 ± 0.35
Backbone atoms (residues 3-18)	0.96 ± 0.33	0.63 ± 0.24

The side chains of amino acid residues threonine 11 and 15, (corresponding to threonine 13 and 17 in the p22 sequences) expected to line the inside of the assembled channel, align with the hydrophobic side of the helix, while the side chain of threonine18 (threonine 20 in the p22 sequences) is part of the observed turn and is in an orientation that would need to change during the process of forming the channel in order to become part of the interior surface.

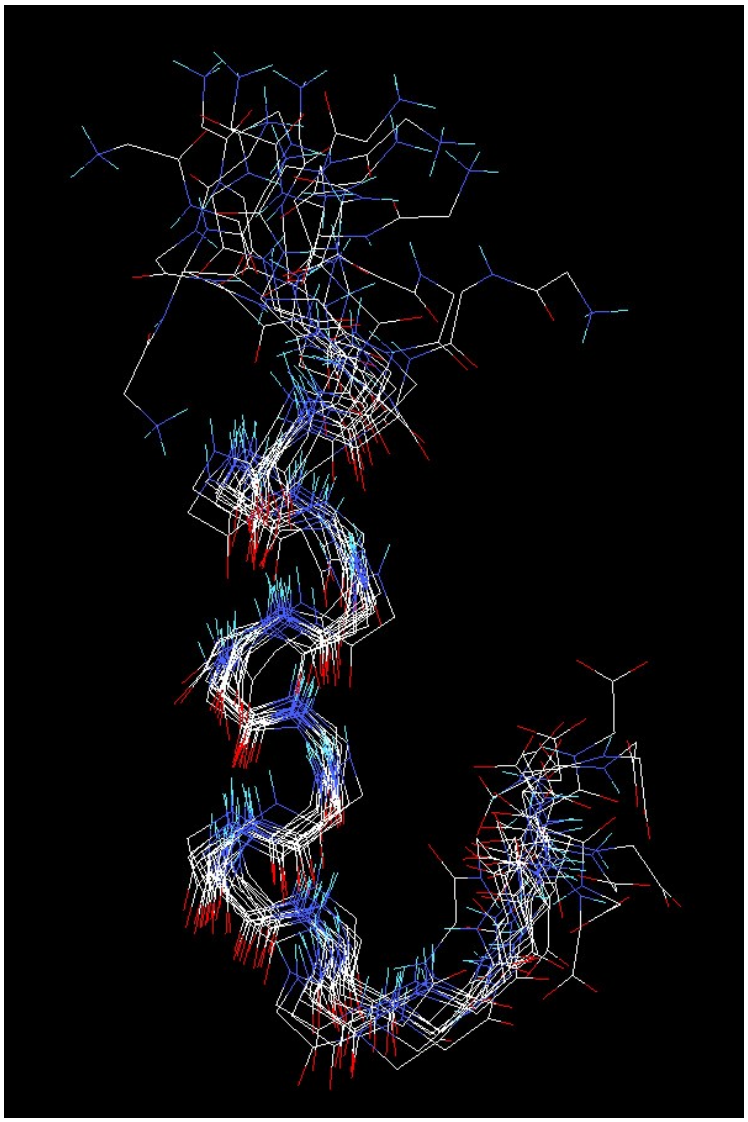

Figure 3-15. Solution monomeric structure of peptide NK_4-M2GlyR-p20 T17R S20W in 50% TFE. Cluster of the 15 calculated structures with the lowest average energy superimposed (only backbone atoms are displayed)

Figure 3-16 presents a cluster of 15 calculated structures for peptide NK_4-M2GlyR-p20 T17R S20W in SDS micelles. The 15 calculated structures with lowest average total energy were clustered by RMSD using backbone atoms of the residues. The cluster of 15 conformers represents the predominant structure of peptide NK_4-M2GlyR-p20 T17R S20W in SDS micelles.

The predominant structural features for the peptide in SDS micelles include a well-defined α helix in the central part of the peptide (spanning from lysine 4 to methionine 16); and a segregation of the hydrophobic and hydrophilic side chains to different sides of the helix. The N-terminal three lysines are unstructured, but appear to be more restricted than in the structures calculated for this peptide in TFE solution. The four C-terminal residues (arginine 17, threonine 18, glutamine 19, and tryptophan 20) form an incomplete helix turn and present some variability within the cluster of structures.

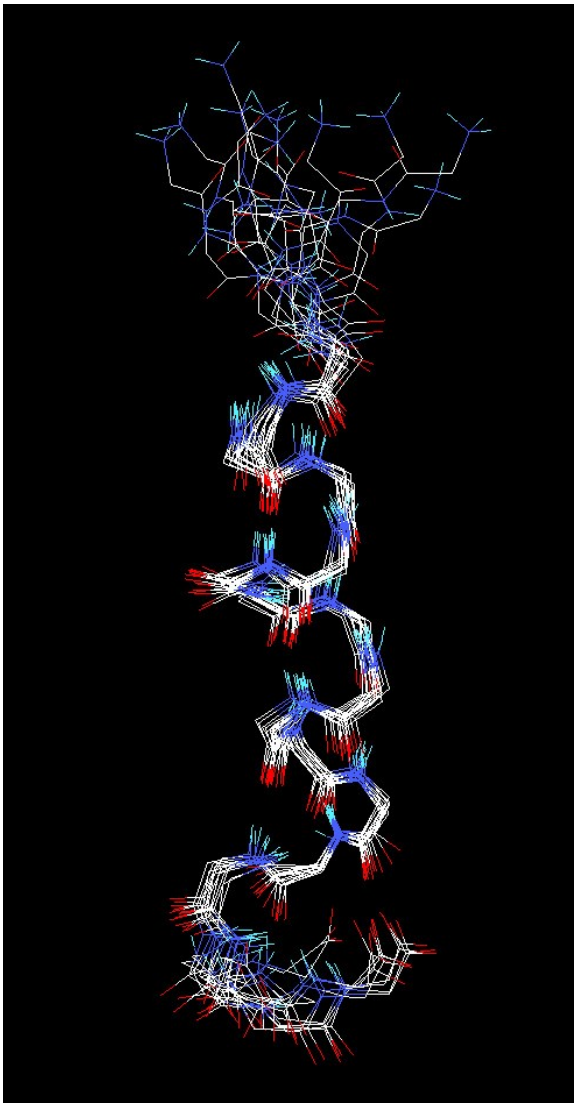

Figure 3-16. Solution monomeric structure of peptide NK_4-M2GlyR-p20 T17R S20W in SDS micelles. Cluster of the 15 calculated structures with the lowest average energy superimposed (only backbone atoms are displayed)

Discussion and Analysis

A comparison of the concentration dependence of the I_{SC} stimulated by peptide NK_4-M2GlyR-p20 T17R S20W in MDCK cell, with that of other M2GlyR derived peptides previously reported (Broughman et al., 2004;Bukovnik et al., 2012;Cook et al., 2004;Shank et

al., 2006) shows that peptide NK_4-M2GlyR-p20 T17R S20W has both a higher I_{MAX} and a lower $K_{1/2}$, characteristics that are desirable for a potential therapeutic peptide (Figure 4-2).

The calculated average structure for peptide NK_4-M2GlyR-p20 T17R S20W under both experimental conditions tested (50% TFE, SDS micelles) is predominantly α-helical as is expected for the channel forming peptides of this family (Figure 3-17). Differences between the structures calculated in TFE solution and SDS micelles for peptide NK_4-M2GlyR-p20 T17R S20W are detected. The most notable difference is in the C-terminal residues (17-20), for both sample conditions these residues are not part of the main α helix. For the 50% TFE sample, the C-terminal residues form a bend that folds back towards the helix, and that seems to be stabilized by a hydrogen bond between the side chain hydroxyl of threonine 12 and the carbonyl from threonine 18. For the structures calculated from the SDS micelles sample the C-terminal residues continue in the same general direction of the main α helix axis but do not come in enough proximity to form the characteristic hydrogen bond with the amino acids in the helix. Notable changes in structure between samples in TFE solution compared to in SDS micelles have previously been reported for peptide NK_4-M2GlyR-p22 S22W another member of the family of M2GlyR derived peptides. The changes for NK_4-M2GlyR-p22 S22W are attributed to the formation of a hydrophobic pocket in the central part of the peptide (Cook et al., 2004). For peptide NK_4-M2GlyR-p20 T17R S20W this does not appear to be the case, as no hydrophobic side chains are located towards the inside of the bend.

Comparison between the 2D ^1H-^1H TOCSY spectra for both sample conditions reveals a greater dispersion in the H^N resonances for the SDS micelles sample (Figure 3-8 and Figure 3-12 are at

the same scale), this dispersion in the chemical shift scale is indicative of a better defined secondary structure in SDS micelles, and is consistent with the calculated structures (the upfield shift of the resonances in the 50%TFE can be attributed to the difference in temperature). The calculated chemical shift index of the H^{α} further supports that the secondary structure adopted by the peptide in the micelle environment is better defined. For the SDS micelles sample the CSI is consistently negative for almost the full length of the peptide (Figure 3-14), whereas for the 50% TFE sample the CSI shows changes in sign frequently along the sequence (Figure 3-10). In Chapter 2 it was mentioned that the CSI was found to be of limited predicting value for the M2GlyR peptides, but perhaps it can be indicative of stability of the secondary structure elements.

The apparently more restricted N-terminus for the peptide in SDS micelles compared with the peptide in 50% TFE can be explained by the presence of the hydrophilic heads of the SDS molecules around the peptide, exerting force into the lysine residues, a similar effect could be responsible for a more restricted structure overall for the SDS micelles sample, that was calculated to have a RMSD of 0.63 ± 0.24 Å in the helical region, compare to 0.96 ± 0.33 Å for the TFE sample (Table 2-3). Since every residue is expected to be in contact with the SDS molecules, the conformation adopted by the shorter peptide (2 residues less than the peptides previously studied) in SDS micelles could potentially be more affected by the environment than the conformation of the 22 residue peptides that have been postulated to have their N-terminus exposed to the bulk water.

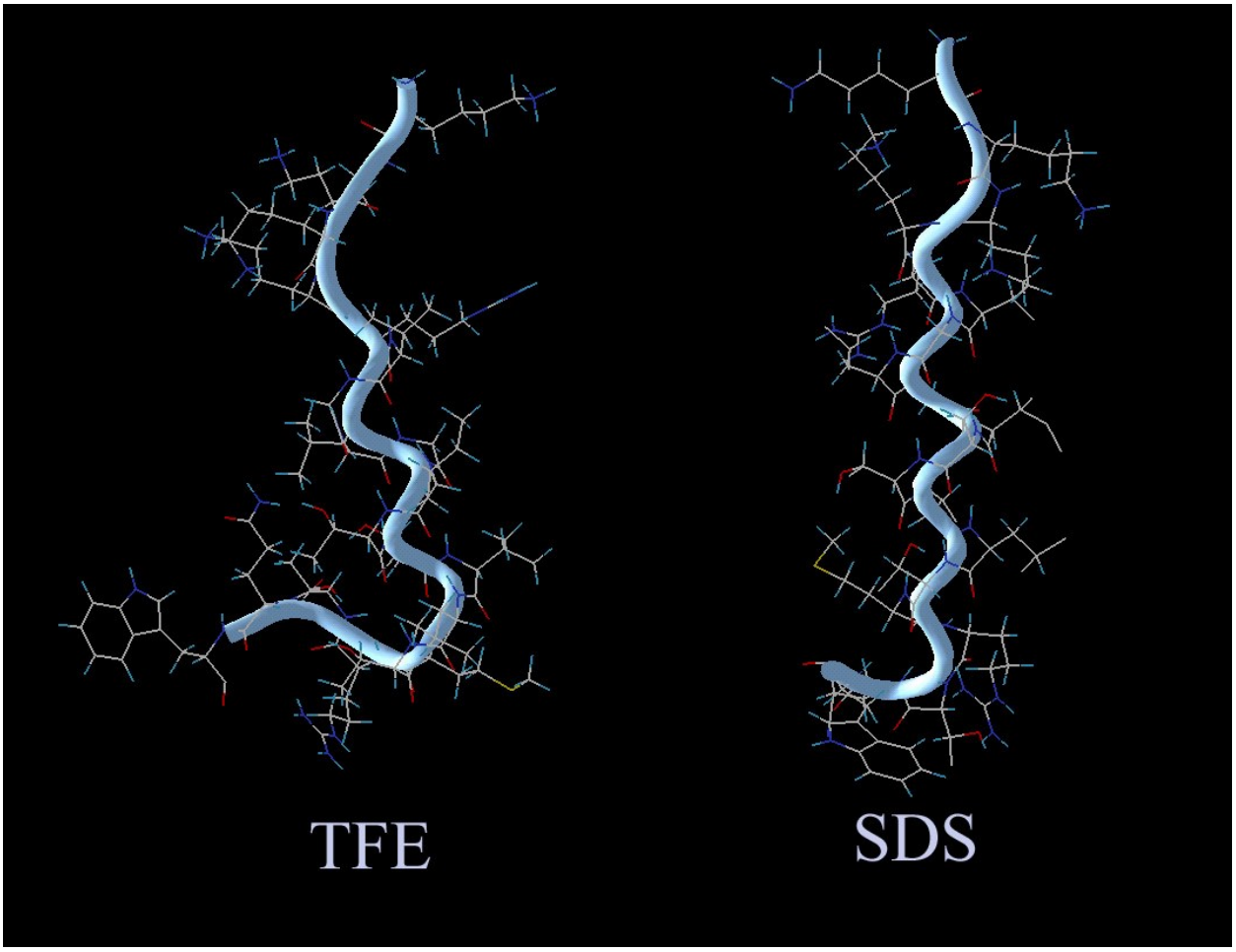

Figure 3-17. Comparison between the average determined structures for channel forming peptide NK_4-M2GlyR-p20 T17R S20W in 50% TFE and SDS micelles

The terminal lysines of NK_4-M2GlyR-p20 T17R S20W are more restricted also than the terminal lysines reported in the NMR structures for other M2GlyR derived peptides (Cook et al., 2004;Herrera et al., 2010), this could be explained by the shorter axial length of the NK_4-M2GlyR-p20 T17R S20W peptide when compared with 22 residue sequences. The presence of membrane anchoring residues in the C-terminus could force the N-terminal lysines into the interior of the micelle.

The calculated structures for the SDS micelles samples are expected to be a better representation of the structure adopted by the peptide in the interior of a membrane bilayer, than the structures calculated in the TFE solution. There are expected limitations to the SDS calculated structures as well, SDS molecules have 12 carbon alkyl tails whereas cellular membranes are mainly composed by lipids with longer acyl chains, 16 to 20 carbons mostly (Spector and Yorek, 1985)). With the radius of an SDS micelle reported to between 15 Å and 20 Å (Cabane et al., 1985;Duplatre et al., 1996;Pires et al., 2012), and an axial length of the determined structure for NK_4-M2GlyR-p20 T17R S20W of ~30 Å, the peptide is expected to barely cross the micelles. The structure calculated is not expected to be able to span across an unperturbed cellular membrane to form ion channels.

The findings on peptide NK_4-M2GlyR-p20 T17R S20W make it a step forward towards the optimization of the peptide sequence for an optimal channel forming peptide, further study of the permselectivity of the formed channels is needed to characterize the ion current induced by the peptide, since the removed amino acids from the sequence may play a role in the filter of the ion channel.

References

Arseniev, A. S., Barsukov, I. L., Bystrov, V. F., Lomize, A. L. and Ovchinnikov Yu, A. (1985). 1H-NMR study of gramicidin A transmembrane ion channel. Head-to-head right-handed, single-stranded helices. *FEBS Lett* **186**, 168-174.

Broughman, J. R., Brandt, R. M., Hastings, C., Iwamoto, T., Tomich, J. M. and Schultz, B. D. (2004). Channel-forming peptide modulates transepithelial electrical conductance and solute permeability. *American journal of physiology. Cell physiology* **286**, C1312-1323.

Broughman, J. R., Mitchell, K. E., Sedlacek, R. L., Iwamoto, T., Tomich, J. M. and Schultz, B. D. (2001). NH(2)-terminal modification of a channel-forming peptide increases capacity for epithelial anion secretion. *American journal of physiology. Cell physiology* **280**, C451-458.

Broughman, J. R., Shank, L. P., Takeguchi, W., Schultz, B. D., Iwamoto, T., Mitchell, K. E. and Tomich, J. M. (2002). Distinct structural elements that direct solution aggregation and membrane assembly in the channel-forming peptide M2GlyR. *Biochemistry* **41**, 7350-7358.

Brunger, A. T., Adams, P. D., Clore, G. M., DeLano, W. L., Gros, P., Grosse-Kunstleve, R. W., Jiang, J. S., Kuszewski, J., Nilges, M., Pannu, N. S., Read, R. J., Rice, L. M., Simonson, T. and Warren, G. L. (1998). Crystallography & NMR system: A new software suite for macromolecular structure determination. *Acta Crystallogr D Biol Crystallogr* **54 (Pt 5)**, 905-921.

Bukovnik, U., Gao, J., Cook, G. A., Shank, L. P., Seabra, M. B., Schultz, B. D., Iwamoto, T., Chen, J. and Tomich, J. M. (2012). Structural and biophysical properties of a synthetic channel-forming peptide: designing a clinically relevant anion selective pore. *Biochimica et biophysica acta* **1818**, 1039-1048.

Cabane, B., Duplessix, R. and Zemb, T. (1985). High-Resolution Neutron-Scattering on Ionic Surfactant Micelles - Sds in Water. *Journal De Physique* **46**, 2161-2178.

Cammers-Goodwin, A., Lee, T. C. and Walgers, R. (1998). The mechanism of fluoroalcohol-mediated conformational purturbation of peptides. *Abstracts of Papers of the American Chemical Society* **216**, U216-U216.

Carlin, R. W., Sedlacek, R. L., Quesnell, R. R., Pierucci-Alves, F., Grieger, D. M. and Schultz, B. D. (2006). PVD9902, a porcine vas deferens epithelial cell line that exhibits neurotransmitter-stimulated anion secretion and expresses numerous HCO3(-) transporters. *American journal of physiology. Cell physiology* **290**, C1560-1571.

Cook, G. A., Prakash, O., Zhang, K., Shank, L. P., Takeguchi, W. A., Robbins, A., Gong, Y. X., Iwamoto, T., Schultz, B. D. and Tomich, J. M. (2004). Activity and structural comparisons of solution associating and monomeric channel-forming peptides derived from the glycine receptor m2 segment. *Biophys J* **86**, 1424-1435.

Cornell, W. D., Cieplak, P., Bayly, C. I., Gould, I. R., Merz, K. M., Ferguson, D. M., Spellmeyer, D. C., Fox, T., Caldwell, J. W. and Kollman, P. A. (1995). A 2nd Generation Force-Field for the Simulation of Proteins, Nucleic-Acids, and Organic-Molecules. *Journal of the American Chemical Society* **117**, 5179-5197.

D'Andrea-Winslow, L., Strohmeier, G. R., Rossi, B. and Hofman, P. (2001). Identification of a sea urchin Na(+)/K(+)/2Cl(-) cotransporter (NKCC): microfilament-dependent surface expression is mediated by hypotonic shock and cyclic AMP. *The Journal of experimental biology* **204**, 147-156.

D.A. Case, D. A. P., J.W. Caldwell, T.E. Cheatham III, J. Wang, W.S. Ross, C.L. Simmerling, T.A. Darden, K.M. Merz, R.V. Stanton, A.L. Cheng, J.J. Vincent, M. Crowley, V. Tsui, H. Gohlke, R.J. Radmer, Y. Duan, J. Pitera, I. Massova, G.L. Seibel, U.C. Singh, P.K. Weiner and P.A. Kollman (2002). AMBER 7.

Delaglio, F., Grzesiek, S., Vuister, G. W., Zhu, G., Pfeifer, J. and Bax, A. (1995). NMRPipe: a multidimensional spectral processing system based on UNIX pipes. *J Biomol NMR* **6**, 277-293.

Devor, D. C., Singh, A. K., Frizzell, R. A. and Bridges, R. J. (1996). Modulation of Cl- secretion by benzimidazolones. I. Direct activation of a Ca(2+)-dependent K+ channel. *The American journal of physiology* **271**, L775-784.

Duplatre, G., Marques, M. F. F. and daGracaMiguel, M. (1996). Size of sodium dodecyl sulfate micelles in aqueous solutions as studied by positron annihilation lifetime spectroscopy. *Journal of Physical Chemistry* **100**, 16608-16612.

Goddard, T. D. and Kneller, D. G. (2004). SPARKY 3. University of California, San Francisco.

Grantham, J. J., Uchic, M., Cragoe, E. J., Jr., Kornhaus, J., Grantham, J. A., Donoso, V., Mangoo-Karim, R., Evan, A. and McAteer, J. (1989). Chemical modification of cell proliferation and fluid secretion in renal cysts. *Kidney international* **35**, 1379-1389.

Herrera, A. I., Al-Rawi, A., Cook, G. A., Gao, J., Iwamoto, T., Prakash, O., Tomich, J. M. and Chen, J. (2010). Structural characterization of two pore-forming peptides: consequences of introducing a C-terminal tryptophan. *Proteins* **78**, 2238-2250.

Jasanoff, A. and Fersht, A. R. (1994). Quantitative determination of helical propensities from trifluoroethanol titration curves. *Biochemistry* **33**, 2129-2135.

Kirnarsky, L., Prakash, O., Vogen, S. M., Nomoto, M., Hollingsworth, M. A. and Sherman, S. (2000). Structural effects of O-glycosylation on a 15-residue peptide from the mucin (MUC1) core protein. *Biochemistry* **39**, 12076-12082.

MacPhee, C. E., Perugini, M. A., Sawyer, W. H. and Howlett, G. J. (1997). Trifluoroethanol induces the self-association of specific amphipathic peptides. *Febs Letters* **416**, 265-268.

Pervushin, K. V., Arseniev, A. S., Kozhich, A. T. and Ivanov, V. T. (1991). Two-dimensional NMR study of the conformation of (34-65)bacterioopsin polypeptide in SDS micelles. *J Biomol NMR* **1**, 313-322.

Piotto, M., Saudek, V. and Sklenar, V. (1992). Gradient-Tailored Excitation for Single-Quantum Nmr-Spectroscopy of Aqueous-Solutions. *Journal of Biomolecular Nmr* **2**, 661-665.

Pires, J. M., de Moura, A. F. and Freitas, L. C. G. (2012). Investigating the Spontaneous Formation of Sds Micelle in Aqueous Solution Using a Coarse-Grained Force Field. *Quimica Nova* **35**, 978-U352.

Rizo, J., Blanco, F. J., Kobe, B., Bruch, M. D. and Gierasch, L. M. (1993). Conformational behavior of Escherichia coli OmpA signal peptides in membrane mimetic environments. *Biochemistry* **32**, 4881-4894.

Roccatano, D., Colombo, G., Fioroni, M. and Mark, A. E. (2002). Mechanism by which 2,2,2-trifluoroethanol/water mixtures stabilize secondary-structure formation in peptides: a molecular dynamics study. *Proceedings of the National Academy of Sciences of the United States of America* **99**, 12179-12184.

Shank, L. P., Broughman, J. R., Takeguchi, W., Cook, G., Robbins, A. S., Hahn, L., Radke, G., Iwamoto, T., Schultz, B. D. and Tomich, J. M. (2006). Redesigning channel-forming peptides: amino acid substitutions that enhance rates of supramolecular self-assembly and raise ion transport activity. *Biophys J* **90**, 2138-2150.

Spector, A. A. and Yorek, M. A. (1985). Membrane lipid composition and cellular function. *Journal of lipid research* **26**, 1015-1035.

Stein, E. G., Rice, L. M. and Brunger, A. T. (1997). Torsion-angle molecular dynamics as a new efficient tool for NMR structure calculation. *Journal of magnetic resonance* **124**, 154-164.

Tomich, J. M., Wallace, D., Henderson, K., Mitchell, K. E., Radke, G., Brandt, R., Ambler, C. A., Scott, A. J., Grantham, J., Sullivan, L. and Iwamoto, T. (1998). Aqueous solubilization of transmembrane peptide sequences with retention of membrane insertion and function. *Biophysical journal* **74**, 256-267.

Wallace, D. P., Tomich, J. M., Iwamoto, T., Henderson, K., Grantham, J. J. and Sullivan, L. P. (1997). A synthetic peptide derived from glycine-gated Cl- channel induces transepithelial Cl- and fluid secretion. *Am J Physiol* **272**, C1672-C1679.

Wüthrich, K. (1986). *NMR of proteins and nucleic acids*. The George Fisher Baker non-resident lectureship in chemistry at Cornell University, Wiley, New York.

Wüthrich, K., Billeter, M. and Braun, W. (1983). Pseudo-structures for the 20 common amino acids for use in studies of protein conformations by measurements of intramolecular proton-proton distance constraints with nuclear magnetic resonance. *J Mol Biol* **169**, 949-961.

Chapter 4 - Comparison between NMR determined monomeric structures for Channel-Forming Peptides and analysis of the potential of the monomeric structure as a predictor of channel activity

Introduction

NMR data based protein structures can provide information about the conformation of a molecule at atomic resolution level under solution condition. For a protein with a well-defined secondary and tertiary structure, an NMR determined structure describes a complex set of short, medium, and long range dipole interactions. Therefore NMR spectroscopy provides a very valuable technique for the description and study of the protein topology and function. In the case of small monomeric peptides the question of structure determination could be a simple one, and complete description could be just assigning a secondary structural elements (α-helix, β-strand, random coil) to each residue in the sequence. The molecular structure of membrane active peptides is much more dynamic in nature, and depends strongly on the environment surrounding the peptide at any given moment (e.g. extracellular space, membrane surface, membrane interior) (Bechinger, 2008) and on the peptide's oligomerization state (Bartels et al., 2011).

For the structure determination of any protein by NMR spectroscopy, careful consideration should be given to the conditions used for sample preparation. The sample conditions should be similar enough to the "natural" environment of the protein such that the resulting structure can be considered biologically relevant, but cannot go beyond the instrumental limitations of the

technique in general, and of the available resources. Structural studies of membrane associated proteins have always been considered challenging for NMR spectroscopy. Two approaches are available for the study of membrane associated proteins by NMR: (A) The use of oriented phospholipid bilayers in solid state NMR (Marassi and Opella, 1998) and (B) the use of membrane mimetics in solution NMR (Warschawski et al., 2011).

The oligomeric state and structure of M2GlyR derived peptides in solutions was initially assessed by chemical cross-linking and circular dichroism studies, respectively (Broughman et al., 2002b). Looking for a more detail description of the structure in solution, the use of NMR spectroscopy was implemented, first as an indicator of secondary structure elements (Broughman et al., 2002a), and later in the complete determination of the solution structure (Cook et al., 2004). Membrane mimetics were later used to determine the monomeric structure of M2GlyR derived peptides a membrane like environment (Herrera et al., 2010).

Most NMR determined structures for M2GlyR peptides present a high degree of similarity. Determination of the molecular structure by NMR for newly designed M2GlyR peptides requires a considerable investment of both material and human resources, i.e. peptide purification, sample preparation, data acquisition, data analysis and structure calculations. The question has arisen of whether or not there is compelling need to determine the NMR structure of the peptides that constitute the most recent developments in the optimization of the M2GlyR family of channel forming peptides. This report tries to provide arguments to answer that question, taking into consideration all the available NMR determined structures for M2GlyR derived channel forming peptides, an evaluation of whether the structures provide valuable information not otherwise

available is attempted. How well the changes in ion conductance between peptide sequences can be explained by the differences in structure, the potential of the structure as a predictor of electrophysiological characteristics, and the usefulness of the structure as an aid in the design of improved peptide sequences are the characteristics evaluated.

Materials and Methods

Peptide Synthesis and Purification

All peptides consider for this analysis (Figure 4-1) were chemically synthesized as described in the previous chapters at the Biotechnology Core Facility of Kansas State University by solid phase peptide synthesis methodology using 9-fluorenylmethoxycarbonyl (Fmoc) chemistry (Tomich et al., 1998). CLEAR amide resin (0.3 mmol/g) was purchased from Peptides International Inc. (Louisville, KY) and N^{α}-Fmoc amino acids were purchased from Anaspec (Fremont, CA), Bachem Inc. (Torrance, CA), and Peptides International Inc. (Louisville, KY). The peptides were purified using a System Gold HPLC system (Beckman Instruments Inc., Fullerton, CA) and eluted from the column using a linear gradient of acetonitrile containing 0.1% trifluoroacetic acid (TFA). HPLC-purified peptides were characterized by matrix-assisted-laser desorption time-of-flight mass spectroscopy (MALDI-TOF/TOF) using a Bruker Ultraflex II mass spectrometer (Bruker Instruments Inc., Billerica, MA) and after characterization, peptides were lyophilized and stored as dry powder until used.

Transepithelial ion transport measurements

Transepithelial ion transport measurements in Madin-Darby canine kidney (MDCK) epithelial cells were performed as described in Chapter 3, briefly cells were maintained as subconfluent monolayers and were allowed to propagate until they were harvested. MDCK cells were plated onto permeable culture support wells (Snapwell, 12 mm diameter. CoStar, Cambridge, MA). Snapwell supports were placed in a six-well plate with DMEM/F-12 plus P/S and FBS, monolayers of MDCK cells were used 7-14 days after reaching confluency. Transepithelial ion transport was evaluated with the use of a modified Ussing chambers (Model DCV9, Navicyte, San Diego, CA). MDCK cell monolayers in the Snapwells were mounted vertically in the chambers. Apical and basolateral surfaces of the monolayers were bathed in a modified Ringer solution (120 mM NaCl, 25 mM $NaHCO_3$, 3.3 mM KH_2PO_4, 0.8 mM K_2HPO4, 1.2 mM $MgCl_2$, and 1.2 mM $CaCl_2$), which was prepared daily. The solution bathing the monolayers was kept at 37 °C and continuously bubbled with 5% CO_2/ 95% O_2 , experiments were conducted on monolayers with a resistance of at least 600 Ohms cm^2 (Grantham et al., 1989;Shank et al., 2006;Wallace et al., 1997). The transepithelial membrane potential (V_{TE}) was clamped to 0 mV and the short-circuit current measured continuously with a voltage clamp apparatus (Model 558C, University of Iowa, Department of Bioengineering, Iowa City, IA). Data was acquired at a rate of 1 Hz. Reported data points represent the mean I_{SC} stimulated by the peptide at the indicated concentrations; bars indicate the standard error of the mean. Continuous lines presented in Figure 4-2 represent the best fit of the data to a modified Hill equation.

Circular Dichroism

Circular Dichroism (CD) spectroscopy measurements were performed on a Jasco J-720 or a Jasco J-815 spectropolarimeter (Jasco Inc., Tokyo, Japan) using a quartz cuvette with a path length of 0.1 mm or 1.0 mm (Fisher Scientific, Waltham, MA). All spectra were recorded from 260 to 190 nm wavelength using a 1.0 nm spectral bandwidth, 0.2 nm step resolution, 20 nm/min scan speed, and 2 second response time. Also a baseline measurement was performed at the beginning of each run to check instrument stability. The CD spectra presented for the peptide solutions are an average of eight scans with background subtraction. Peptide stock solution was prepared to a concentration of 1 mM in water, stock solution concentration was determined using fluorescence at 278 nm, and final peptide concentration in all CD samples was 50 μM. Bovine serum albumin (BSA) served as the protein standard. The DI (deionized)-distilled H_2O peptide sample (0% TFE) was prepared by diluting 50 μL peptide stock solution with 950 μL DI H_2O. TFE:water peptide samples were prepared by vortexing 50 μL of peptide stock solution with calculated volumes of TFE (Sigma-Aldrich Inc., St. Louis, MO) and DI-distilled H_2O to produce a final TFE concentration of 25% and 50% by volume. The SDS micelles peptide sample was prepared by adding 50 μL of peptide stock solution with two minute sonication to calculated volumes to yield 10 mM SDS, 10 mM NaCl, and 10 mM phosphate buffer at pH 7.0 concentrations.

NMR Spectroscopy

NMR samples for each peptide considered in this analysis were prepared in a slightly different way, as a result of progressive optimization of the procedure and to the particular challenges presented by each peptide. NMR studies on peptide NK_4-M2GlyR-p27 were performed by J.R. Broughman (Broughman et al., 2002a). NMR studies on peptide NK_4-M2GlyR-p22 were performed by G. A. Cook and A. I. Herrera (Cook et al., 2004;Herrera et al., 2010). NMR studies on peptide NK_4-M2GlyR-p22 S22W were performed by G. A. Cook (Cook et al., 2004;Herrera et al., 2010). NMR studies on peptide NK_4-M2GlyR-p22 T19R S22W were performed by G. A. Cook (Bukovnik et al., 2012). NMR studies on peptide NK_4-M2GlyR-p20 T17W S20W were performed by A. I. Herrera (Chapter 2). The protocols involved in TFE solution and SDS micelles sample preparation are described in the Materials and Methods section of Chapter 3. The peptide concentration and solvent concentration for each sample are presented in Table 4-1.

Table 4-1. Sample and experimental conditions for NMR structural studies of NK_4-M2GlyR peptides (peptide concentration, solvent concentration, sample temperature, NMR instrument proton frequency)

Peptide	*Solvent System*	
	TFE solution	*SDS Micelles*
NK_4-M2GlyR-p27	3 mM 30% TFE 30°C 500 MHz	
NK_4-M2GlyR-p22	3 mM 40% TFE 10°C	2.5 mM 500 mM SDS 45°C

NK_4-M2GlyR-p22 S22W	500 MHz	800 MHz
	3 mM 40% TFE 10°C 500 MHz	2.5 mM 500 mM SDS 45°C 600 MHz
NK_4-M2GlyR-p22 T19R S22W		2.5 mM 500 mM SDS 40°C 800 MHz
NK_4-M2GlyR-p20 T17R S20W	5.7 mM 50% TFE 15°C 500 MHz	2.5 mM 500 mM SDS 25°C 800 MHz

NMR experiments on the NK_4-M2GlyR peptide samples were performed at 3 different locations, each one with an instrument having a different magnetic field strength. The 11.75 tesla 500 MHz Varian NMR spectrometer (Varian now Agilent Inc., Palo Alto, CA) is located at the Biomolecular NMR facility of the Biochemistry and Molecular Biophysics Department at Kansas State University, the 18.8 tesla 800 MHz Bruker NMR spectrometer (Bruker Instruments Inc., Billerica, MA) is located at the Biomolecular NMR laboratory at the University of Kansas (Lawrence, KS), and 14.1 tesla 600 Mhz Bruker NMR spectrometer is located at the laboratory of Professor Yan Xu at the University of Pittsburgh (Pittsburgh, PA). The instrument used for data acquisition on each sample, and the temperature of the sample during data acquisition are specified on Table 4-1. The use of higher field instruments (compared with the instrument available at Kansas State University) and higher temperatures were needed to obtain data with the required signal resolution for structure determination on the SDS micelles samples as discussed in Chapter 2.

2D ^{1}H-^{1}H TOCSY experiments and 2D ^{1}H-^{1}H NOESY experiments with different mixing times were acquired for each NMR sample. For some samples additional 2D ^{1}H-^{1}H DQF-COSY or 2D ^{1}H-^{1}H rotating frame nuclear Overhauser effect spectroscopy (ROESY) experiments were performed. Data processing and analysis were carried out using one or more of the following programs: Varian software VNMR versions 6.1B or 6.1C or VNMRj version 2.3, NMRPipe (Delaglio et al., 1995), Sparky software (Goddard and Kneller, 2004). More details on the NMR experiments are discussed in the corresponding publication (Broughman et al., 2002a;Bukovnik et al., 2012;Cook et al., 2004;Herrera et al., 2010) and in the Materials and Methods sections of Chapter 2 and Chapter 3.

NMR Structure Calculations

NMR monomeric solution structures at the atomic resolution were calculated for each of the samples described in Table 4-1, except for the NK_4-M2GlyR-p27 peptide sample. The structure calculations for all peptides were carried out following the standard protocol (Wüthrich et al., 1983). Upper distance limits, derived from specifically assigned NOESY cross peaks, and dihedral angle constraints, derived from coupling constant values, were used along with the amino acid sequence of each peptide as the input for the structure calculations. The programs used for structural calculations were DYANA (DYnamics Algorithm for NMR Applications, Peter Güntert Scientific Software) or CNS (crystallography and NMR system), (Brunger et al., 1998). Additional software used for energy minimization and clustering were: SYBYL versions 6.7 and 7.1 (Tripos Inc. St. Louis, MO) and Insight II (Accelrys, San Diego, CA). Further details

on the structure calculations are included in the corresponding publication (Broughman et al., 2002a;Bukovnik et al., 2012;Cook et al., 2004;Herrera et al., 2010) and in the Materials and Methods sections of Chapter 2 and Chapter 3.

Computational Methods

Increasingly complex computational methods have been used in the study of the NK_4-M2GlyR family of channel forming peptides. In the first attempt to simulate the structure of an M2GlyR derived peptide in solution, Broughman et al. built a computational model of peptide NK_4-M2GlyR-p27 using the Biopolymer module of Sybyl 6.7 (Tripos Inc., St. Louis, MO) with electrostatics calculated by the Kollman method (Singh and Kollman, 1984) and a distance dependent dielectric constant of ($e = 4 \cdot r$) rather than explicit solvation. Backbone dihedral angles φ and ψ for residues 5 to 27 (from the M2GlyR sequence) were set to an α-helical conformation. Lysine residues 1 to 4 were set to random coil conformation. Refinement of the structure was done by performing 100 iterations of steepest descent energy minimization followed by 5 cycles of optimization using the conjugate gradient method until convergence was reached. The energy minimized structure was subjected to molecular dynamics simulations for 10 psec at 300K to create the final reported structure (Broughman et al., 2002a).

Johnston et al. from the group of Dr. Sansom in the Department of Biochemistry at the University of Oxford UK used as starting point for molecular dynamics simulations the NMR solution structures calculated for peptides NK_4-M2GlyR-p22 and NK_4-M2GlyR-p22 S22W in 40% TFE. These simulations were performed using GROMACS v3 (Lindahl et al., 2001) with

ffgmx43a1 force field in four different environments: TFE:water, SDS micelles, dodecylphosphocholine (DPC) micelles, and a dimyristoylphosphatidylcholine (DMPC) bilayer. Between 0.2 and 1.0 ns of equilibration and 20 ns of production simulation were performed at a temperature of 300 K for TFE:water, SDS micelles, and DPC micelles simulations. A temperature of 310 K was used for DMPC simulations. Further experimental details can be found in the original report (Johnston et al., 2006).

As a first attempt to constructing a computational model for the assembled ion channels formed by M2GlyR derived peptides in lipid bilayers, the NMR determined monomeric structures in deuterated SDS micelles of peptides NK_4-M2GlyR-p22 S22W, and NK_4-M2GlyR-p22 T19R S22W were assembled each into a pentameric bundle based on experimental work indicating that this family of peptides spontaneously assembled into pentameric structures when inserted into synthetic bilayers or cell membranes (Reddy et al., 1993). Starting from the energy minimized average structure of the corresponding peptide, the structure of the pore was modeled by placing five identical copies of the peptide in a radial penta-symmetric array. Peptides were oriented with the hydrophilic side-chains known to be in the interior of the pore facing each other and the hydrophobic side-chains facing the exterior of the pore. The initial distance between peptides was adjusted to bring the adjacent peptides into contact. Dynamic simulations were ran on a Silicon Graphics O2 workstation for 10 ps using AMBER7 force field (Cornell et al., 1995;D.A. Case, 2002) with the software Sybyl version 7.1 (Tripos Inc., St. Louis, MO) with a dielectric constant of 1.0, followed by 100 steps of energy minimization by Powell method (Powell, 1977). The resulting pore structures were analyzed by determining the average internal diameter of the pore at 20 positions equidistantly distributed along the pore axis.

Drs. Chen and Al-Rawi in the Department of Biochemistry and Molecular Biophysics at Kansas State University constructed structural models of the putative pentameric channels formed by peptides NK_4-M2GlyR-p22 and NK_4-M2GlyR-p22 p22-S22W as described in Appendix A-Chapter 2. Briefly the GBSW implicit membrane model (Im et al., 2003) was used to refine the structures calculated by NMR. The refined monomer NMR structures were assembled into pentamers using CHARMM (Brooks et al., 2009;Brooks et al., 1983). The assembled channels were subject to energy minimization and then solvated in a pre-equilibrated POPC bilayer membrane using the CHARMM-GUI automated Membrane Builder (Jo et al., 2007;Jo et al., 2008). NAMD software(Phillips et al., 2005) was used for 20 ns of production simulation.

Results and Discussion

Monomeric peptide structures have been calculated using NMR data or predicted based on NMR data for the M2GlyR peptides described in Figure 4-1. Two solvent systems were used: deuterated TFE:water mixtures and deuterated SDS Micelles in water. A summary of the NMR experimental conditions is presented in Table 4-1. The data from transepithelial ion transport measurements using MDCK cells, CD spectra, and computer generated models are available also for the peptides described in Figure 4-1.

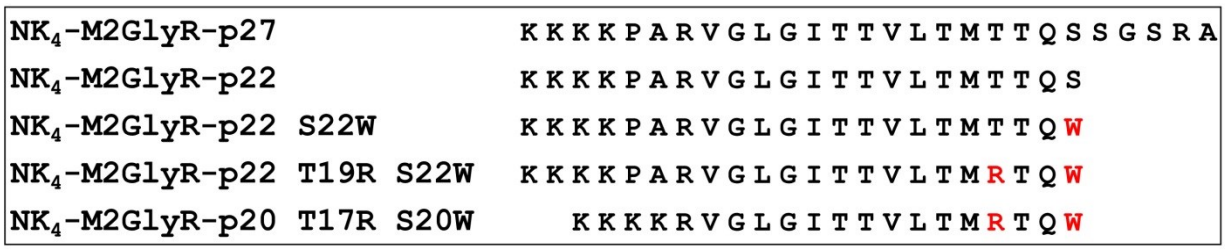

Figure 4-1. Channel forming peptides derived from M2GlyR that have NMR based structures

The M2GlyR derived peptides included in Figure 4-1 are only a few of the many sequences tested throughout the project of developing a peptide based channel replacement therapeutic for cystic fibrosis. These sequences were selected as the leading candidates at their corresponding time during the evolution of the project, and because of their importance their structure was determined by NMR. The change in the leading sequence over time can be describe as a series of single differences between each peptide and the next, e.g. deletion of 5 C-terminal residues between NK_4-M2GlyR-p27 and NK_4-M2GlyR-p22, and deletion of PA at positions 5 and 6 between NK_4-M2GlyR-p22 T19R S22W and NK_4-M2GlyR-p20 T17R S20W. This creates an opportunity to try to correlate the observed changes in the kinetic properties of the peptides with the changes detected from the techniques that provide structural information.

Transepithelial ion transport measurements

MDCK monolayers were used to assess peptide-dependent ion transport. Short circuit current (I_{SC}) is an extremely sensitive indicator of net ion flux (Tomich et al., 2012). Figure 4-2 shows the concentration dependence of I_{SC} induced by NK_4-M2GlyR derived peptides when applied to

the apical membrane of MDCK epithelial monolayers in the presence of 1-EBIO (Shank et al., 2006 and Chapter 3).

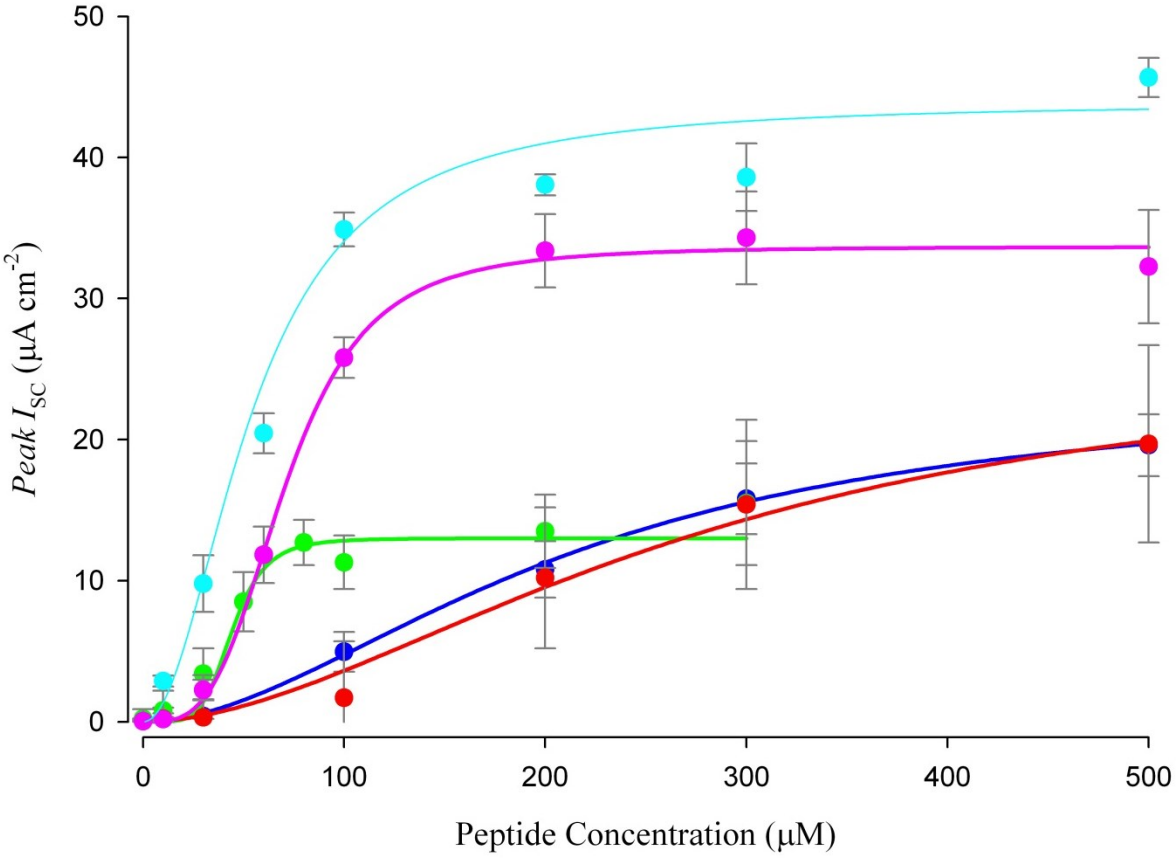

Figure 4-2. Concentration dependence of I_{SC} induced by M2GlyR derived peptides on MDCK epithelial monolayers. ●NK$_4$-M2GlyR-p27 ●NK$_4$-M2GlyR-p22 ●NK$_4$-M2GlyR-p22 S22W ●NK$_4$-M2GlyR-p22 T19R S22W ●NK$_4$-M2GlyR-p20 T17R S20W. Composite figure with data from Shank et al. 2006 and Chapter 3

The best fit of the data presented in Figure 4-2 to a modified Hill equation, as described in Chapter 3, produced the kinetic parameters reported in Table 4-2, where the parameters determined for peptide NK$_4$-M2GlyR-p20 T17R S20W (Chapter 3) are added to the ones previously reported (Tomich et al., 2012).

Table 4-2. Kinetic properties of M2GlyR derived peptides on MDCK epithelial monolayers. Data from Tomich et al., 2012 and Chapter 3

Peptide	I_{max} ($\mu A/cm^2$)	$K_{1/2}$ (μM)	*Hill coefficient*
NK_4-M2GlyR-p27	26.2 ± 5.7	271 ± 71	1.9
NK_4-M2GlyR-p22	23.7 ± 5.6	210 ± 70	1.9 ± 0.6
NK_4-M2GlyR-p22 S22W	13.0 ±1.0	45 ± 6	5.4 ± 2.9
NK_4-M2GlyR-p22 T19R S22W	33.7 ± 1.3	71 ± 5	3.5 ± 0.7
NK_4-M2GlyR-p20 T17R S20W	43.8 ± 2.8	58 ± 8	1.8 ± 0.4

Table 4-3. Change in kinetic properties between leading M2GlyR derived peptide candidates in response to change in peptide sequence

Change in Peptide	ΔI_{max} ($\mu A/cm^2$)	$\Delta K_{1/2}$ (μM)	*Δ Hill coefficient*
Δ(S23 G24 S25 R26 A27)	-2.5 ± 8.0	-61 ± 100	0 ± 0.6
S22W	-10.7 ± 5.7	-166 ± 70	3.5 ± 3.0
T19R	20.7 ± 1.6	26 ± 8	-1.9 ± 3.0
Δ(P5 A6)	10.1 ± 3.1	-13 ± 9	-1.7 ± 0.8

Circular Dichroism

The CD spectra of all NK_4-M2GlyR peptides in water show the characteristic shape of the spectra for peptides in random coil conformation, with a minimum near 195 nm (Broughman et al., 2002b;Cook et al., 2004) and (Figure 3-4). Increasing concentrations of TFE change the spectra to one characteristic of α-helix with minima at 208 nm and 222 nm, for all peptides as well except for peptide NK_4M2GlyR-p22 S22W that lacks the minimum at 222nm, and has a

spectrum indicative of only partial α-helix (Broughman et al., 2002b;Cook et al., 2004) and (Figure 3-4).

The CD spectra in 10 mM SDS micelles with peptide concentrations of 50 μM of all the peptides considered in this chapter is presented in Figure 4-3 and have the characteristics of the spectra for α-helical peptides.

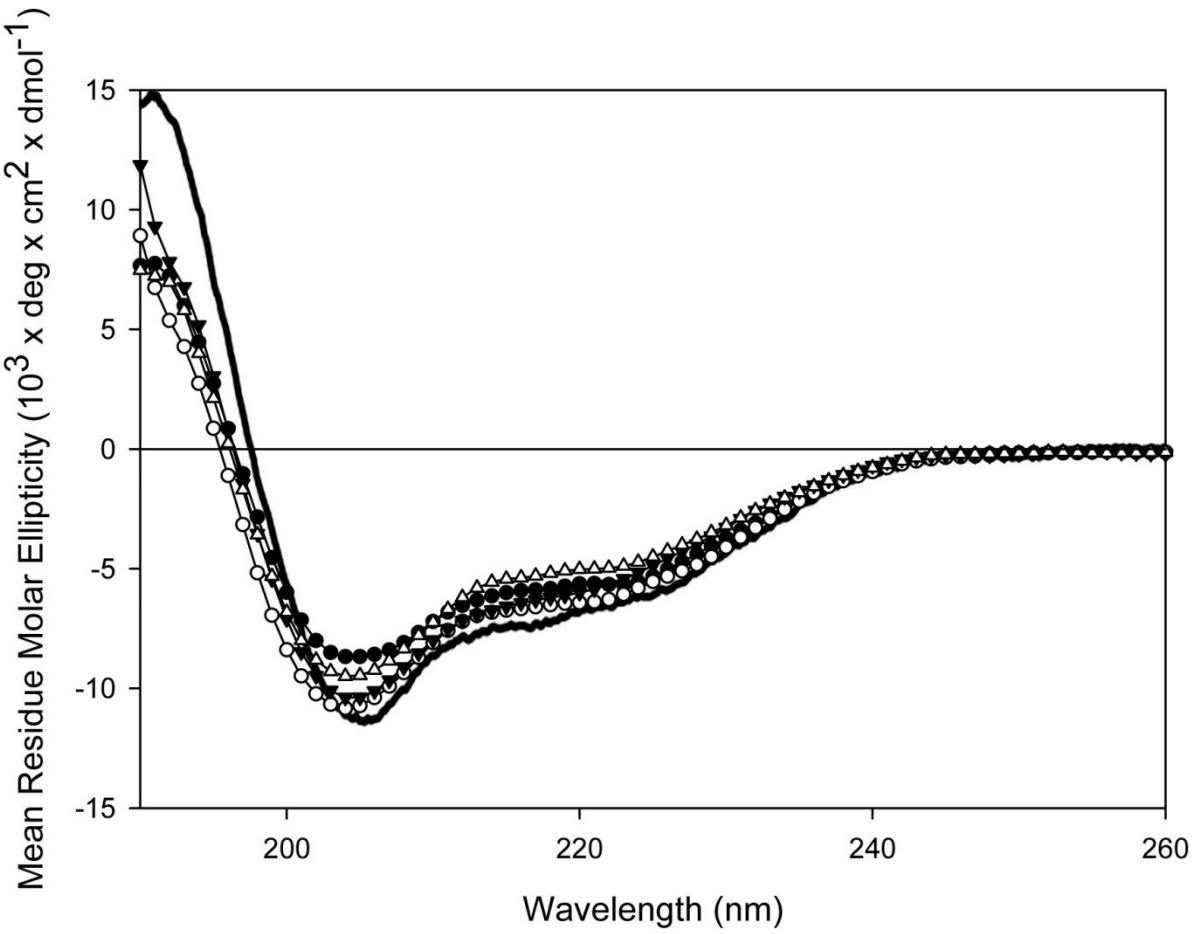

Figure 4-3. Circular dichroism spectra of NK_4-M2GlyR derived peptides in 10 mM SDS micelles. NK_4-M2GlyR p27 WT (●), NK_4-M2GlyR p22 (○), NK_4-M2GlyR p22 S22W (▼), NK_4-M2GlyR p22 T19R S22W (Δ) and NK_4-M2GlyR p20 T17R S20W (─). Composite figure with data from Broughman et al., 2002b , Cook et al., 2004 and Chapter 3

CD data collected on M2GlyR derived peptides in water, TFE:water mixtures and SDS micelles provides reliable structural information about the peptides in each environment. CD spectra for all the considered peptides supports the conformational transition experimented by the peptides with the change in the sample conditions. The CD spectrum of peptide NK_4-M2GlyR p22 S22W in TFE:water is a particular case, it was shown in (Cook et al., 2004) that the just partial α-helical character of the spectrum correlates with the NMR structure determined for the same conditions, and it was postulated there as well that the CD spectrum together with the NMR structure in TFE solution (Table 4-1), provide an explanation to the change in the kinetic properties of peptide NK_4-M2GlyR p22 S22W compared with NK_4-M2GlyR p22 (Table 4-3), in particular to the reduction of $K_{1/2}$ by 166 μM. The explanation presented was that the backbone structure allows the C-terminus to loop over into a closed structure reducing the exposure of the hydrophobic residues to water; this in turn reduces the aggregation, making more monomeric peptide available for interaction with the membrane (Cook et al., 2004). This rational appears logical, but raises the question of what should be the interpretation of the NMR structure of the peptides in TFE solutions in the context of their physiological environment, where TFE is not expected to be present. The report presented the argument that since solution aggregation was greatly decreased the determined conformer or a similar one had to be sampled at a relatively high frequency in water solution.

CD spectroscopy provides information about the secondary structure of a peptide but is not able to indicate where in the sequence the detected secondary structure elements are located. The CD spectra in SDS micelles, of the peptides here considered, are almost superimposable (Figure 4-3), provide no additional information beyond confirmation that the peptides in SDS are folded, and

have no potential for providing explanation to the changes in ion conductance between the considered sequence variations. Even though the extracted structural information is very limited, the small quantities of material needed and the short time required to collect CD data make it practical to continue its use as a preliminary test in the future. A major change in the structure due to an error in synthesis or due to the unexpected result of a new modification in the sequence could be easily detected by CD.

NMR Structures

CD spectra showing that M2GlyR derived peptides are predominantly unstructured in water solution prompted us to use a different solvent system for 3D solution structure determination by NMR. A TFE:water solution system was considered based on the known secondary structure stabilizing property of TFE (Nelson and Kallenbach, 1989), and the expected helical secondary structure of the parent sequence based on earlier studies (Tomich et al., 1998). CD studies in TFE:water confirmed the formation of α-helical structures and indicated a correlation between helical content in TFE solution and channel activity (Broughman et al., 2002b). These results made TFE solutions a convincing choice for the initial NMR solution studies.

NMR was initially used to evaluate the structure of the 4 N-terminal lysines of peptide NK_4-M2GlyR-p27 in deuterated TFE solution. TOCSY spectra were used to evaluate the dispersion of the lysine resonances and NOESY spectra were used to detect medium range connectivities that would be indicative of participation of the lysines in the formation of a helix (Broughman et al., 2002a). The molecular model shown in Table 4-4 for NK_4-M2GlyR-p27 was computationally

constructed based on the NMR evidence as described in the methods section. The first NMR structures calculated for M2GlyR derived peptides were the structures of NK_4-M2GlyR-p22 and NK_4-M2GlyR-p22 S22W in TFE solution (Cook et al., 2004). The structure of NK_4-M2GlyR-p22 was described as a continuous helix with an extended N-terminal segment formed by the lysine residues, and having a length of more than 32 Å. NK_4-M2GlyR-p22 S22W adopts a much less linear structure made of a single-turn helix (residues 11 – 14), a stretched beta-like turn (residues 14 – 17), and then another two-turn helix (residues 15 – 21) (Tomich et al., 2012).

Table 4-4. Average calculated structures of M2GlyR derived peptides

Peptide	*Solvent System*	
	TFE:water	*SDS Micelles*
NK_4-M2GlyR-p27	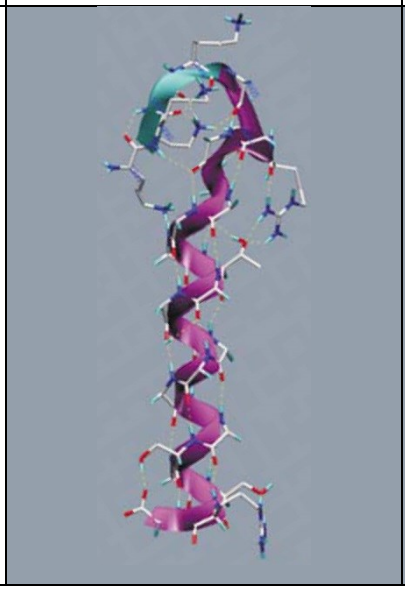	

NK_4-M2GlyR-p22	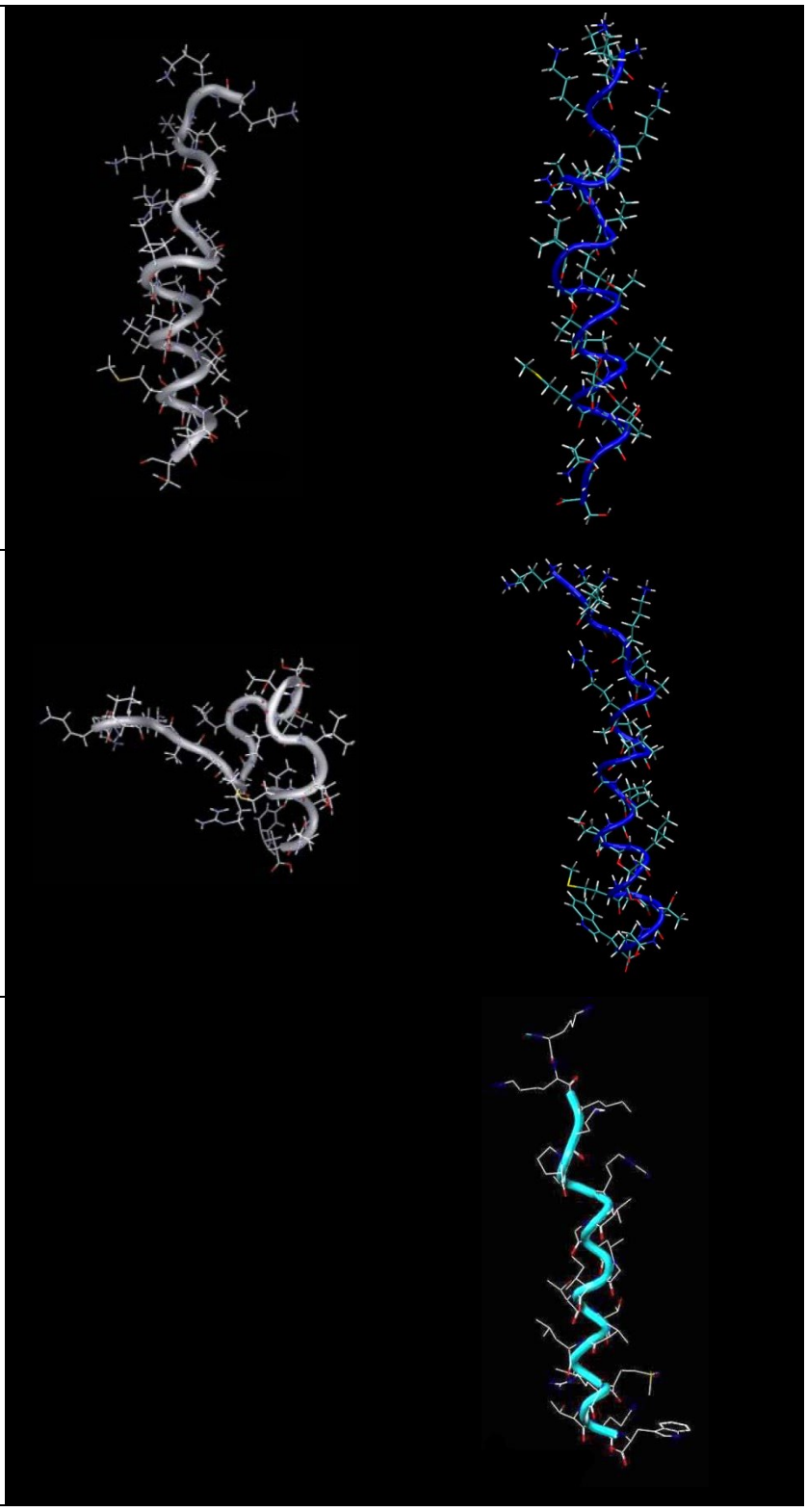
NK_4-M2GlyR-p22 S22W	
NK_4-M2GlyR-p22 T19R S22W	

NK_4-M2GlyR-p20 T17R S20W	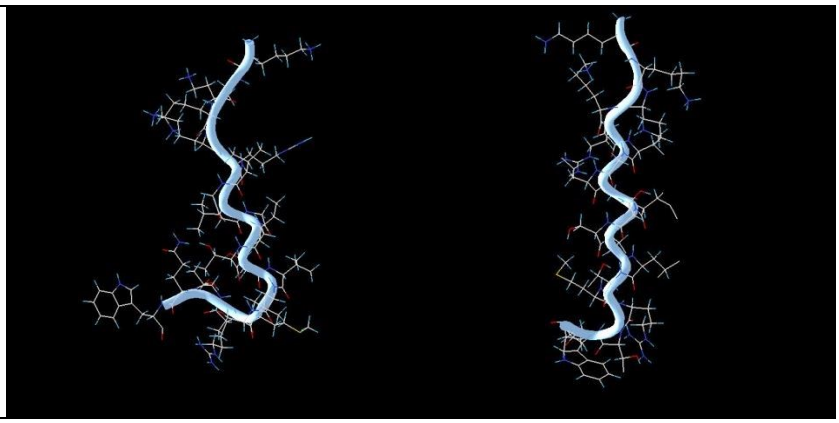

Looking for better evaluation of the molecular structure that would be a better representation of the conformations sampled by the M2GlyR peptides when inserted into lipid bilayers, the protocol for the structure determination by NMR was changed to preparing the NMR sample with the peptide inserted into SDS micelles. The instrumental challenges and the consequences on the data quality brought upon by this change were discussed in Chapter 2.

The first two reported structures calculated by NMR in SDS micelles for M2GlyR derived peptides were the ones for peptide NK_4-M2GlyR-p22 and peptide NK_4-M2GlyR-p22 S22W (Chapter 2 and Herrera et al., 2010). The average calculated structures in SDS micelles for peptides NK_4-M2GlyR-p22 and NK_4-M2GlyR-p22 S22W appear very similar (Table 4-4). Their most prominent features are helical conformation for residues residue 6-20 and extended conformation for residues 1-5. Detailed comparison between the two average structures, as discussed in Chapter 2 shows that NK_4-M2GlyR-p22 S22W has a slight convexity, while NK_4-M2GlyR-p22 has a more linear axis in the central portion of the structure. The C-terminus of NK_4-M2GlyR-p22 S22W appears to have a more stable configuration according to the ensemble of NMR structures calculated.

The substitution of residue 22 from a serine to a tryptophan reflected in the ion conductance kinetic parameter with a decrease in I_{max} of 10.7 ± 5.7 μA/cm^2, a decrease in $K_{1/2}$ of 166 ± 70 μM and an increase in the Hill coefficient of 3.5 ± 3.0 (Table 4-3). Although the NMR structures calculated for NK_4-M2GlyR-p22 and NK_4-M2GlyR-p22 S22W are consistent with the kinetic properties of each peptide, and with the changes in those properties, the differences between the structures do not provide an explanation for the kinetic changes. Determination of the structure for NK_4-M2GlyR-p22 S22W in SDS micelles alone would have not made any prediction about ion conductance possible apart from it being somehow comparable to the ion conductance of NK_4-M2GlyR-p22 peptide. The explanation given to the large reduction in $K_{1/2}$, as mentioned before is that reduced tendency to aggregation is responsible for more peptide available for membrane interaction. The calculated structure for NK_4-M2GlyR-p22 S22W does not contradict this explanation. However it does not provide any additional evidence in favor either. The increase in the Hill coefficient (to 5.4 ± 2.9 the highest amongst the tested sequences) is indicative of an increase in the cooperativity of the channel assembly process. This change is attributed to the membrane anchoring effect of the tryptophan residue at position 22. The C-terminal tryptophan is speculated to anchor the membrane to the bilayer interface reducing the possibility of peptide movement in the direction normal to the bilayer, making alignment more favorable during assembly (Tomich et al., 2012). The increased stability of the C-terminus of NK_4-M2GlyR-p22 S22W described from the calculated NMR structure in SDS micelles makes a positive argument for this explanation.

The substitution of residue 19 from a threonine to an arginine caused ion conductance kinetic parameters to change with an increase in I_{max} of 20.7 ± 1.6 μA/cm^2 (the largest increase for a

single sequence change), an increase in $K_{1/2}$ of 26 ± 8 μM and a decrease in the Hill coefficient of 3.2 ± 3.1(Table 4-3). Comparison between the calculated average structures in SDS micelles for peptides NK_4-M2GlyR-p22 S22W and NK_4-M2GlyR-p22 T19R S22W reveals no apparent major differences (Table 4-4). Once again their most prominent features are a helical conformation for residues 6-20 and an extended conformation for residues 1-5. NK_4-M2GlyR-p22 T19R S22W adopts a more linear conformation, not displaying the slight convexity reported for M2GlyR-p22 S22W (Bukovnik et al., 2012). The differences between the NMR structures in SDS micelles of peptides NK_4-M2GlyR-p22 S22W and NK_4-M2GlyR-p22 T19R S22W also do not provide an explanation for the kinetic changes in the ion conductance. The structure for NK_4-M2GlyR-p22 T19R S22W in SDS micelles also does not have predicting potential over the ion conductance.

The deletion of residues proline 5 and alanine 6 caused the I_{max} to increase by 10.1 ± 3.1 μA/cm^2, the $K_{1/2}$ to decrease by 13 ± 9 μM and the Hill coefficient to decrease by 1.7 ± 0.8. This changes are among the smallest cause be a single change in the sequence (Table 4-3). Although the changes in I_{max} and $K_{1/2}$ are in the favorable direction with respect to increasing ion conductance, it is somehow surprising that are smaller compared with the changes produced by the single residue substitutions (S22W and T19R).

The general appearance of the average structures in SDS micelles for peptides NK_4-M2GlyR-p22 T19R S22W and NK_4-M2GlyR-p20 T17R S20W seems similar with a long central helix and an extended N-terminus (Table 4-4). Detailed analysis of both structures reveals considerable differences. The structure calculated in SDS micelles for NK_4-M2GlyR-p20 T17R S20W is the

only one that has one of the N-terminal lysines as part of the helix. Proline is known to be α-helix breaker residue, while alanine favors α-helix formation (Chou and Fasman, 1974;Fujiwara et al., 2012). When prolines are part of an α-helix, they are frequently found at the first N-terminal turn, where the loss of the hydrogen bond to the amide nitrogen does not cause significant effects (Woolfson and Williams, 1990). The presence of a proline residue at position 5 in the NK_4-M2GlyR-p22 sequences is probably limiting the participation of the N-terminal lysines in the α-helix. At the same time it has been reported that proline residues occur with higher frequency in transmembrane α helices, compared to α helices for soluble proteins (Cordes et al., 2002). It has been suggested by experimental and computational studies that proline containing motifs can form molecular hinges that act as conformational switches in transmembrane α-helices (Tieleman et al., 2001). The deletion of proline 5 and alanine 6 in NK_4-M2GlyR-p20 T17R S20W could be affecting the dynamics of the ion channels.

Due to the shorter amino acid sequence of NK_4-M2GlyR-p20 T17R S20W the axial length of the structured peptides is also shorter. The axial length of NK_4-M2GlyR-p20 T17R S20W in SDS micelles is ~30 Å. A shorter conduction pathway for the channels is a possible explanation for the changes in I_{max} and $K_{1/2}$. It should also be considered that a length of ~30 Å makes the peptide in the determined conformation incapable of spanning across most unperturbed cellular membranes (Mitra et al., 2004). Since the detection of ion current induced by the peptide gives a strong indication that the peptide does form ion channels, there are two possible explanations to how it does it. The peptide either adopts a less tilted stretched structure inside the bilayer, which could reduce the helical portion of the structure and affect the amphipathic distribution of the side chains. Or the peptide induces thinning of the lipid bilayer. Membrane thinning has been

reported to be involved in the mechanisms of channel forming peptides (Chen et al., 2003), and has been observed during simulations of channels formed by M2GlyR peptides (Herrera et al., 2010). The reduction in the Hill coefficient observed can also be caused by the length reduction and needed membrane thinning. Lateral movement of the inserted peptide can be restricted by the need of moving not only the peptide but also the defect in the bilayer around it in order to find oligomerizing partners (assuming insertion occurs as a separate event to channel formation).

The information that can be extracted from the NMR structure of peptide NK_4-M2GlyR-p20 T17R S20W in SDS micelles is also not sufficient to explain the changes in ion conductance, but correlates well with the observations. It is notable that the residue deletions (Δ(S23 G24 S25 R26 A27) and Δ(P5 A6)) produce in general smaller changes in the kinetic parameters than the amino acid substitutions, considering that deletions change the size, mass and even charge of the peptides. This observation suggests that the remaining core of the M2GlyR is a highly efficient ion channel forming sequence and these other residues could exist outside the bilayer in nature. In fact the PA N-terminal segment of the NK_4-M2GlyR-p22 peptides corresponds in the glycine receptor channel to a segment that has been proposed to be part of an internal loop connecting the M2 transmembrane segment with the previous transmembrane segment M1 (Lynch, 2004).

An apparently common feature of the NMR structures calculated for the peptides in SDS micelles is the unstructured or extended configuration of the N-terminal lysine residues. In order to extract more information from the NMR data about these residues, an analysis of their chemical shifts was carried out.

The standard protocol for structure determination using multidimensional NMR data is based on distance and angle constraints calculated from NOE cross peaks and J-couplings respectively (Wüthrich, 1986). Chemical shift information is used to complete the task of identifying specific residues, but in essence the calculation of the structure is chemical shift independent. The chemical shift parameter is a sensible indicator of the chemical environment that surrounds a nucleus, and can also be indicative of the conformation of an amino acid (Wishart and Nip, 1998). The chemical shifts of the amide protons of the N-terminal lysine residues were collected from the reported assignment tables or directly from the ^{1}H-^{1}H TOCSY spectra used in the structure determination for each NMR structure included in Table 4-4. Table 4-5 shows the minimum and the maximum chemical shifts values and the difference between the two numbers indicates the dispersion of the lysine chemical shifts.

Table 4-5. Chemical shifts (ppm) and dispersion (Δ) for the amide protons of the N-terminal lysine residues in M2GlyR derived peptides

Peptide	*TFE*			*SDS*		
	Min	Max	Δ	Min	Max	Δ
	Chemical Shift (ppm)					
NK_4-M2GlyR-p27	8.10	8.55	0.45			
NK_4-M2GlyR-p22	8.21	8.59	0.38	8.12	8.58	0.46
NK_4-M2GlyR-p22 S22W	8.21	8.59	0.38	8.02	8.54	0.52
NK_4-M2GlyR-p22 T19R S22W				7.90	8.40	0.50
NK_4-M2GlyR-p20 T17R S20W	8.07	8.19	0.12	8.16	8.58	0.42

The peptide in SDS micelles with the smallest dispersion of the lysine chemical shifts is NK_4-M2GlyR-p20 T17R S20W. This observation can be interpreted as the 4 lysine residues of this peptide being in a more restrictive environment compared with the other peptides. This is

consistent with the finding that lysine 4 is part of the α-helix (Chapter 3), and can be due to the shorter length of the peptide combined with the anchoring effect of the C-terminal tryptophan, pulling the hydrophobic side chains for one or more lysine residues into the hydrophobic interior of the micelles. The data reported in Table 4-5 also show that for each peptide the dispersion of the lysine chemical shifts is smaller for the sample in TFE solution than for the sample in SDS micelles. The possible reason may be the samples in TFE solution are surrounded by the solvent, and although micro-heterogeneity of the TFE:water solvent around the peptides has been postulated based on computer simulations (Johnston et al., 2006;Roccatano et al., 2002), any amino acid in an extended conformation is exposed to the solvent in a similar way.

Since lysine residue 4 of the NK_4-M2GlyR-p20 T17R S20W peptide participates of the α-helix conformation and is predicted to be inside the lipid bilayer, the structure of the assembled ion channels should be able to accommodate for this. The deletion of amino acid residues at the carboxyl or amino end of an amphipathic sequence does not change the registry between amino acids, not affecting the amphipathic character of the sequence. The helical wheel diagrams in Figure 4-4 show that the amino acid distribution in NK_4-M2GlyR-p20 T17R S20W and NK_4-M2GlyR-p22 T19R S22W is almost the same. The polar and non-polar residues are equally segregated and the membrane anchoring reside tryptophan 22 is in the same relative position, opposite to the polar residues, in what should be the surface of the channel that faces the interior of the lipid bilayer. Accommodating the lysine 4 residue should not be problematic for the channel, as seen in the diagram (Figure 4-4B) this residue would face the hydrophilic side of the peptide.

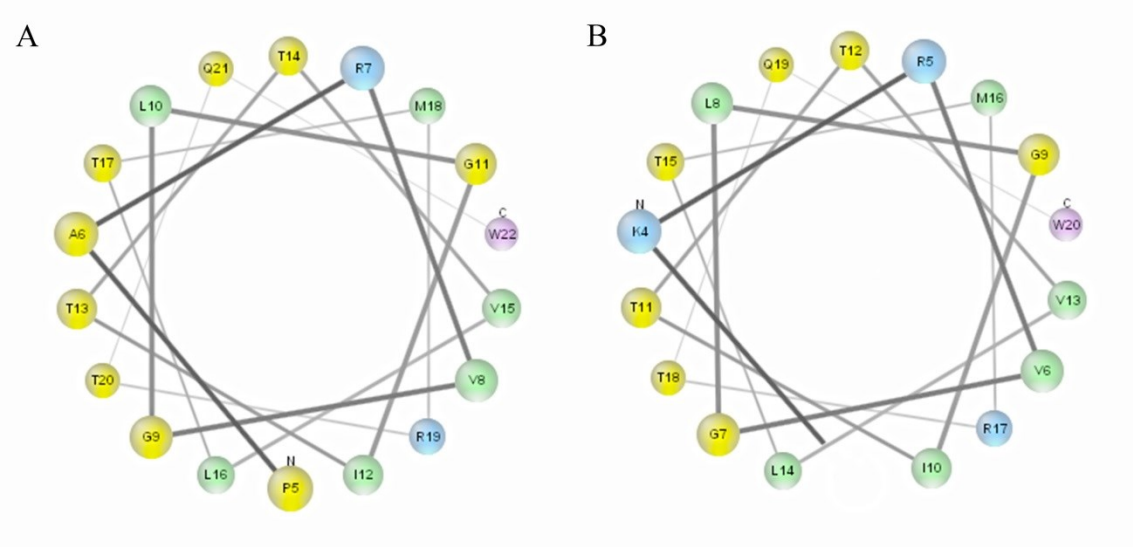

Figure 4-4. Helical wheel diagrams of peptides A) NK_4-M2GlyR-p22 T19R S22W and B) NK_4-M2GlyR-p20 T17R S20W. Green circles represent nonpolar residues, yellow polar uncharged residues, blue basic residues and purple aromatic residues. Diagrams created using MPEx (Snider et al., 2009)

A common feature to all the calculated structures by NMR for M2GlyR derived peptides in SDS micelles, is that the segment that could be predicted to form the transmembrane α-helix, and was modelled as one for peptide NK_4-M2GlyR-p27 (Broughman et al., 2002a), has never been determined by NMR to be a perfect α-helix going from residue 5 to the end of the sequence. As it can be seen in Table 4-4 the reported helices have imperfections mostly at the start and end of the helix. This feature is not an artifact of the structure averaging since the individual structures in the clusters of reported structures present the same deviations from the canonical α-helix. This deviation could be involved in accommodating the reported curvature of the helix, but could potentially also be created by the strong curvature of the SDS micelle around the peptide. Whether or not this feature of the NMR structures in SDS micelles has any relevance or biological significance is yet to be determined.

Computer Simulations

Representative examples of the different types of computational studies performed on M2GlyR derived peptides are presented to highlight their relationship to the structures determined by NMR. The increasing complexity of the computer simulations performed on the M2GlyR derived peptides is a reflection of advances in the field and of the material an human resources available to the project at each point in time. To help answer the question of the relevance of determining new NMR structures for M2GlyR derived peptides, an informal evaluation of how the computational results complement, or contradict or replace the NMR studies is presented here.

As mentioned before the first atomic model of an M2GlyR derived peptide was the product of combining NMR derived information with a peptide building computational protocol. The protocol included structure refinement by energy minimization and molecular dynamics. During the simulation on peptide NK_4-M2GlyR-p27 the N-terminal lysine residues showed some motion, but remained mostly extended and not interacting with the helix constructed for residues 5 to 27. There was also very little motion of the helix during the simulation (Broughman et al., 2002a).

The first use of M2GlyR derived peptide structures determined by NMR in molecular dynamics simulations was reported in Johnston et al. 2006. The structures used were the TFE solution structures of NK_4-M2GlyR-p22 and NK_4-M2GlyR-p22 S22W. The stability of the helical

structure was evaluated in four membrane-mimetic environments, as described in the methods section, and in more detail in the original report (Johnston et al., 2006). The results of the simulation for NK_4-M2GlyR-p22 S22W in SDS are not fully consistent with the structure calculate by NMR in the same environment. The simulation shows only a small helical fragment at the C-terminus with a bend in the middle region and a disordered N-terminal segment. The resulting structures from the simulations in DMPC bilayers are in close agreement to the calculated NMR structure in SDS micelles. A result of particular relevance to the present discussion is reproduced in Figure 4-5, where a simulation snapshot shows an M2GlyR peptide inside a micelle. The shape of the simulated micelle is far from the idealized sphere that is usually envisioned when considering the SDS micelle samples. This should be considered in the potential case of developing an improved protocol for the determination of NMR structures of M2GlyR derived peptides in a membrane-mimetic environment.

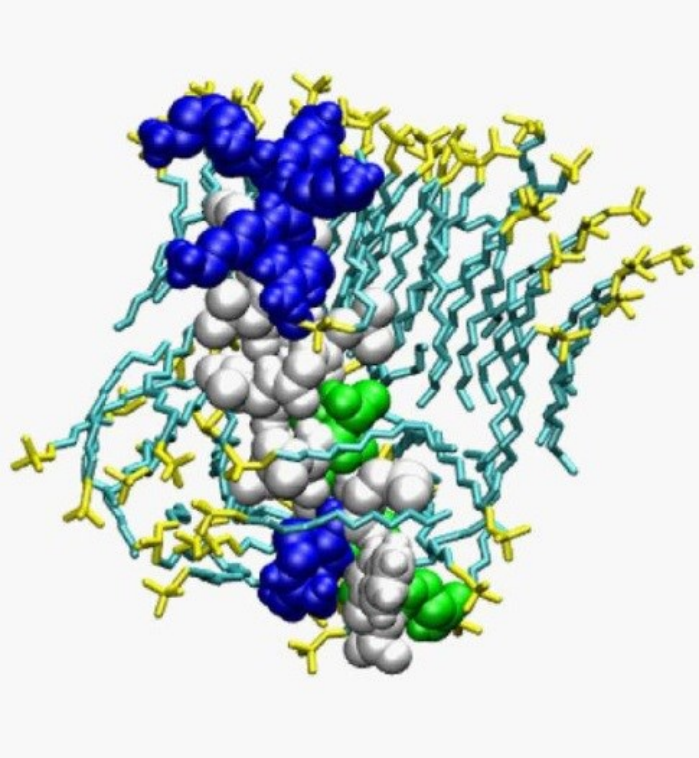

Figure 4-5. Snapshot of an M2GlyR derived peptide in an SDS micelle. Peptide is represented as van der Waals spheres and colored by residue type: white hydrophobic, green polar uncharged, and blue polar charged (Johnston et al., 2006)

Since all the NMR structures in SDS for the M2GlyR derived peptides appear very similar, and seem to provide little new information about the ion conducting channels therefore a protocol described in the methods section was developed. Rather than a dynamic model, the constructed assemblies were intended to be a geometric representation of the channels that potentially could help in the interpretation of the information already contained in the NMR structures calculated from samples in SDS micelles.

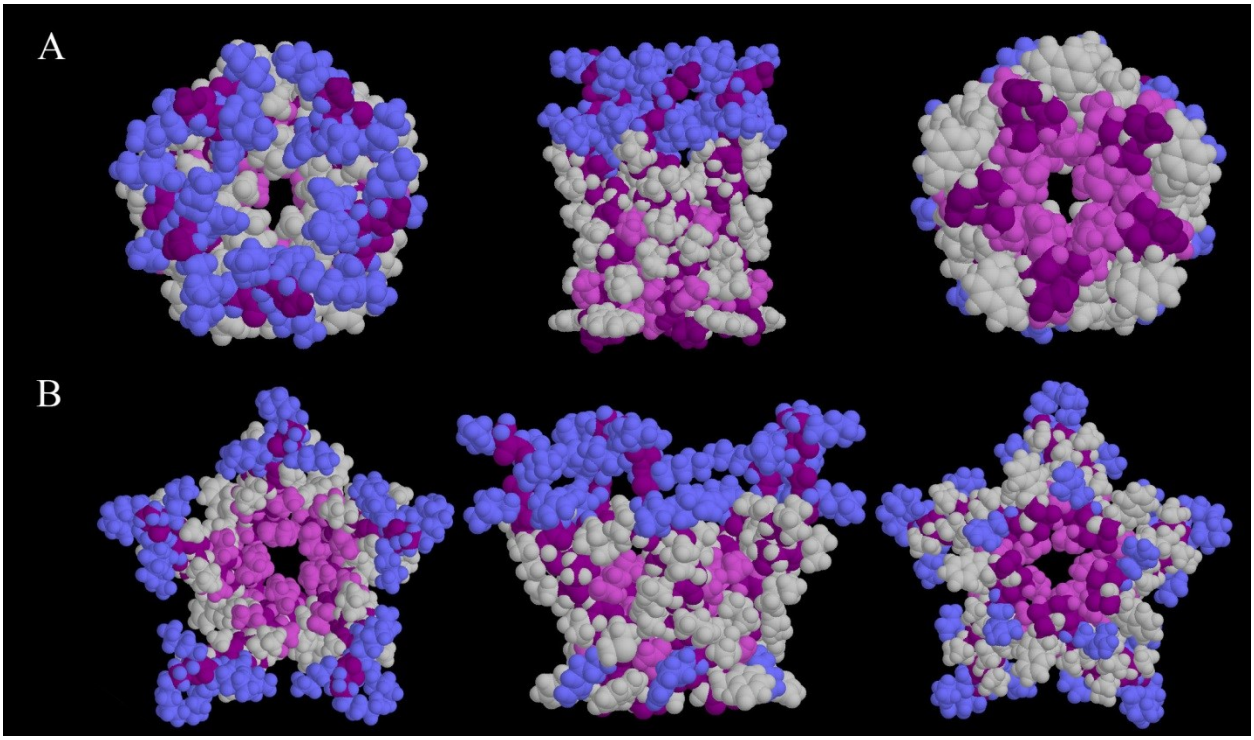

Figure 4-6. Computational models of assembled channels of A) NK_4-M2GlyR p22 B) NK_4-M2GlyR p22 S22W. Top, side and bottom view from left to right. Space-filing representation with backbone in purple, charged side chains blue, polar side chains magenta, and non-polar side chains grey

Differences between the structures determined for NK_4-M2GlyR p22 and NK_4-M2GlyR p22 S22W peptide monomers cause appreciable differences in the overall shape and interior diameter profile between the respective constructed channels. Information extracted from these models was used to analyze the modification made to the next generation of M2GlyR derived peptides. The complete absence of solvent interactions makes the constructed channel models of limited biological significance.

The next generation of computational studies on ion channels formed by M2GlyR derived peptides, performed by Dr. Chen's group, has been described in Appendix A- Chapter 2, and

briefly in the methods section of this chapter. The NMR structures in SDS along with a range of additional experimental data and theoretical considerations were used to create the starting points for these simulations (Tomich et al., 2012).

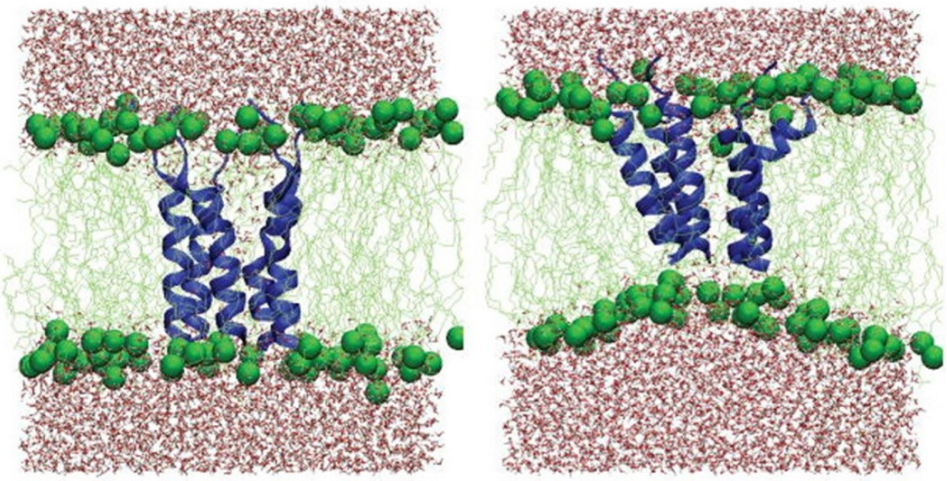

Figure 4-7. Snapshots of NK_4-M2GlyR p22 S22W channel in POPC bilayer before (left) and after (right) 20 ns of production simulation (Herrera et al., 2010)

The channel models generated by the simulation provide a structural basis for understanding the differences in channel activities between the tested sequences (Figure 4-7). The membrane anchoring effect of the C-terminal tryptophan residue as an explanation for the changes in the kinetic characteristics of ion conductance caused by the S22W substitution is supported by these simulations. Greater stability of the M2GlyR p22 S22W channel provides an explanation for the large reduction in $K_{1/2}$ (Herrera et al., 2010). The current protocols for computational simulation of the M2GlyR derived channels provide evidence that static structures determined by NMR cannot provide alone.

Concluding remarks

An essential characteristic of the optimized channel forming sequence, which has not been discussed, is ion selectivity. The limited availability of ion selectivity data on the peptides with an NMR determined structure makes it unfeasible to evaluate the correlation between changes in the selectivity of each peptide and the corresponding NMR structures. Anion selectivity of the M2GlyR peptides could be affected by changes in hydrogen bonding potential and electrostatics of the pore lining residues, pore length and pore rigidity. NK_4-M2GlyR-p22 T17R S22W is known to be only slightly anion selective (Tomich et al., 2012). Changes in ion selectivity could have occurred on a progressive matter as the sequence was modified, or could be the consequence of a single sequence modification. In either case it is improbable that the NMR structures provide an explanation to the changes in ion selectivity. At this point the best way to evaluate the mechanism of ion selectivity is perhaps by computational methods that use channels generated from NMR structures of the peptide monomer in SDS micelles as starting point (Chen and Tomich, 2014).

The question of the significance of the structures calculated by NMR from the TFE solution samples remains unanswered. Since these structures represent a condition that is not expected to be encountered under physiological conditions by the peptide, it could be argued that NMR structures for the peptides in TFE solution should no longer be determined. But the analysis presented here advocates for the contrary. The structure for NK_4-M2GlyR-p22 S22W is the most distinct among all the NMR structures calculated, and is the one that has the largest capacity to aid in the explanation of the characteristics of that peptide in solution and the changes in the kinetic parameters of the corresponding channels. Not all of the calculated structures in TFE

solution are as informative, and perhaps calculation of an NMR structure in TFE solution should not be attempted for every new lead sequence. Determination of an NMR structure in TFE solution should be performed when a new sequence behaves in an unexpected way, or when the CD spectrum of a peptide predicts a conformation not predominantly helical in solution.

The structures calculated by NMR for M2GlyR derived peptides in SDS micelles appear to be an adequate approximation to the actual structure of the peptides in the assembled channel. They are in agreement with the all the experimental data and the theoretical considerations on this family of channel forming peptides. However the capability of providing evidence for the explanation of changes in the ion conductance is limited. An improvement in the protocol for structure determination of M2GlyR derived peptides by solution NMR should be performed. One possible area of improvement is in the selection of the membrane mimicking agent. A screen of various detergents to establish which detergents prevents aggregation while supporting native structure as reflected by well-dispersed and well-resolved NMR spectra has been suggested as the best way to make a selection (Sanders and Sonnichsen, 2006). Another direction that should be explored is the structure determination of an oligomeric form of the M2GlyR peptides. Recently the structure of the human α7 nicotinic acetylcholine receptor (nAChR) transmembrane domain was reported using solution NMR (Bondarenko et al., 2014). Samples were made using detergent Lauryldimethylamine-oxide. α7 nAChR transmembrane domain contains 137 residues with 4 transmembrane helices. Adapting this protocol to the M2GlyR derived peptides may require the synthesis of the transmembrane sequences attached to a scaffold element, something that has been done previously for M2GlyR peptides, and also ^{15}N and ^{13}C isotopic enrichment of the sample.

The calculated NMR structures have provided experimental evidence of the structure in a membrane-like environment for the M2GlyR family of peptides. Although the structure found was predictable, particularly for the later calculated structures, if the structure was never determined it would have remained as an unproven conjecture. Future predictions about the structure, in the lipid bilayer environment, for new members of this family of peptides are well supported. Cost effective methodologies like CD spectroscopy can provided complementary evidence for the prediction of the structure of a new modified sequence.

The NMR structures determined for SDS micelles samples have provided a needed experimentally rooted starting point for computational studies. The current state of development of the computational techniques and the available resources give computer simulations a predicting ability and potential for explaining observations on M2GlyR derived channels far superior to the possibilities of solution NMR using the current protocol.

If the optimization of the channel forming sequence continues to follow successive modifications has it has until now, eventually the question will arise of where or not the NMR structures now available can be used as evidence to predict or simulate the structure and characteristics of the new peptides.

References

Bartels, T., Choi, J. G. and Selkoe, D. J. (2011). alpha-Synuclein occurs physiologically as a helically folded tetramer that resists aggregation. *Nature* **477**, 107-U123.

Bechinger, B. (2008). A dynamic view of peptides and proteins in membranes. *Cellular and molecular life sciences : CMLS* **65**, 3028-3039.

Bondarenko, V., Mowrey, D. D., Tillman, T. S., Seyoum, E., Xu, Y. and Tang, P. (2014). NMR structures of the human alpha7 nAChR transmembrane domain and associated anesthetic binding sites. *Biochimica et biophysica acta* **1838**, 1389-1395.

Brooks, B. R., Brooks, C. L., 3rd, Mackerell, A. D., Jr., Nilsson, L., Petrella, R. J., Roux, B., Won, Y., Archontis, G., Bartels, C., Boresch, S., Caflisch, A., Caves, L., Cui, Q., Dinner, A. R., Feig, M., Fischer, S., Gao, J., Hodoscek, M., Im, W., Kuczera, K., Lazaridis, T., Ma, J., Ovchinnikov, V., Paci, E., Pastor, R. W., Post, C. B., Pu, J. Z., Schaefer, M., Tidor, B., Venable, R. M., Woodcock, H. L., Wu, X., Yang, W., York, D. M. and Karplus, M. (2009). CHARMM: the biomolecular simulation program. *Journal of computational chemistry* **30**, 1545-1614.

Brooks, B. R., Bruccoleri, R. E., Olafson, B. D., States, D. J., Swaminathan, S. and Karplus, M. (1983). CHARMM: A program for macromolecular energy, minimization, and dynamics calculations. *Journal of Computational Chemistry* **4**, 187-217.

Broughman, J. R., Shank, L. P., Prakash, O., Schultz, B. D., Iwamoto, T., Tomich, J. M. and Mitchell, K. (2002a). Structural implications of placing cationic residues at either the NH2- or COOH-terminus in a pore-forming synthetic peptide. *The Journal of membrane biology* **190**, 93-103.

Broughman, J. R., Shank, L. P., Takeguchi, W., Schultz, B. D., Iwamoto, T., Mitchell, K. E. and Tomich, J. M. (2002b). Distinct structural elements that direct solution aggregation and membrane assembly in the channel-forming peptide M2GlyR. *Biochemistry* **41**, 7350-7358.

Brunger, A. T., Adams, P. D., Clore, G. M., DeLano, W. L., Gros, P., Grosse-Kunstleve, R. W., Jiang, J. S., Kuszewski, J., Nilges, M., Pannu, N. S., Read, R. J., Rice, L. M., Simonson, T. and Warren, G. L. (1998). Crystallography & NMR system: A new software suite for

macromolecular structure determination. *Acta Crystallogr D Biol Crystallogr* **54 (Pt 5)**, 905-921.

Bukovnik, U., Gao, J., Cook, G. A., Shank, L. P., Seabra, M. B., Schultz, B. D., Iwamoto, T., Chen, J. and Tomich, J. M. (2012). Structural and biophysical properties of a synthetic channel-forming peptide: designing a clinically relevant anion selective pore. *Biochimica et biophysica acta* **1818**, 1039-1048.

Chen, F. Y., Lee, M. T. and Huang, H. W. (2003). Evidence for membrane thinning effect as the mechanism for peptide-induced pore formation. *Biophysical Journal* **84**, 3751-3758.

Chen, J. H. and Tomich, J. M. (2014). Free energy analysis of conductivity and charge selectivity of M2GlyR-derived synthetic channels. *Biochimica Et Biophysica Acta-Biomembranes* **1838**, 2319-2325.

Chou, P. Y. and Fasman, G. D. (1974). Conformational parameters for amino acids in helical, beta-sheet, and random coil regions calculated from proteins. *Biochemistry* **13**, 211-222.

Cook, G. A., Prakash, O., Zhang, K., Shank, L. P., Takeguchi, W. A., Robbins, A., Gong, Y. X., Iwamoto, T., Schultz, B. D. and Tomich, J. M. (2004). Activity and structural comparisons of solution associating and monomeric channel-forming peptides derived from the glycine receptor m2 segment. *Biophys J* **86**, 1424-1435.

Cordes, F. S., Bright, J. N. and Sansom, M. S. P. (2002). Proline-induced distortions of transmembrane helices. *Journal of Molecular Biology* **323**, 951-960.

Cornell, W. D., Cieplak, P., Bayly, C. I., Gould, I. R., Merz, K. M., Ferguson, D. M., Spellmeyer, D. C., Fox, T., Caldwell, J. W. and Kollman, P. A. (1995). A 2nd Generation Force-Field for the Simulation of Proteins, Nucleic-Acids, and Organic-Molecules. *Journal of the American Chemical Society* **117**, 5179-5197.

D.A. Case, D. A. P., J.W. Caldwell, T.E. Cheatham III, J. Wang, W.S. Ross, C.L. Simmerling, T.A. Darden, K.M. Merz, R.V. Stanton, A.L. Cheng, J.J. Vincent, M. Crowley, V. Tsui, H. Gohlke, R.J. Radmer, Y. Duan, J. Pitera, I. Massova, G.L. Seibel, U.C. Singh, P.K. Weiner and P.A. Kollman (2002). AMBER 7.

Delaglio, F., Grzesiek, S., Vuister, G. W., Zhu, G., Pfeifer, J. and Bax, A. (1995). NMRPipe: a multidimensional spectral processing system based on UNIX pipes. *J Biomol NMR* **6**, 277-293.

Fujiwara, K., Toda, H. and Ikeguchi, M. (2012). Dependence of alpha-helical and beta-sheet amino acid propensities on the overall protein fold type. *BMC structural biology* **12**, 18.

Goddard, T. D. and Kneller, D. G. (2004). SPARKY 3. University of California, San Francisco.

Grantham, J. J., Uchic, M., Cragoe, E. J., Jr., Kornhaus, J., Grantham, J. A., Donoso, V., Mangoo-Karim, R., Evan, A. and McAteer, J. (1989). Chemical modification of cell proliferation and fluid secretion in renal cysts. *Kidney international* **35**, 1379-1389.

Herrera, A. I., Al-Rawi, A., Cook, G. A., Gao, J., Iwamoto, T., Prakash, O., Tomich, J. M. and Chen, J. (2010). Structural characterization of two pore-forming peptides: consequences of introducing a C-terminal tryptophan. *Proteins* **78**, 2238-2250.

Im, W., Feig, M. and Brooks, C. L., 3rd. (2003). An implicit membrane generalized born theory for the study of structure, stability, and interactions of membrane proteins. *Biophysical journal* **85**, 2900-2918.

Jo, S., Kim, T. and Im, W. (2007). Automated builder and database of protein/membrane complexes for molecular dynamics simulations. *PloS one* **2**, e880.

Jo, S., Kim, T., Iyer, V. G. and Im, W. (2008). CHARMM-GUI: a web-based graphical user interface for CHARMM. *Journal of computational chemistry* **29**, 1859-1865.

Johnston, J. M., Cook, G. A., Tomich, J. M. and Sansom, M. S. (2006). Conformation and environment of channel-forming peptides: a simulation study. *Biophysical journal* **90**, 1855-1864.

Lindahl, E., Hess, B. and van der Spoel, D. (2001). GROMACS 3.0: a package for molecular simulation and trajectory analysis. *Journal of Molecular Modeling* **7**, 306-317.

Lynch, J. W. (2004). Molecular structure and function of the glycine receptor chloride channel. *Physiological Reviews* **84**, 1051-1095.

Marassi, F. M. and Opella, S. J. (1998). NMR structural studies of membrane proteins. *Current Opinion in Structural Biology* **8**, 640-648.

Mitra, K., Ubarretxena-Belandia, T., Taguchi, T., Warren, G. and Engelman, D. M. (2004). Modulation of the bilayer thickness of exocytic pathway membranes by membrane proteins rather than cholesterol. *Proceedings of the National Academy of Sciences of the United States of America* **101**, 4083-4088.

Nelson, J. W. and Kallenbach, N. R. (1989). Persistence of the alpha-helix stop signal in the S-peptide in trifluoroethanol solutions. *Biochemistry* **28**, 5256-5261.

Phillips, J. C., Braun, R., Wang, W., Gumbart, J., Tajkhorshid, E., Villa, E., Chipot, C., Skeel, R. D., Kale, L. and Schulten, K. (2005). Scalable molecular dynamics with NAMD. *J Comput Chem* **26**, 1781-802.

Powell, M. J. D. (1977). Restart procedures for the conjugate gradient method. *Mathematical Programming* **12**, 241.

Reddy, G. L., Iwamoto, T., Tomich, J. M. and Montal, M. (1993). Synthetic peptides and four-helix bundle proteins as model systems for the pore-forming structure of channel proteins. II. Transmembrane segment M2 of the brain glycine receptor is a plausible candidate for the pore-lining structure. *The Journal of biological chemistry* **268**, 14608-14615.

Roccatano, D., Colombo, G., Fioroni, M. and Mark, A. E. (2002). Mechanism by which 2,2,2-trifluoroethanol/water mixtures stabilize secondary-structure formation in peptides: a molecular dynamics study. *Proceedings of the National Academy of Sciences of the United States of America* **99**, 12179121-84.

Sanders, C. R. and Sonnichsen, F. (2006). Solution NMR of membrane proteins: practice and challenges. *Magnetic resonance in chemistry : MRC* **44 Spec No**, S24-40.

Shank, L. P., Broughman, J. R., Takeguchi, W., Cook, G., Robbins, A. S., Hahn, L., Radke, G., Iwamoto, T., Schultz, B. D. and Tomich, J. M. (2006). Redesigning channel-forming peptides: amino acid substitutions that enhance rates of supramolecular self-assembly and raise ion transport activity. *Biophys J* **90**, 2138-2150.

Singh, U. C. and Kollman, P. A. (1984). An Approach to Computing Electrostatic Charges for Molecules. *Journal of Computational Chemistry* **5**, 129-145.

Snider, C., Jayasinghe, S., Hristova, K. and White, S. H. (2009). MPEx: A tool for exploring membrane proteins. *Protein Science* **18**, 2624-2628.

Tieleman, D. P., Shrivastava, I. H., Ulmschneider, M. R. and Sansom, M. S. P. (2001). Proline-induced hinges in transmembrane helices: Possible roles in ion channel gating. *Proteins-Structure Function and Genetics* **44**, 63-72.

Tomich, J. M., Bukovnik, U., J., L. and Schultz, B. D. (2012). Channel Replacement Therapy for Cystic Fibrosis. In *Cystic Fibrosis - Renewed Hopes Through Research* (Sriramulu, D., ed.). InTech.

Tomich, J. M., Wallace, D., Henderson, K., Mitchell, K. E., Radke, G., Brandt, R., Ambler, C. A., Scott, A. J., Grantham, J., Sullivan, L. and Iwamoto, T. (1998). Aqueous solubilization of transmembrane peptide sequences with retention of membrane insertion and function. *Biophysical journal* **74**, 256-267.

Wallace, D. P., Tomich, J. M., Iwamoto, T., Henderson, K., Grantham, J. J. and Sullivan, L. P. (1997). A synthetic peptide derived from glycine-gated Cl- channel induces transepithelial Cl- and fluid secretion. *Am J Physiol* **272**, C1672-C1679.

Warschawski, D. E., Arnold, A. A., Beaugrand, M., Gravel, A., Chartrand, E. and Marcotte, I. (2011). Choosing membrane mimetics for NMR structural studies of transmembrane proteins. *Biochimica Et Biophysica Acta-Biomembranes* **1808**, 1957-1974.

Wishart, D. S. and Nip, A. M. (1998). Protein chemical shift analysis: a practical guide. *Biochemistry and cell biology = Biochimie et biologie cellulaire* **76**, 153-163.

Woolfson, D. N. and Williams, D. H. (1990). The Influence of Proline Residues on Alpha-Helical Structure. *Febs Letters* **277**, 185-188.

Wüthrich, K. (1986). *NMR of proteins and nucleic acids*. The George Fisher Baker non-resident lectureship in chemistry at Cornell University, Wiley, New York.

Wüthrich, K., Billeter, M. and Braun, W. (1983). Pseudo-structures for the 20 common amino acids for use in studies of protein conformations by measurements of intramolecular proton-proton distance constraints with nuclear magnetic resonance. *J Mol Biol* **169**, 949-961

Chapter 5 - Summary and Final Discussion

A review on membrane active peptides highlighting their ubiquitous presence in nature, and their diversity of origin was presented in the first chapter. Membrane active peptides were classified according to their function as: antimicrobial, cell-penetrating, channel/pore forming and amyloids. A description of the historical development, the mode of action and the recent developments in their field was given for each of the four categories of membrane active peptides. Similarities, such as the amphipathic distribution of residues, are found in the structural characteristics of all membrane active peptides and are likely to have common mechanistic significance. New general models for peptide-membrane interaction have been recently proposed focusing on the membrane as an active participant with regard to which peptides will interact and form pores. The intent of the review was to present a framework for the structural studies on a family of channel forming peptides presented in the other chapters of this dissertation, bringing attention to the involvement of membrane active peptides in diseases, immunity and the development of potential pharmaceutical applications.

One pharmaceutical application, currently being explored in the laboratory of Dr. John Tomich at Kansas State University, is the development of a channel forming peptide (CFP) with the potential to be used in the treatment of the symptoms caused by cystic fibrosis (CF). A treatment for the respiratory symptoms of CF has the potential of slowing down the degenerative consequences of the progression of the disease, and enhancing the quality of life for CF patients. The starting sequence for the family of M2GlyR peptides was the second transmembrane segment of the α subunit of the glycine receptor. Modifications that increase solubility in

aqueous solution and decrease aggregation have been made to the sequence yet at the expense of anion specific conductance.

An answer to the question, of whether or not there is compelling need to determine the NMR structure of the peptides that constitute the most recent developments in the optimization of the M2GlyR family of CFPs, has been explored by: -presenting the structures determined by solution NMR for NK_4-M2GlyR-p22 and NK_4-M2GlyR-p20 T17R S20W sequences -comparing all the structures determined by NMR for the M2GlyR family of peptides – looking for differences between structures that can correlate with the observed changes in the ion conductance between peptide sequences and – assessing the contribution to the project that the NMR determined structures have had to date.

The kinetic parameters (I_{max}, $K_{1/2}$ and Hill coefficient) derived from fitting the I_{SC} vs concentration data to a modified Hill equation were used to compare the ion conductance properties of the different peptide sequences. Increasing I_{max} while decreasing $K_{1/2}$ are among the desired results of the sequence modifications. Peptide NK_4-M2GlyR-p22 has an I_{max} of 23.7 ± 5.6 μA/cm^2, a $K_{1/2}$ of 210 ± 71 μM and a Hill coefficient of 1.9 ± 0.6. The determined NMR structure for NK_4-M2GlyR-p22 peptide in SDS micelles is in a helical conformation from residues 6 to 20. The N-terminal lysine residues are unstructured and flexible. The hydrophobic and hydrophilic side chains of the residues in the helix are segregated to different sides of the helix. The structure of NK_4-M2GlyR-p22 in SDS micelles is very similar to the previously reported structure in 40% TFE for the same peptides. The cluster of structures in TFE was reported to have a RMSD to the mean structure for residues 9-20 of 1.95± 0.6 Å (Cook et al.,

2004), whereas the cluster of structures in SDS micelles showed a RMSD to the mean structure (residues 6-20) of 0.46 ± 0.12 Å.

The average structure for peptide NK_4-M2GlyR-p22 in SDS micelles and the average structure calculated for peptide NK_4-M2GlyR-p22 S22W in the same environment (Herrera et al., 2010) both have a similar helical conformation on most of the length (residue 6-20) of the peptide. NK4-M2GlyR-p22 S22W shows a convexity along the axis of the helix, while NK4-M2GlyR-p22 has a more linear axis in the central portion of the structure. Both peptides have an unstructured state of the N-terminal lysines that is more pronounced for the NK4-M2GlyR-p22 sequence due to lacking the anchoring tryptophan residue.

The substitution of residue 22 from a serine to a tryptophan produced a decrease in I_{max} of 10.7 ± 5.7 μA/cm^2, a decrease in $K_{1/2}$ of 166 ± 70 μM and an increase in the Hill coefficient of 3.5 ± 3.0. These changes in the kinetic parameter could not have been predicted from the NMR structures alone. The higher peptide concentration required by NK_4-M2GlyR-p22 compared with NK_4-M2GlyR-p22 S22W to reach one-half I_{max} could be attributed to the soluble associations formed by the peptide in the aqueous environment, and also to the higher conformational flexibility in the membrane environment, that may negatively impact the stability of the assembled ion channel. Computational assemblies and molecular dynamics simulations have been performed on peptide NK_4-M2GlyR-p22 and peptide NK_4-M2GlyR-p22 S22W based on the calculated NMR solution structures (as described in Appendix A – Chapter 2). According to the simulations, the introduction of the C-terminal tryptophan appears to lead to global changes of the channel structure.

For peptide NK_4-M2GlyR-p20 T17R S20W the kinetic parameters of ion conductance across monolayers of MDCK cells have been determined, and the NMR solution structure was determined in a TFE:water solution and also in SDS micelles. The NK_4-M2GlyR-p20 T17R S20W sequence is a modification of a previously studied leading sequence candidate NK_4-M2GlyR-p22 T19R S22W. The shorter sequence was created by removing residues proline 5 and alanine 6. These two residues are predicted to be part of an internal loop connecting the M2 transmembrane segment to the M1 transmembrane segment in the Glycine receptor channel sequence.

Peptide NK_4-M2GlyR-p20 T17R S20W has both a higher I_{MAX} (43.8 ± 2.8 $\mu A/cm^2$) and a lower $K_{1/2}$ (58 ± 8 μM) compared to other M2GlyR derived peptides with calculated NMR structures. The average structures for peptide NK_4-M2GlyR-p20 T17R S20W under both experimental conditions (TFE solution and SDS micelles) were calculated and were found to be predominantly α-helical. The most notable difference between the structure calculated in TFE solution and the one calculate in SDS micelle is in the C-terminal region (residues 17-20). For both sample conditions the C-terminal residues are not part of the main α helix, but for the structure in TFE the C-terminal residues form a hydrogen bond stabilized bend that folds back towards the helix. For the structure in SDS micelles the C-terminal residues continue in the same general direction of the main α helix axis.

Another difference between the structures calculated for NK_4-M2GlyR-p20 T17R S20W, in TFE solution and in SDS micelles, is the apparently more restricted N-terminus for the conformation

in SDS. This difference could be explained by the interaction of the N-terminal lysines with the hydrophilic heads of the SDS molecules. A similar interaction could be responsible for a more restricted structure overall for the SDS micelles sample, that has a RMSD to the mean structure of 0.63 ± 0.24 Å in the helical region, compare to 0.96 ± 0.33 Å for the TFE sample.

The presence of the membrane anchoring residue in the C-terminus of NK_4-M2GlyR-p20 T17R S20W, combined with the shorter axial length of the peptide structure could force the hydrophobic side chains for one or more of the N-terminal lysines into the hydrophobic interior of the micelles. The location of the N-terminal lysines partially in the interior of the micelles explains the observed more restricted conformation of the N-terminus compared to other NMR structures of M2GlyR derived peptides (Cook et al., 2004;Herrera et al., 2010). Another suggested explanation is that the absence of the proline residue, a known helix breaker (Chou and Fasman, 1974;Fujiwara et al., 2012), allows lysine 4 to participate in the helix, partially restricting the conformation of the N-terminal residues. Proline residues are actually found in many transmembrane α-helix sequences (e.g. CFP alamethicin, S6 from voltage-gated potassium channels, D5 from voltage-gated chloride channels), where they induce a hinge in the helix that has been associated with channel gating (Tieleman et al., 2001). The absence of the proline residue in NK_4-M2GlyR-p20 T17R could be affecting the dynamic properties of the formed channels as well.

The structure determined for NK_4-M2GlyR-p20 T17R S20W in SDS micelles is expected to be a better representation of the structure adopted by the peptide in the interior of a membrane bilayer, than the structures calculated in the TFE solution. Even so there are expected limitations

to the reported structure in SDS micelles. The axial length of the structure in SDS micelles is ~30 Å, the peptide in the reported structure would not be able to span across an unperturbed cellular membrane to form ion channels.

The deletion of residues proline 5 and alanine 6 from the sequence of peptide NK_4-M2GlyR-p22 T19R S22W produced an increase in I_{max} of 10.1 ± 3.1 μA/cm^2, a decrease in $K_{1/2}$ of 13 ± 9 μM and a decrease in the Hill coefficient of 1.7 ± 0.8. These changes in the kinetic parameters cannot be fully explained by the differences in the NMR solution structures. A prediction, based on the NMR structure, of a shorter conduction pathway in the formed channels is a possible explanation to the increase in ion conductance.

The characterization of the ion conductance induced by peptide NK_4-M2GlyR-p20 T17R S20W presents this sequence as a step in the right direction towards the optimization of a channel forming peptide with potential as a therapeutic for the treatment of CF. Study of the ion selectivity of the channels formed by this peptide is needed to further characterize the ion current induced.

The anion selectivity of the M2GlyR peptides is expected to be affected by the changes made to the sequence. Selective anion permeability could be affected by pore length and pore rigidity or changes in hydrogen bonding potential and electrostatics of the pore lining residues. The NK_4-M2GlyR-p22 T17R S22W is known to be only slightly anion selective (Tomich et al., 2012). Evaluation of the ion selectivity mechanism of the M2GlyR derived peptides has been reported

by computational methods that use the NMR structures determined in SDS micelles as starting point (Chen and Tomich, 2014).

Having developed the ability to determine the structure of peptides from the M2GlyR family in a membrane mimicking environment has decreased the relevance of performing new determinations using the TFE solution environment. At the same time the structure in TFE solution of peptide M2GlyR-p22 S22W sets a precedent for the contribution to the understanding of the behavior in water solution that TFE solution structures can give. Not all the structures in TFE solution are as informative, suggesting that determination of an NMR structure in TFE solution should only be attempted when a new sequence behaves in an unexpected way, or when the CD spectrum of a peptide predicts a conformation not predominantly helical in solution.

Based on theoretical considerations and all other experimental data available (CD spectra, structure of similar sequences, computer simulations), the structures calculated by NMR for the M2GlyRfamily of peptides in SDS micelles appear to be an adequate approximation to the actual structure of the peptides in the assembled channel. However limited capability of providing on their own evidence for the explanation of changes in the ion conductance has been found. The NMR structures currently available have provided supporting evidence for the rationalization of the observed differences in the solubility, oligomerization states, and ion conductance between the considered sequences. In nature the peptides will be paired with other transmembrane segments as oligomeric bundles with water-lined pores. Packing interactions will most likely stabilize aspects of these assemblies. Using the current protocols these interactions cannot be analyzed by solution NMR.

The contribution of the NMR structures with the largest impact is to the computer simulation of the ion conducting channels formed by the family of M2GlyR peptides. NMR structures for SDS micelles samples have provided an experimentally based starting point for computational studies. Future predictions about the dynamics of the channels and newly explored modifications to the leading peptide sequences are well supported. The current availability of computational techniques and resources make computer simulations the best choice as the primary source of structural information about the M2GlyR family of ion channels.

Improvements to the protocols used for structure determination of M2GlyR derived peptides by solution NMR need to be considered in order to justify new structure determinations. A sample environment that better resembles the cellular membrane may be incorporated to the protocols. The use of vesicles (Warschawski et al., 2011) or phospholipid bilayer nanodiscs (Hagn et al., 2013) as the membrane mimicking environment may be considered. The feasibility of determining the structure by NMR of assembled peptide channels is an important possibility to be explored. The determination of the assembled channel would require the use of a doubly isotopically labeled (^{15}N, ^{13}C) sample for multinuclei/multidimensional, triple-resonance 3D NMR experiments. And the implementation of Transverse Relaxation-Optimized Spectroscopy (TROSY) experiments, currently use to solve the structure of very large biological macromolecules in solution (Pervushin et al., 1997).

A complementary approach for the study of the assembled peptide channels is the use of Solid state NMR. There are two kinds of sample preparations commonly used in the study of

membrane interacting proteins and peptides by solid state NMR. In one kind of samples the protein has to be reconstituted in micelles or vesicles and then packed in to "magic angle spinning" rotors. In the other kind of samples the protein is reconstituted in lipid bicelles or a lipid bilayer that have a determined orientation with respect to the magnetic field of the instrument.

Structural and dynamics studies of full length channels and channels formed by CFPs have been reported using magic angle spinning (MAS) (Varga et al., 2007;Williams et al., 2013). For solid state MAS NMR samples 2D ^{13}C–^{13}C homonuclear correlation spectra (DARR) and 3D inter-residue (NCOCx) and intra-residue (NCαCX) NMR experiments are used to perform backbone assignments. A typical sample preparation consists of: - expression (for proteins) or synthesis (for peptides) followed by purification of an isotopically labeled protein of peptide – reconstitution of the sample in lipid vesicles (components optimized for each sample) – dialysis of the proteoliposomes and – packing into MAS rotors of the NMR instrument. Using MAS samples the dynamics of the channels formed by M2glyR derived peptides could be studied following chemical shift perturbations as it has been reported in the study of the channel forming M2 protein from the influenza A virus (Liao et al., 2013).

Solid state NMR on magnetically oriented samples can also provide useful complementary information on the structure of assembled channel formed by M2GlyR derived peptides. For solid state NMR on oriented samples the channels need to assemble in lipid bicelles or a lipid bilayer. The bicelles used in solid state NMR studies are a mixture of long chain lipids (e.g. DMPC) and short chain lipids or detergents (e.g. DHPC) (Warschawski et al., 2011). The

relative orientation to the magnetic field of the helical axis of the monomers can be determined under different sample conditions using the oriented samples (Bechinger et al., 1996). This could provide experimental confirmation to the packing geometries observed in the computational studies.

In general the field of NMR currently offers possibilities that if implemented can make a contribution to the study and improvement of M2GlyR derived channel forming peptide assemblies. Substantial investment of time and resources would be needed to implement the required changes to the NMR protocols use in the study of the M2GlyR family of peptides. Collaboration with a group having experience in using the required NMR techniques on similar samples is a possible way to facilitate the transition.

References

Bechinger, B., Gierasch, L. M., Montal, M., Zasloff, M. and Opella, S. J. (1996). Orientations of helical peptides in membrane bilayers by solid state NMR spectroscopy. *Solid State Nuclear Magnetic Resonance* **7**, 185-191.

Chen, J. H. and Tomich, J. M. (2014). Free energy analysis of conductivity and charge selectivity of M2GlyR-derived synthetic channels. *Biochimica Et Biophysica Acta-Biomembranes* **1838**, 2319-2325.

Chou, P. Y. and Fasman, G. D. (1974). Conformational parameters for amino acids in helical, beta-sheet, and random coil regions calculated from proteins. *Biochemistry* **13**, 211-222.

Cook, G. A., Prakash, O., Zhang, K., Shank, L. P., Takeguchi, W. A., Robbins, A., Gong, Y. X., Iwamoto, T., Schultz, B. D. and Tomich, J. M. (2004). Activity and structural comparisons of solution associating and monomeric channel-forming peptides derived from the glycine receptor m2 segment. *Biophys J* **86**, 1424-1435.

Fujiwara, K., Toda, H. and Ikeguchi, M. (2012). Dependence of alpha-helical and beta-sheet amino acid propensities on the overall protein fold type. *BMC structural biology* **12**, 18.

Hagn, F., Etzkorn, M., Raschle, T. and Wagner, G. (2013). Optimized Phospholipid Bilayer Nanodiscs Facilitate High-Resolution Structure Determination of Membrane Proteins. *Journal of the American Chemical Society* **135**, 1919-1925.

Herrera, A. I., Al-Rawi, A., Cook, G. A., Gao, J., Iwamoto, T., Prakash, O., Tomich, J. M. and Chen, J. (2010). Structural characterization of two pore-forming peptides: consequences of introducing a C-terminal tryptophan. *Proteins* **78**, 2238-2250.

Liao, S. Y., Fritzsching, K. J. and Hong, M. (2013). Conformational analysis of the full-length M2 protein of the influenza A virus using solid-state NMR. *Protein Science* **22**, 1623-1638.

Pervushin, K., Riek, R., Wider, G. and Wuthrich, K. (1997). Attenuated T-2 relaxation by mutual cancellation of dipole-dipole coupling and chemical shift anisotropy indicates an avenue to NMR structures of very large biological macromolecules in solution. *Proceedings of the National Academy of Sciences of the United States of America* **94**, 12366-12371.

Tieleman, D. P., Shrivastava, I. H., Ulmschneider, M. R. and Sansom, M. S. P. (2001). Proline-induced hinges in transmembrane helices: Possible roles in ion channel gating. *Proteins-Structure Function and Genetics* **44**, 63-72.

Tomich, J. M., Bukovnik, U., J., L. and Schultz, B. D. (2012). Channel Replacement Therapy for Cystic Fibrosis. In *Cystic Fibrosis - Renewed Hopes Through Research* (Sriramulu, D., ed.). InTech.

Varga, K., Tian, L. and McDermott, A. E. (2007). Solid-state NMR study and assignments of the KcsA potassium ion channel of S. lividans. *Biochimica Et Biophysica Acta-Proteins and Proteomics* **1774**, 1604-1613.

Warschawski, D. E., Arnold, A. A., Beaugrand, M., Gravel, A., Chartrand, E. and Marcotte, I. (2011). Choosing membrane mimetics for NMR structural studies of transmembrane proteins. *Biochimica Et Biophysica Acta-Biomembranes* **1808**, 1957-1974.

Williams, J. K., Tietze, D., Wang, J., Wu, Y. B., DeGrado, W. F. and Hong, M. (2013). Drug-Induced Conformational and Dynamical Changes of the S31N Mutant of the Influenza M2 Proton Channel Investigated by Solid-State NMR. *Journal of the American Chemical Society* **135**, 9885-9897.